

[NiFe] and [FeFe] Hydrogenases Studied by Advanced Magnetic Resonance Techniques

Wolfgang Lubitz,* Eduard Reijerse, and Maurice van Gastel

Max-Planck-Institut für Bioanorganische Chemie, Stiftstrasse 34-36, D-45470 Mülheim an der Ruhr, Germany

Received March 12, 2007

Contents

1. Introduction	4331	6.7.1. Origin of the ^{57}Fe hyperfine couplings in the H-Cluster	4354
2. Structure of [NiFe] and [FeFe] Hydrogenases	4333	6.7.2. Redox States of the Iron Atoms in the Binuclear Cluster	4354
2.1. [NiFe] Hydrogenases	4333	6.8. Possible Mechanisms for the Catalytic Cycle	4355
2.2. [FeFe] Hydrogenases	4335	7. Concluding Remarks	4356
3. Redox States of Hydrogenases	4336	8. List of Abbreviations	4357
3.1. [NiFe] Hydrogenase	4336	9. Acknowledgments	4358
3.2. [FeFe] Hydrogenase	4337	10. Appendix I. Advanced EPR Methods Used in Hydrogenase Research	4358
4. A Survey of Structural Methods Used in Hydrogenase Research	4338	10.1. FID-Detected EPR	4358
5. Magnetic Resonance Studies of [NiFe] Hydrogenases	4339	10.2. ESE-Detected EPR	4358
5.1. Overview of EPR Spectra in the Various Redox States of the Enzyme	4339	10.3. Three-Pulse Electron Spin Echo Envelope Modulation (ESEEM) Spectroscopy	4359
5.2. The Presence of Ni and Fe in the Active Site	4340	10.4. Four-Pulse ESEEM (HYSCORE)	4359
5.3. The Oxidized (As-Isolated) States	4341	10.5. Pulse Electron–Nuclear Double Resonance (ENDOR) Spectroscopy	4359
5.3.1. g Tensor Analysis and the Ligand Field	4341	10.6. Pulse Electron–Nuclear–Nuclear Triple Resonance	4359
5.3.2. Hyperfine Interactions	4342	10.7. Pulse Electron–Electron Double Resonance (PELDOR/DEER) Spectroscopy	4359
5.3.3. Activation and Inactivation Studies	4343	10.8. ELDOR-Detected NMR	4360
5.3.4. The Fe–S Clusters	4344	11. Appendix II. Crystal Field Considerations for Ni^{III} and Ni^{I} in a Square Pyramidal Crystal Field	4360
5.4. The Active Intermediate State	4344	12. Appendix III. The Spin Exchange Model of the H-cluster in [FeFe] Hydrogenase	4360
5.4.1. g Tensor Analysis and the Ligand Field	4344	13. References	4361
5.4.2. Hyperfine Interactions	4345		
5.4.3. The Fe–S Clusters	4345		
5.5. Inhibition of the Enzyme	4346		
5.5.1. Inhibition by O_2	4346		
5.5.2. Inhibition by CO	4346		
5.5.3. Other Inhibitory Agents	4346		
5.6. Light Sensitivity of the Enzyme	4346		
5.7. EPR-Silent States	4347		
5.8. Other Hydrogenases Containing Nickel	4347		
5.9. DFT Calculations and Electronic Structure	4347		
5.10. The Catalytic Cycle	4349		
6. Magnetic Resonance Studies of [FeFe] Hydrogenases	4350		
6.1. Overview of EPR Spectra in Various Redox States of the Enzyme	4350		
6.2. The Oxidized (As Isolated) State	4350		
6.3. The Intermediate States	4351		
6.4. The H_2 -Reduced State	4352		
6.5. The CO-Inhibited State	4353		
6.6. Light Sensitivity of the CO-Inhibited State	4354		
6.7. Electronic Structure of the H-Cluster	4354		

1. Introduction

Fossil fuels like coal, oil, and natural gases are not renewable on a human time scale and when combusted they pollute the earth's atmosphere with carbon dioxide. The latter is believed to contribute to global warming and climate changes hazardous for our world and human life. Thus, the search for alternative sustainable fuels to satisfy the worldwide increasing energy demand has become a major issue in recent years.^{1–6} One possible solution is provided by the use of hydrogen as a “clean fuel”.^{1–4,7,8} However, free hydrogen is not a natural energy source on earth as it is incompatible with the high oxygen content of the atmosphere. The generation of hydrogen from bound compounds (e.g., hydrocarbons) is a highly energy-consuming process in which the greenhouse gas CO_2 is released. The ideal source of hydrogen is water that can for example be split electrolytically using electricity from renewable, nonfossil energy sources.^{3,9} Water splitting and release of oxygen and protons is performed in nature in oxygenic photosynthesis by green plants, algae, and some bacteria, a process powered by

* To whom correspondence should be addressed. E-mail: lubitz@mpi-muelheim.mpg.de.

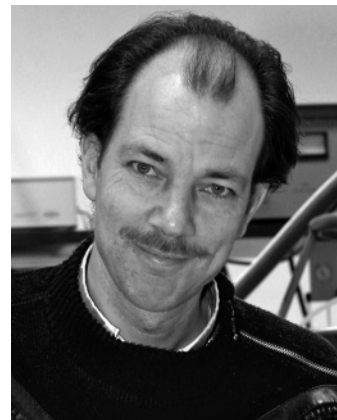
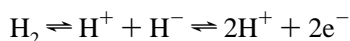


Wolfgang Lubitz, born 1949 in Berlin, studied chemistry at the Freie Universität (FU) Berlin (1969–1974), where he also received his doctoral degree (1977) and habilitation in organic chemistry in 1982. From 1983 to 1984 he worked as a Max Kade Fellow at UC San Diego (department of physics), from 1979 to 1989 as assistant and associate professor at the FU Berlin, from 1989 to 1991 as professor at the Universität Stuttgart (experimental physics/biophysics), and from 1991 to 2001 as full professor of physical chemistry at the Max Volmer Institute, Technische Universität Berlin. In 2000 he became a Scientific Member of the Max Planck Society and Director at the Max Planck Institute for Radiation Chemistry in Mülheim/Ruhr (later renamed Max Planck Institute for Bioinorganic Chemistry). He is Honorary Professor at the Heinrich Heine Universität Düsseldorf and currently Managing Director of the Max Planck Institute in Mülheim. He is member of the International EPR/ESR Society (IES), ISMAR and AMPERE Society, the International Photosynthesis Society, and several other professional organizations such as the GDCh, ACS, and RSC. Since 2004 he is a member of the Council for the Meetings of the Nobel Laureates in Lindau and since 2005 President of the IES. He is on the editorial board of five journals. Among other awards and fellowships he recently received the Zavoisky Award (Russia, 2002), the Bruker Prize (U.K., 2003) and the Gold Medal of the International EPR Society (2005). Wolfgang Lubitz is (co)author of more than 250 publications in scientific journals and has contributed to books and written about 15 review articles. In the past his group has substantially contributed to light-induced charge separation in bacterial and plant photosynthesis by studying the radicals, radical pairs, and triplet states that are created in this process. In recent years, the focus has been shifted to the investigation of catalytic metal centers in metalloproteins, for example in [NiFe]- and [FeFe]-hydrogenases and the Mn₄-cluster in the water splitting complex of photosynthesis. An important aspect of his work is the development and application of advanced EPR methods in different frequency bands, which is supplemented by quantum chemical calculations and other spectroscopic techniques.

sunlight.^{10–12} Many of the photosynthetic microorganisms also contain an enzyme that can convert the released protons into dihydrogen. This enzyme is called hydrogenase.¹³

The understanding of the basic principles of hydrogen production and utilization in microbes is a goal of major importance both for basic research and possible applications in our society.⁷ A mechanistic knowledge of the hydrogen conversion and consumption process would allow us to use the organisms or the isolated enzymes in biotechnological hydrogen production processes.^{14–23} Furthermore, this would provide the necessary fundamental knowledge for designing biomimetic or bioinspired artificial “hydrogenase catalysts” for large-scale hydrogen production in the future.^{24–35}

Hydrogenases are ancient enzymes that facilitate the uptake and oxidation of dihydrogen to protons and release of electrons and also the reverse reaction in a true equilibrium process



Edward Reijerse received his B.Sc. and his M.Sc. in Chemistry from the University of Nijmegen, the Netherlands in 1978 and 1982 (respectively). He obtained his Ph.D. in physical chemistry in 1986 on the subject of advanced electron paramagnetic resonance under the guidance of Prof. E. de Boer and Dr. C. P. Keijzers at the University of Nijmegen, the Netherlands. He spend one year in industry as group leader product development at Powers Chemco, Soest BV in the Netherlands. In 1986 he was appointed as assistant professor at the Department of Molecular Spectroscopy at the University of Nijmegen, the Netherlands. In the same group he worked as associate professor from 1992 to 2002. His research interests involve the development of advanced EPR techniques and their application to bioinorganic systems and transition metal model complexes. Since 2002 he is working as group leader at the Max Planck institute for Bioinorganic Chemistry in Mülheim, Germany.



Maurice van Gastel (Ph.D. in Physics at Leiden University, the Netherlands) did his graduate research with Prof. Dr. E. J. J. Groenen on copper proteins by magnetic resonance, optical and theoretical methods. He then went to industry and worked for two years at the MRI department of Philips Medical Systems. In 2002 he returned to science and joined the group of Prof. Dr. W. Lubitz. Presently he works as a group leader at the MPI in Mülheim and studies bacterial photosynthesis and hydrogen production.

The *in vivo* situation may, however, not correspond to an equilibrium situation. From isotope exchange experiments, according to $\text{H}_2 + \text{D}_2\text{O} \rightleftharpoons \text{HD} + \text{HDO}$ it has been deduced that the H_2 molecule is split heterolytically at the metal rather than homolytically.³⁶ The enzyme also catalyzes the conversion of para- (parallel nuclear spins) to ortho-dihydrogen.^{37,38} The enzymatic reaction takes place at specialized metal centers which are turned to high efficiency via a unique ligand sphere.

The enzyme hydrogenase is found in many microorganisms from bacteria and archae to eukarya¹³ (see also article by Vignais and Billoud in this issue). It represents a diverse class of enzymes. While nature has found several solutions for hydrogen conversion, in all cases the simple looking task

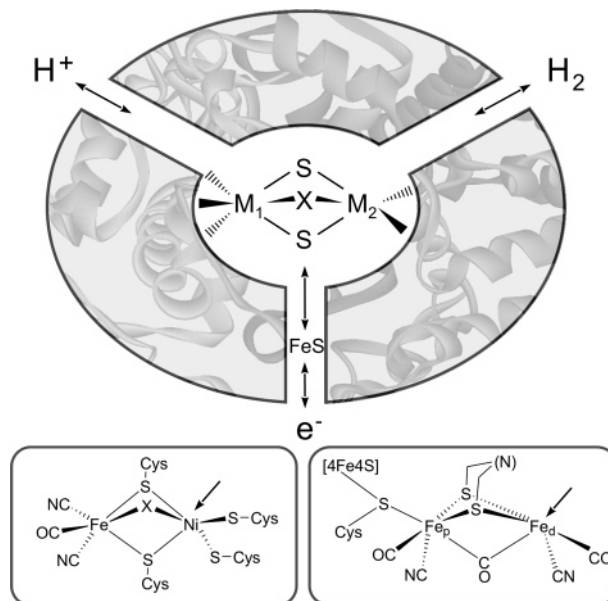
is solved by a highly sophisticated molecular mechanism that is not yet understood in detail.

Hydrogenases can be classified according to the metal content of the active site into [NiFe], [FeFe], and [Fe] hydrogenases. A characteristic feature of all hydrogenases is that the iron atoms are ligated by small inorganic ligands (CO, CN⁻), which were first detected by FTIR spectroscopy.^{39,40} The [NiFe] and [FeFe] hydrogenases contain sulfur-bridged bimetallic centers, typically with an open coordination site on one metal. A subgroup of the first class comprises the [NiFeSe] hydrogenases, in which one of the cysteine ligands of the nickel atom is replaced by a selenocysteine.⁴¹ The third class of enzymes has long been thought to contain no metal. However, it was recently shown that the active site harbors a single iron atom^{42–45} with an unusual coordination sphere. These enzymes are now called [Fe]-hydrogenases or iron-sulfur cluster-free hydrogenases. They can activate H₂ only in the presence of a second substrate (methyl tetrahydromethanopterin).⁴⁶ They are quite different from the first two classes and will therefore only briefly be discussed in this review. Other classifications of hydrogenases¹³ according to the redox partner, NAD(P)⁺ or cytochromes, have also been described.

Hydrogenases are present in the periplasm or in the cytosol, either in soluble form or membrane bound. In eukarya hydrogenases are often found in specialized cellular compartments.^{13,47} Two important functions of hydrogenases are to balance the redox potential in the cell and also to provide energy by oxidation of molecular hydrogen. They may remove reducing equivalents by production of molecular hydrogen or provide electrons by splitting H₂. Depending on the location in the cell, hydrogenases may either be tuned for hydrogen evolution or hydrogen uptake. They may also be involved in establishing transmembrane proton gradients.¹³ The same principle to bind hydrogen at the active site (e.g., [NiFe] center) during the catalytic process has also been used to sense the presence of hydrogen and regulate the expression of genes required for the biosynthesis of hydrogenases (see article by Friedrich et al.⁴⁸). These proteins are called sensory or regulatory hydrogenases in contrast to the catalytic hydrogenases and show a much lower activity.^{49,50} Accordingly, hydrogenases are also classified as membrane-bound (MBH), soluble (SH), or regulatory hydrogenases (RH), e.g., in the species *Ralstonia (R.) eutropha*, where all three classes are present and have been characterized (see article by Friedrich et al.⁴⁸). Many catalytic hydrogenases are bidirectional, that is, they act both as H₂-uptake and H₂-producing enzymes.^{51–53} The [NiFe] hydrogenases are often more active in H₂ oxidation and the [FeFe] hydrogenases in the production of molecular hydrogen. The activity can be measured by several assays described in the literature.^{13,47} Some [FeFe] hydrogenases are, for example, extremely active in H₂-generation,⁵⁴ each molecule of enzyme can produce up to ~10⁴ molecules of H₂ per second at room temperature.⁵⁵ The reported lower catalytic activity of [NiFe] as compared to the [FeFe] hydrogenases using assays with artificial electron acceptors (e.g., methyl viologen) has recently been critically discussed by Armstrong et al.,⁵⁶ who showed that the H₂ uptake reaction for a monolayer of enzyme on the electrode is diffusion limited.

In all hydrogenases the protein matrix plays an important role in providing (i) the ligand sphere for binding of the active metal site, (ii) an optimized pocket for the catalytic reaction, and (iii) pathways between the active site and the surface for both the substrate and products of the enzymatic

Scheme 1



reaction. This is shown for the bimetallic [NiFe] and [FeFe] hydrogenases in Scheme 1 that schematically depicts the three-channel motif found in these hydrogenases. It shows the active site, the H₂ access channel, the electron and proton-transfer chains, and the chemical constitutions of the bimetallic complexes forming the active sites.

There are many features of hydrogenase catalysis that are not yet understood. This article is intended to show what specific spectroscopic methods—like magnetic resonance—can contribute to this field. Before starting this endeavor we will briefly discuss the structure of [NiFe] and [FeFe] hydrogenases, the various states of these enzymes that occur in their activation/deactivation, inhibition, and catalytic cycles and outline the techniques used to study the structure—in particular the electronic structure—of these enzymes. The active site of the [Fe] hydrogenase is different.^{42,45,57–59} This class of enzymes will therefore not be further discussed in this review.

2. Structure of [NiFe] and [FeFe] Hydrogenases

In Scheme 1 a general view of the [NiFe] and [FeFe] hydrogenases is given. The H₂ transfer channel has been mapped out by modeling studies and by introducing Xe atoms in single crystals^{60,61} and subsequent X-ray crystallography (see article by Fontecilla-Camps et al. in this issue). The H⁺ transfer chain has been located by a search for protonable residues^{61–64} combined with site-directed mutagenesis.⁶⁵ A Mg atom has been located in the H⁺ transfer pathway for several [NiFe] hydrogenases.^{64,66} The electron transfer is in general performed by iron–sulfur clusters. The number and type of these clusters vary in different species, in particular in the case of the [FeFe] hydrogenase.⁶⁷ Of central importance are the active sites of the [NiFe] and [FeFe] hydrogenases (Scheme 1, bottom) which show remarkable similarities. In the following, details of the structure of the [NiFe] and [FeFe] hydrogenases relevant to the spectroscopic studies are outlined.

2.1. [NiFe] Hydrogenases

[NiFe] hydrogenase was first crystallized in 1987 from *Desulfovibrio (D.) vulgaris* Miyazaki F by Higuchi et al.,⁶⁸

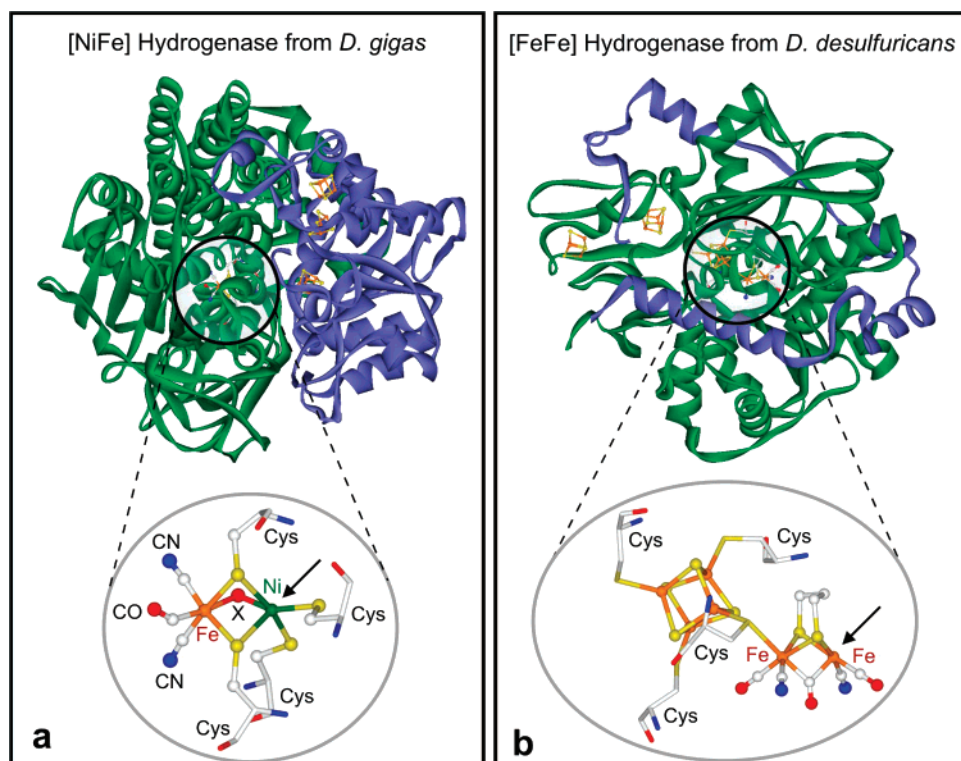


Figure 1. (a) Structure of [NiFe] hydrogenase from *D. gigas* (PDB 1FRV) from ref 63 detailing the two protein subunits (small, blue; large, green), the electron-transfer chain with three Fe–S centers in the small subunit, and the active site in the large subunit. The structure of the active site is shown enlarged at the bottom (see text). The arrow indicates the sixth coordination site at Ni which is found to be unoccupied. The enzyme resided mainly in the unready state. (b) Structure of [FeFe] hydrogenase from *D. desulfuricans* (PDB 1HFE) from ref 61, detailing the two protein subunits (small, blue; large, green). The H-cluster (hydrogen-activating cluster) and the two additional [4Fe–4S] clusters are all located in the large subunit. The molecular structure of the H-cluster with the cubane [4Fe–4S]_H and the dinuclear [2Fe]_H subclusters is shown enlarged at the bottom. The arrow indicates the free coordination site at the distal iron Fe_d found in ref 61.

Table 1. Crystal Structures of Different Hydrogenases

organism and functional state of the enzyme	class	method	resolution nm	year	PDB file	reference
<i>D. gigas</i> unready	[NiFe]	MIR	0.285	1995	1FRV	Volbeda et al. ⁶³
<i>D. gigas</i> unready	[NiFe]	MR	0.254	1996	2FRV	Volbeda et al. ⁷⁰
<i>D. gigas</i> active	[NiFe]	MR	0.27	1998		Garcin thesis ³⁴¹
<i>D. gigas</i> unready	[NiFe]	MR	0.235	2005	1YQ9	Volbeda et al. ⁷¹
<i>D. vulgaris</i> ready	[NiFe]	MIR	0.18	1997	1H2A	Higuchi et al. ⁶⁶
<i>D. vulgaris</i> active	[NiFe]	MR	0.14	1999	1H2R	Higuchi et al. ⁷²
<i>D. vulgaris</i> CO-inhibited	[NiFe]	MR	0.118–0.14	2002	1UBH-U	Ogata et al. ⁷³
<i>D. vulgaris</i> unready, ready	[NiFe]	MR	0.104–0.14	2005	1WUI-L	Ogata et al. ⁷⁴
<i>D. fructosovorans</i> unready	[NiFe]	MR	0.27	1997	1FRF	Montet et al. ⁶⁰
	[NiFe]	MR	0.18	2002		Volbeda et al. ⁷⁶
<i>D. fructosovorans</i> ready	[NiFe]	MR	0.21	2005	1YRQ	Volbeda et al. ⁷¹
<i>D. fructosovorans</i> unready	[NiFe]	MR	0.183	2005	1YQW	Volbeda et al. ⁷¹
<i>D. desulfuricans</i>	[NiFe]	MR	0.18	2001	1E3D	Matias et al. ⁷⁵
<i>D. baculatum</i> active	[NiFeSe]	MR	0.215	1999	1CC1	Garcin et al. ⁴¹
<i>C. pasteurianum</i>	[FeFe]	MAD	0.18	1998	1FEH	Peters et al. ⁶²
<i>C. pasteurianum</i> inhibited	[FeFe]	MR	0.24	1999	1C4A-C	Lemon et al. ¹²³
<i>D. desulfuricans</i>	[FeFe]	MAD	0.16	1999	1HFE	Nicolet et al. ⁶¹
<i>D. desulfuricans</i> active	[FeFe]	MR	0.185	2001		Nicolet et al. ¹²¹
<i>M. jannaschii</i>	[Fe]	MR	0.175	2006	2B0J	Pilak et al. ⁵⁸
<i>M. kandleri</i>	[Fe]	MAD	0.24	2006		Pilak et al. ⁵⁸

and in the same year from *D. gigas* by Niviere et al.⁶⁹ It took almost a decade before a crystal structure was reported by Volbeda and co-workers for the *D. gigas* enzyme.^{63,70} At present structures from five [NiFe] hydrogenases from closely related sulfate-reducing bacteria are known (see also article by Fontecilla-Camps et al. in this issue). These are the enzymes from *D. gigas*,^{63,64,70,71} *D. vulgaris* Miyazaki F,^{66,72–74} *D. desulfuricans*,⁷⁵ *D. fructosovorans*^{60,76} and *Desulfomicrobium* (*Dm.*) *baculatum*⁴¹. Structures were obtained for different states of the enzymes and for some mutants of

D. fructosovorans.^{65,76–78} No crystal structures of other [NiFe] hydrogenases, for example, from photosynthetic organisms are known. The structural data obtained so far have been reviewed and critically evaluated.^{64,70,79–81} For an overview see Table 1.

In Figure 1a the structure of the [NiFe] hydrogenase of *D. gigas* is shown.⁷⁰ It consists of two subunits with molecular weights of about 28 and 60 kDa. For many membrane-bound enzymes a small membrane anchor is additionally present, which is cleaved during enzyme puri-

fication. The large subunit contains the active site, which is deeply buried in the protein. The geometry of this site is highly conserved throughout all [NiFe] hydrogenases (cf. article by Vignais and Billoud in this issue). The nickel and iron atoms are separated by a distance of about 2.5–2.9 Å⁶⁴ and are bridged by the sulfur atoms of two cysteines. The nickel atom is coordinated by two more cysteines bound in a terminal position. For some hydrogenases one of the latter cysteines is replaced by a selenocysteine and these enzymes form the subclass of [NiFeSe] hydrogenases.^{41,82–84} The iron atom carries three inorganic diatomic ligands that have been identified by infrared spectroscopy as two CN[−] and one CO.^{39,85–88} In the aerobically isolated enzyme (oxidized state: in general a mixture of the so-called “unready” or Ni-A and the “ready” or Ni-B states), additional electron density is detectable between nickel and iron which stems from a third bridging ligand “X”.^{66,70} This bridging ligand has been postulated to be, in catalytic hydrogenases, an oxygen⁷⁰ or a sulfur species.^{66,75} The former hypothesis has been supported by spectroscopic studies using ¹⁷O labeling,^{89,90} but the presence of sulfur cannot be ruled out, for example, in *D. vulgaris* Miyazaki F.^{91,92} In the active state of the enzyme (Ni-C/Ni-R) this electron density is absent.^{41,72} However, it is unclear whether the position X is empty or occupied by an atom or molecule with low electron density (e.g., hydrogen). Spectroscopic studies clearly showed that in the active Ni-C state a hydride (H[−]) is present in the bridge between the Ni and the Fe.^{93–95} In all states of standard hydrogenases the nickel atom has an open coordination site, which defines an axial direction, (marked by an arrow in Figure 1a, bottom) and it is therefore believed that the Ni represents the primary hydrogen binding site. This is supported by the fact that the inhibitor CO binds at this position⁷³ and also that the H₂ transfer channel ends near the Ni (see Scheme 1).^{60,79}

The small subunit contains three Fe–S clusters that are involved in the electron transport to/from the active [NiFe] center (Figure 1a). In the catalytically active hydrogenases, a proximal [4Fe–4S] cluster is located near the [NiFe] center, flanked by a [3Fe–4S] cluster. Near the protein surface a distal [4Fe–4S] cluster is present. In the [NiFeSe] hydrogenase of *D. baculatum* the [3Fe–4S] is replaced by a [4Fe–4S] cluster.⁴¹ The distance between the iron–sulfur clusters is ~12 Å, that is suited for biological electron transfer.⁹⁶ A magnesium atom is found in the crystal structure,⁶⁶ which is probably involved in proton transfer.^{64,66} A possible pathway for molecular hydrogen to travel between the protein surface and the active site has been found in molecular dynamics calculations using a probe radius of 0.1 nm.⁶⁰ Additional information came from crystallographic studies using high-pressure Xe gas.^{60,64,80} Strikingly, the channel seems to end at the vacant sixth coordination position of the nickel atom. It has been speculated that this channel used by hydrogen may also allow access of CO and O₂ which lead to inhibition of the enzyme. Recently, crystal structures at higher resolution for both the ready (Ni-B) and the unready (Ni-A) states were published.^{71,74} In the unready state the electron density for the bridging ligand was found to be elongated, and it was suggested that this ligand is possibly a hydroperoxide, OOH[−].⁷¹ Furthermore, additional electron density was observed in these structures^{71,74} near the cysteine sulfur atoms, indicating the formation of sulfoxides and/or sulfenic acids possibly resulting from trapped O atoms.^{97–100}

It was proposed that the type of bridging ligand may be the cause for the slow activation of the unready state and the fast activation of the ready state.⁷¹ Ogata et al.⁷⁴ compared their highly resolved Ni-A structure with that of the CO-inhibited enzyme⁷³ and could show that the extra density assigned to an additional oxygen is located in the same position as the CO ligand that blocks the sixth coordination position of the nickel atom (see also Figure 5 in Lubitz et al.¹⁰⁰). This would prevent binding of dihydrogen. More details on the structure of [NiFe] hydrogenase are found in the cited literature and in the article by Fontecilla-Camps et al. in this issue.

2.2. [FeFe] Hydrogenases

In early biochemical studies^{101–103} on [FeFe] hydrogenases it was found that the prosthetic groups are located in only one subunit and consist of several [4Fe–4S] clusters and an active site of (at that time) unknown structure, which was termed the “H-cluster” (from “hydrogen-activating cluster”). The gram positive bacterium *Clostridium (C.) pasteurianum* was the first organism that was found to contain no nickel but only iron atoms in the hydrogenase.¹⁰⁴ Initially, the iron and sulfur content of hydrogenases were widely underestimated because of limited purity of the protein, inaccuracies in the determined molecular weights, and a nearly 2-fold overestimation of the protein content of the preparations. Two [FeFe] hydrogenase preparations from *C. pasteurianum* have been described.^{102,103,105,106} Since they showed distinct difference in their catalytic behavior, these preparations were associated with two different types of [FeFe] hydrogenase. One type of [FeFe] hydrogenase from *C. pasteurianum*, called hydrogenase I, catalyzes the two-electron reduction of two protons to yield dihydrogen and was eventually found to contain 20 atoms of iron per protein molecule arranged into five distinct Fe–S clusters. This hydrogenase is very active in catalyzing both oxidation and evolution of H₂ and was thus named “bidirectional” hydrogenase.¹⁰² The second type of hydrogenase from *C. pasteurianum*, called hydrogenase II,^{105,106} is very active in H₂ oxidation but the rates of H₂ evolution are very low. Therefore, it was referred to as “uptake” hydrogenase. The analysis of the iron content (after various corrections) showed that this hydrogenase contains 14 iron atoms distributed over three Fe–S clusters.^{102,103,106} However, the physiological role of this hydrogenase is as yet unknown. It should be noted that after the initial description of this preparation, no follow-up studies have been published. Later the [FeFe] hydrogenases from *Megasphaera (M.) elsdenii*,^{107–110} *Desulfovibrio (D.) vulgaris* Hildenborough,^{111–118} and *Desulfovibrio (D.) desulfuricans*^{55,102,119,120} have been characterized. All these enzymes contain 14 Fe atoms per protein molecule arranged in three Fe–S clusters including the H-cluster.

So far, only two [FeFe] hydrogenases from different organisms have been crystallographically studied. The first one is the cytoplasmic, monomeric [FeFe] hydrogenase I from *C. pasteurianum*, the structure of which has been resolved with a resolution of 1.8 Å.⁶² The second known structure is that of the periplasmic, heterodimeric [FeFe] hydrogenase from *D. desulfuricans* (ATCC 7757)^{61,121} which was resolved to 1.6 Å, see Table 1. The structural features of [FeFe] hydrogenases have also been reviewed.^{67,122} Both structures contain, apart from the H-cluster, a chain of iron–sulfur clusters assumed to provide an electron transport path. In hydrogenase I from *C. pasteurianum* this chain

consists of three ferredoxin-like [4Fe–4S] clusters and one [2Fe–2S] cluster, while in the *D. desulfuricans* enzyme this chain only holds two [4Fe–4S] clusters. Owing to their Mössbauer properties and the sequence similarity of their binding domains to that of ferredoxin Fe–S clusters, these clusters are termed “F-clusters”. In addition to the two crystal structures mentioned above, there are also structures available of the [FeFe] hydrogenase I from *C. pasteurianum* in the CO-inhibited form^{123,124} and the *D. desulfuricans* enzyme prepared under 6 bar H₂ (“reduced” form).¹²¹ In Figure 1b the structure of the [FeFe] hydrogenase of *D. desulfuricans* is shown together with the structure of the active site (“H-cluster”).^{61,121}

The H-cluster, a six-iron cluster, consists of a cubane, [4Fe–4S]_H, connected via the sulfur ligand of cysteine (Cys 382) to the proximal iron (Fe_p) of the binuclear iron cluster [2Fe]_H, as shown in Figure 1b (bottom). The X-ray structure of [FeFe] hydrogenase I of *C. pasteurianum* reveals an almost identical structure of the active center.^{62,125} In both structures the [2Fe]_H cluster is coordinated by a total of 5 diatomic ligands modeled as CO/CN[−] and by a dithiolate ligand not associated with the protein. In the structure of hydrogenase I of *C. pasteurianum* also a H₂O or (OH[−]) molecule was modeled weakly coordinating the distal iron (Fe_d). It was absent in the *D. desulfuricans* structure. Here Fe_d has an open coordination site where presumably the substrate (H₂) or inhibitors bind. The dithiolate ligand is not defined very well in either structure. For *D. desulfuricans* initially the ligand was identified as propane dithiol (PDT) but later mechanistic and stereochemical considerations led to a reinterpretation of this ligand which is now assumed to be a di-thiomethylamine (DTN)^{121,122} (see Figure 1b and Scheme 1). Although largely speculative, this assignment is more likely than PDT since the amine could act as proton acceptor in the catalytic cycle.

As for [NiFe] hydrogenase, it was found that also [FeFe] hydrogenases show FTIR bands in the 1850–2100 cm^{−1} region (typical for CN[−] and CO), which strongly shift upon changes in the redox state of the enzyme.^{40,126–128} In addition, early studies of the active site of [FeFe] hydrogenase I from *C. pasteurianum* and the hydrogenase of *D. vulgaris* Hildenborough using ESEEM and HYSCORE (see appendix) reveal ¹⁴N nuclear couplings with quadrupole splittings fitting those of cyanide^{129–131} On the basis of these observations the CN[−]/CO diatomic moieties in the crystal structures were assigned to two terminal CN[−], two terminal CO, and one bridging CO. The X-ray structure of the reduced *D. desulfuricans* enzyme shows that this bridging CO becomes a terminal ligand to Fe_d upon reduction¹²¹ For the hydrogenase I of *C. pasteurianum* the structure of crystals grown under CO shows that in the inhibited state a single “external” CO is bound terminally to the binuclear cluster at Fe_d, thus replacing the water molecule.

Since the [FeFe] hydrogenases from *D. vulgaris* Hildenborough and *D. desulfuricans* have identical amino acid sequences,^{55,118,132} these enzymes are considered to be identical. The IR spectra of the enzymes from *D. vulgaris*, Hildenborough,^{40,133} *M. elsdenii*,¹³³ *D. desulfuricans*,^{121,126} and of hydrogenase I from *C. pasteurianum*^{128,134} are very similar. Other spectroscopic methods such as electron paramagnetic resonance (EPR), electron–nuclear double resonance (ENDOR), and Mössbauer spectroscopy also revealed similar properties of the H-clusters in these hydrogenases.^{117,131,135–139} Therefore it is expected that all these enzymes have virtually identical active sites (see Figure 1b, bottom; Scheme 1).

3. Redox States of Hydrogenases

3.1. [NiFe] Hydrogenase

In the process of enzyme “activation” and during the catalytic cycle, the [NiFe] hydrogenase passes through a number of intermediate states. They have first been observed and characterized by EPR spectroscopy (for a review see ref 140), which showed that the enzyme cycles between EPR-silent and EPR-detectable (paramagnetic) nickel-centered states. They were named Ni-A, Ni-B, Ni-C (paramagnetic, EPR active), Ni-L (light-induced, EPR active), Ni-SI (EPR silent) and Ni-R (reduced, EPR-silent). For historical reasons these “names” have been retained until today although other nomenclatures have also been used by various authors.^{100,140,141} A full characterization has become possible by FTIR spectroscopy by which the IR vibrations of the CN[−] and CO ligands at the iron are monitored. Here, both the paramagnetic and EPR-silent states are detected. The band shifts are usually sufficiently large (e.g., that of $\tilde{\nu}_{\text{CO}}$) for a clear distinction between redox states. Thus, the $\tilde{\nu}_{\text{CO}}$ wave-number has often been used for a characterization of the various states.⁸⁵

The [NiFe] center is rich in redox states. The oxidized states (Ni-A, Ni-B) are catalytically inactive but can be activated by reduction. They differ in their activation kinetics, Ni-A activation is much slower than that of Ni-B.¹⁴² For this reason the Ni-A state is also called the “unready” state and the Ni-B state the “ready” state. Both states are paramagnetic and are characterized by different *g* values. Upon one-electron reduction of Ni-A and Ni-B, the EPR-silent states Ni-SU (silent unready) and Ni-SIR (silent ready) are formed. For *A. vinosum* hydrogenase it has been shown that the Ni-A → Ni-SU reduction is reversible, but the Ni-B → Ni-SIR reduction strongly depends on pH and temperature. At pH 6.0 and 2 °C the reduction of the ready enzyme was completely irreversible; at pH 8 and 30 °C both reductions were reversible.¹⁴³ Under reducing conditions and at temperatures greater than or equal to 30 °C, the Ni-SIR is converted into another EPR-silent state Ni-SIa (silent active), which can be quickly reduced to give another EPR active state Ni-C.¹⁴⁴ The Ni-C state exhibits a characteristic rhombic *g* tensor, and this state is found in all enzymes studied so far. The Ni-C state is light-sensitive. Upon illumination with white light, the characteristic EPR signal disappears and a new signal appears,^{145,146} which is called Ni-L. At least two subforms have been identified with different *g* values, Ni-L1 and Ni-L2, depending on the temperature and the duration of light exposure.¹⁴⁷ Upon further reduction in the presence of H₂, the most reduced state Ni-R is formed. Three subforms of Ni-R have been identified for *A. vinosum* hydrogenase;⁸⁵ however, the presence of all these substates has not yet been experimentally confirmed in hydrogenases from other sources. The [NiFe] hydrogenase can be inhibited by the addition of CO. It has been shown by X-ray crystallography of single crystals treated with CO,⁷³ that the CO binds at the sixth free-coordination site of the nickel atom (see Figure 1a). A paramagnetic Ni-CO state has been described and characterized.^{89,145,148,149} This Ni-CO (active) state is photosensitive and upon illumination at low temperatures, CO photodissociates, resulting in the same Ni-L state as that formed from Ni-C.

The different EPR active and EPR-silent redox states of the [NiFe] hydrogenase are depicted in a scheme shown in Figure 2. Furthermore the characteristic vibrational bands

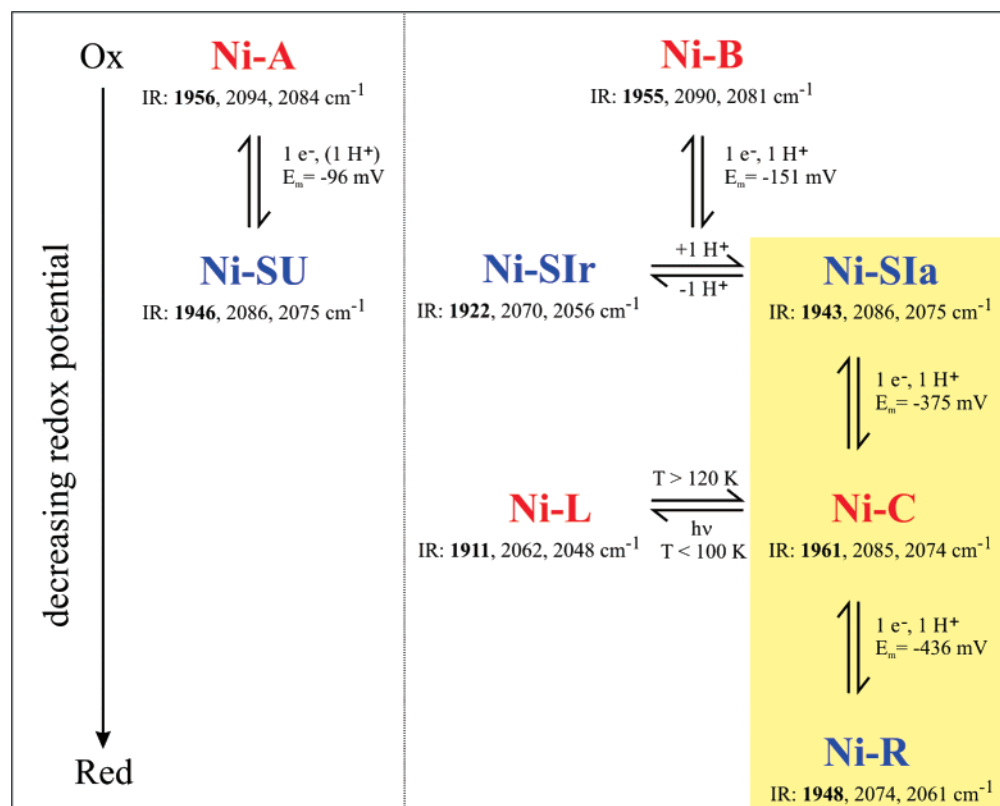


Figure 2. Schematic diagram depicting the various redox states of catalytic [NiFe] hydrogenases: here all numbers are given for *D. vulgaris* Miyazaki F (ref 88). For each state the vibrational frequencies from FTIR (cm^{-1}) for the CO and two CN^- ligands at the Fe (ν_{CO} in bold) are given. All (vertical) transitions are one-electron reduction steps that are accompanied each by a single H^+ transfer. The respective midpoint potentials (E_m) are given (pH = 8, except for Ni-A, pH = 6): EPR-active (paramagnetic) states are given in red and EPR-silent states in blue. The states involved in the catalytic cycle of the enzyme are placed in a yellow box. The silent states Ni-SIr and Ni-SIa are in acid/base equilibrium. Illumination of Ni-C at low temperatures (≤ 100 K) leads to the formation of light-induced states, Ni-L. Treatment with CO (inhibitor) leads to Ni-CO states either from the Ni-SIa or the Ni-C state (not shown, see text). Note that different nomenclatures exist in the literature to describe the same state: Ni-A is also denoted Ni_u^* (u = unready), Ni-B = Ni_r^* (r = ready), Ni-SU = $\text{Ni}_u\text{-S}$, Ni-SI = $\text{Ni}_r\text{-S}$, Ni-SIa = $\text{Ni}_a\text{-S}$, Ni-C = $\text{Ni}_a\text{-C}^*$ and Ni-R = $\text{Ni}_a\text{-SR}$. The asterisk * denotes paramagnetic states.¹⁴¹ Some authors use in addition the vibrational frequency of the CO-band (cm^{-1}) as index for an unequivocal identification of the state. Since these values are not constant, different indices must be used for different species.

of the CO and the 2 CN^- ligands at the iron are given. The midpoint potentials E_m for the various steps obtained by spectroelectrochemical titrations (for details see article by De Lacey et al. in this issue) are given for the enzyme from *D. vulgaris* Miyazaki F.⁸⁸ For the latter enzyme it should be noticed that the changes to lower frequency observed for the Ni-A to Ni-SU transition are atypical, for other enzymes a shift to higher frequency is observed. Similar titrations have been performed by de Lacey et al. for *D. gigas*⁸⁶ and *D. fructosovorans*⁷⁸ and by Albracht and co-workers for *A. vinosum*.⁸⁵ (For details see refs 65, 100, and 141.) Each redox transition is accompanied by a proton-transfer step. The two EPR-silent states Ni-SIr and Ni-SIa are in an acid–base equilibrium.^{86,88}

Here only the [NiFe] active site is shown and the respective redox transitions are given. To complete the picture, also the iron–sulfur centers and their redox states must be included (see e.g, ref 140).

3.2. [FeFe] Hydrogenase

The various redox states and transitions of the active site of the [FeFe] hydrogenase are shown schematically in Figure 3. These have been elucidated by spectroelectrochemistry in combination with EPR/Mössbauer and FTIR techniques, by which the various characteristic states of the H-cluster

are monitored.^{117,127,150,151} In the as-isolated enzyme (in air) the H-cluster is “over-oxidized” ($\text{H}_{\text{ox}}^{\text{air}}$ or H_{inact}). This state is inactive and nonparamagnetic; the cubane subcluster is in the $[\text{4Fe4S}]_{\text{H}}^{2+}$ state, and the two irons in the binuclear subcluster $[\text{2Fe}]_{\text{H}}$ have the same valence. It shows five characteristic IR-bands; two are assigned to CN^- and three to CO bound to the iron atoms of the $[\text{2Fe}]_{\text{H}}$ subcluster. One CO is in a bridging position (cf. Scheme 1), and the open coordination site at Fe_d is occupied by an oxygenic species (OH^- or H_2O) according to X-ray crystallography.^{62,121} The F-clusters in the protein (not shown) are also oxidized (EPR silent).

In the enzyme from *D. sulfuricans* (pH 7) one-electron reduction ($E_m = -75$ mV) generates an EPR active (transient) state (H_{trans}) in which the cubane subcluster $[\text{4Fe-4S}]_{\text{H}}$ is reduced, whereas $[\text{2Fe}]_{\text{H}}$ remains oxidized, but is also affected.¹²⁷ This leads to a change of the position of the IR-bands. In H_{trans} the bridging CO is still present and the $\text{OH}^-/\text{H}_2\text{O}$ ligand is assumed to be retained (Figure 3). Upon further lowering the redox potential another rhombic EPR species (H_{ox}) is formed ($E_m = -261$ mV) in which the reduction equivalent is shifted from the cubane to the binuclear subcluster. This is probably caused by a conformational change in which the $\text{OH}^-/\text{H}_2\text{O}$ ligand is removed leaving an open coordination site at the distal iron Fe_d . The

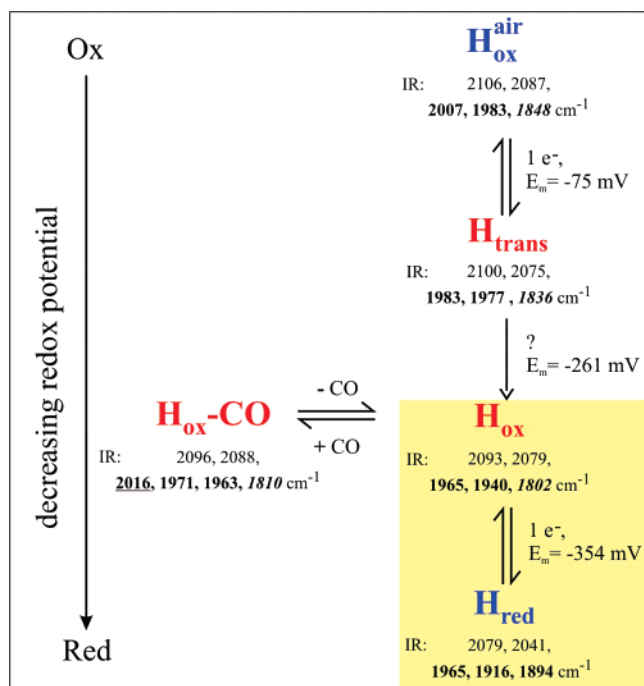


Figure 3. Schematic diagram showing the various redox states of [FeFe] hydrogenase. The numbers are given for the enzyme from *D. desulfuricans* (see ref 135). For each state the vibrational frequencies from FTIR (in cm⁻¹) are given for the two CN⁻ ligands and the three CO (bold) ligands attached to the [2Fe]_H subcluster (cf. Figure 1). The numbers for the bridging CO are given in bold italic. The additional weakly bound CO ligand in the H_{ox}-CO state is in bold underlined. The respective midpoint potentials (E_m) are given for all redox transitions. (The transition from H_{trans} to H_{ox} has been described as a 2e⁻-transition, see ref 127). The light-induced states are not shown (see text). Paramagnetic states are given in red and EPR-silent states in blue.

H_{ox} state is observed in *all* [FeFe] hydrogenases and is regarded as the physiological oxidized intermediate in the catalytic cycle. The [2Fe]_H subcluster is in a mixed-valence state, while the cubane subcluster is in the [4Fe-4S]²⁺ state.

After reduction of the hydrogenase with H₂ the EPR signal of the H-cluster disappears indicating another one-electron reduction step (E_m = -350 mV).¹²⁷ Mössbauer data indicate that the cubane subcluster is still oxidized, the H_{red} cluster must therefore have a further reduced [2Fe]_H cluster. FTIR studies indicate that the bridging CO is lost.^{121,127} According to X-ray crystallographic studies of the reduced enzyme (crystals under 6 bar of H₂) this CO is bound end-on to Fe_d.¹²¹ In this state the F-clusters are also reduced and give rise to characteristic EPR signals. Incubation of H_{red} with argon transforms this state back to H_{ox}. Lower redox potentials (below -500 mV) lead to a destruction of the [2Fe]_H subcluster.

Addition of the inhibitor CO to the H_{ox} state generates the H_{ox}-CO in which the open coordination site at Fe_d is blocked by the incoming CO ligand.^{127,135,152} This is no redox transition. The characteristic IR frequencies of CO (range 1800–2020 cm⁻¹) and CN⁻ (range 2050–2110 m⁻¹) for each state are also given in Figure 3.¹²⁷

4. A Survey of Structural Methods Used in Hydrogenase Research

X-ray Crystallography. For understanding the activation and deactivation, the inhibition and finally the catalytic cycle of the enzyme the structures of all intermediates must be

deduced. This has in part been accomplished by X-ray crystallography of single crystals in which some of the states could be trapped. For nickel iron hydrogenase it was shown that the third bridging ligand X (see Figure 1a) plays a crucial role in the catalytic cycle: in the oxidized (as isolated) enzyme X is present,^{63,66,70} whereas in the reduced enzyme (Ni-C/Ni-R) the electron density is absent⁷² which does not exclude the presence of a light atom (e.g., derived from hydrogen). Furthermore, from the crystal structure of the Ni-CO state,⁷³ evidence for structural features leading to inhibition of the enzyme could be derived. Recent crystallographic work also provided important information for an understanding of the oxygen sensitivity of the catalytic [NiFe] hydrogenases.^{71,74} However, interpretation of X-ray crystallographic data suffers from the difficulty to generate unique intermediate states in the crystals, state transitions are hard to follow, and the resolution is often insufficient to obtain fine structural details that are required for an in-depth understanding. In particular, the resolution of protein crystallography is not high enough to observe protons, that is, the substrate, educts, and products of the hydrogenase enzyme cannot be detected in the crystal structures.

FTIR. Clearly, additional spectroscopic methods are necessary to obtain a complete picture of the intermediate states of the hydrogenase. One important method to characterize and follow the various states is FTIR spectroscopy. This allows the detection of all paramagnetic and diamagnetic states of the enzyme via the CO/CN⁻ vibrations (see for example for [NiFe] hydrogenase refs 39, 70, 85–88, and 153–157, for [FeFe] hydrogenase, refs 40, 126, 127, 133, and 134, and for [Fe] hydrogenase, ref 42). The CO and CN⁻ vibrations occur in a characteristic region of the spectrum that is free from other protein vibrations. The vibrations are sensitive to the charge density at the metal to which these ligands are bound, allowing conclusions about changes of redox states. All electron and proton-transfer reactions can thus be followed as a function of temperature, pH, and time, and the redox potentials can be determined by electrochemical titrations monitoring the vibrational bands (see, e.g., refs 85, 86, 88, and 127). The method has also been used at cryogenic temperatures, for example, for detecting the Ni-L states,^{154,157,158} and in conjunction with stopped-flow techniques to follow species involved in enzyme activation and in the catalytic cycle.^{159,160} Although FTIR is an excellent spectroscopic probe for monitoring changes in the active center of hydrogenase it does not provide complete information about the electronic structure of the active center. For example, in case of the [NiFe] hydrogenase FTIR monitors charge density changes at iron, whereas hydrogen conversion is believed to take place at the nickel atom.

XAS. Another important method for studying metalloenzymes is X-ray absorption (XAS) spectroscopy.¹⁶¹ This technique yields information about the oxidation state(s) of the metal(s) (by XANES) and the number and type of ligands and their distances from the metal center (by EXAFS) that is complementary to X-ray crystallography and other spectroscopies. It has been used mostly for [NiFe] hydrogenase.^{100,156,162–168} Although the interpretation of the Ni EXAFS data has been debated, the information obtained about the oxidation states and their changes are very important. The data are consistent with the formal oxidation state of the Ni metal oscillating between Ni(III) and Ni(II); the occurrence of a Ni(I) is not supported by XAS data (e.g., for Ni-L). Furthermore, Ni L-edge XAS data indicated that the EPR-

silent states (Ni-R, Ni-SI) are probably not diamagnetic Ni(II) low-spin states but are better described by Ni(II) high-spin (hs) states ($S = 1$).¹⁶⁶ XAS spectroscopy on the [FeFe] hydrogenase does not lead to clear results owing to the high iron content of these enzymes.

Mössbauer Spectroscopy. In particular for iron-containing proteins the application of Mössbauer spectroscopy can deliver valuable information.^{169,170} This method has therefore been applied to [NiFe] hydrogenases,^{171–175} [FeFe] hydrogenases,^{115,136,139,151,176–179} and also to the [Fe] hydrogenase (Hmd),^{45,57} all on ⁵⁷Fe-enriched preparations. Mössbauer spectra yield, via the isomer shift and the quadrupole coupling, a detailed picture of the electronic structure of the metal nucleus (oxidation state, orbital occupation), its surrounding (type and symmetry of crystal field), and the changes that occur during the state transitions. In the case of hydrogenases the problem is that *all* iron nuclei in the protein (from the active site and the Fe–S clusters) contribute to the spectral response and it is therefore often difficult to interpret the spectra in a unique way. Nevertheless, valuable information has been obtained for all three classes of hydrogenase.

EPR Spectroscopy. The method of choice to monitor and characterize the paramagnetic redox states of the [NiFe] and [FeFe] hydrogenase is EPR spectroscopy.^{102,135,180,181} A careful analysis of the spectroscopic parameters yields geometric information on one hand but also information about the *electronic structure* of the active center, the electron-transfer chain, and other parts of the protein containing paramagnetic sites. For transition-metal complexes in particular, a variety of information can be obtained, for example concerning the (formal) oxidation state and spin state of the metal, the d-orbital occupation, the symmetry of the crystal field, the type of ligands, the spin distribution, or the exchange coupling with other metal centers.^{182–185} The spectroscopic parameters are the *g* and electron–nuclear hyperfine tensors, nuclear quadrupole tensors, spectral line-widths, relaxation times, and the zero-field splittings (for systems with $S > 1/2$). Standard CW EPR techniques have been instrumental in the early detection and characterization of the various paramagnetic states of [NiFe] hydrogenase^{140,186} and [FeFe] hydrogenases.¹⁰² Of particular importance is the ability to perform EPR experiments not only on liquid and frozen solutions (powders) but also on single crystals^{94,187,188} by which the full tensor information (magnitudes and orientations) can be obtained. The spectral resolution for overlapping sites and species can be dramatically improved by extending EPR to higher magnetic fields as in NMR spectroscopy.^{189–191} In hydrogenase research, in particular the use of Q-band (35 GHz) instead of the conventional X-band (9 GHz) is sufficient for most cases to obtain the required resolution and sensitivity (e.g., for small single crystals).

For the measurement of hfcs and the elucidation of the spin density at nuclei with no magnetic moment isotope labeling is necessary, for example, with ⁶¹Ni and/or ⁵⁷Fe, but also with ¹³C, ¹⁷O, ³³S, and other isotopes. The electron nuclear hyperfine interaction of the ligand nuclei is often too small to be resolved in standard EPR experiments, and more sophisticated pulse techniques must be used to obtain this information. A detailed overview of advanced (pulse-) EPR techniques is given in Appendix I. The standard method to achieve a better nuclear resolution is the electron–nuclear double resonance (ENDOR)¹⁹² experiment with different variants (Mims, Davies, and Schweiger ENDOR; TRIPLE

resonance).¹⁹³ These methods provide magnitudes and signs of the electron–nuclear hyperfine tensors from which distances, geometries, spin densities, and also information about dynamics can be obtained. Furthermore, for nuclei with nuclear spins $I > 1/2$ the nuclear quadrupole couplings become available and thereby valuable information about electrical field gradients at the nuclei. For the detection of nuclei with small magnetic moments and small hf couplings, which are sometimes difficult to detect in conventional X-band ENDOR spectroscopy, special pulse EPR techniques based on ESEEM (electron spin echo envelope modulation)^{193,194} are available (e.g., the 2-dimensional correlation technique HYSORE¹⁹⁵). An alternative to ENDOR is provided by ELDOR-detected NMR¹⁹⁶ that has recently been used to detect the ⁶¹Ni hfcs in [NiFe] hydrogenase. For distance measurements between electron spins various methods are available,¹⁹⁷ the most popular one is pulse electron–electron double resonance (PELDOR)^{198–200} also called double electron–electron resonance (DEER).^{193,201}

The application of modern EPR techniques, together with isotope labeling and crystallization of samples, has provided a wealth of information about the paramagnetic states of [NiFe] and [FeFe] hydrogenase that has been indispensable in the elucidation of the details of the activation/deactivation, the inhibition, and the catalytic cycle of these enzymes. The detailed EPR work performed by various groups and the information obtained from this work is the major topic of this review. We will focus on the [NiFe] and [FeFe] hydrogenases since no EPR experiments have so far been reported for the [Fe] hydrogenase. The older EPR work has authoritatively been covered in various reviews and book articles and the reader is referred to this work for further details.^{52,102,140} Here we will describe the more recent work published during the past decade, including the important EPR experiments on single crystals and the recent work using advanced EPR methods. Furthermore the indispensable support by modern quantum chemical calculations of the magnetic resonance parameters^{202–204} will be highlighted.

5. Magnetic Resonance Studies of [NiFe] Hydrogenases

5.1. Overview of EPR Spectra in the Various Redox States of the Enzyme

The active center in [NiFe] hydrogenases is rich in redox states. In the oxidized enzyme a mixture of two redox states called Ni-A and Ni-B is found. These forms are catalytically inactive and are activated by flushing the enzyme with molecular hydrogen. The Ni-A and Ni-B states have different activation kinetics, Ni-A takes much longer to be activated under hydrogen than Ni-B.¹⁴² For this reason the Ni-A state is also called the “unready” state and the Ni-B state the “ready” state. Characteristic EPR spectra for *A. vinosum* hydrogenase are shown in Figure 4, the *g* values are summarized in Table 2. Upon one-electron reduction of Ni-A and Ni-B, the Ni-SU and Ni-SIr states are formed. These states have an even number of electrons, they are “EPR silent”. Whether or not they are paramagnetic is still a topic of debate (see section 5.7). The Ni-SIr converts into another EPR-silent state Ni-SIa.⁸⁵ The distinction between these two states (“silent ready” and “silent active”) has been attributed to protonation and dissociation of the bridging hydroxyl group. For the hydrogenase of *A. vinosum* at reduced temperature an intermediate state could be distinguished in which the formed water is still present at the active site

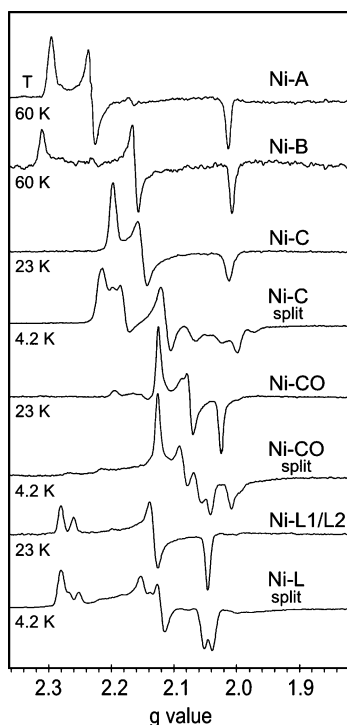


Figure 4. Schematic overview of EPR spectra of the EPR-active redox intermediates in *A. vinosum* hydrogenase; for *g* tensor values see Table 2. Spectra are taken from chapter 7 in ref 7. Reprinted with permission from ref 7. Copyright 2001 Thomson Publishing Services.

Table 2. Overview of *g* Values of the Redox States of the [NiFe] Center Observed in [NiFe] Hydrogenases of *A. vinosum* and *A. ferrooxidans*^a

redox state	<i>g_x</i>	<i>g_y</i>	<i>g_z</i>	species
Ni-A	2.32	2.24	2.01	<i>A. vinosum</i>
Ni-B	2.33	2.16	2.01	<i>A. vinosum</i>
Ni-C	2.21	2.15	2.01	<i>A. vinosum</i>
Ni-L1	2.26	2.12	2.05	<i>A. vinosum</i>
Ni-L2	2.28	2.12	2.05	<i>A. vinosum</i>
Ni-CO	2.12	2.07	2.02	<i>A. vinosum</i>
Ni-B	2.33	2.19	2.00	<i>A. ferrooxidans</i> ^b
Ni _B -L	2.48	2.23	2.17	<i>A. ferrooxidans</i> ^b
Ni-C	2.22	2.15	2.01	<i>A. ferrooxidans</i> ^b
Ni _C -L	2.28	2.12	2.04	<i>A. ferrooxidans</i> ^b

^a Data taken from ref 7 and ref 157. ^b The four states (Ni-B, Ni_B-L, Ni-C, and Ni_C-L) have also been observed in whole cells of *A. ferrooxidans* and gave the same *g* values as in the isolated enzyme within experimental error (0.01).

blocking the H₂-access.⁸⁵ Ni-SIa is highly active and can be quickly reduced to give an EPR active state Ni-C. The *g* values of the Ni-C state in all [NiFe] enzymes studied so far typically amount to 2.01, 2.15, and 2.21 with variation of about 0.01. At low temperature, the Ni-C signal splits owing to spin–spin interaction with the proximal [4Fe–4S] cluster, as will be discussed in section 5.4. Moreover, the Ni-C state can be converted by light into another redox state,^{145,146} which is called Ni-L. Two subforms exist with different *g* values; Ni-L1 and Ni-L2 (see Figure 4 and Table 2). Their relative ratio depends on the time of exposure to light and the temperature.¹⁴⁷ Upon further reduction in the presence of H₂ the most reduced state Ni-R is formed, which is again EPR silent. Three subforms of Ni-R have been identified for *A. vinosum* hydrogenase.⁸⁵ It is unclear whether these substates are also present in other hydrogenases. Upon flushing the Ni-C state with CO, the enzyme is inhibited, and another EPR spectrum appears (see Figure 4).¹⁴⁸ The *g*

values are included in Table 2. Basically the same states with very similar or identical *g* values have been found for a variety of catalytic [NiFe] hydrogenases from other bacteria, including *D. desulfuricans* (Norway strain),²⁰⁵ *D. fructosovorans*,²⁰⁶ *M. voltae*,²⁰⁷ *D. vulgaris* Hildenborough,²⁰⁸ *D. vulgaris* Miyazaki F,¹⁸⁷ and *A. vinosum*.⁸⁵

For the recently published work on the cyanobacterial-like uptake [NiFe] hydrogenase of *Acidithiobacillus* (*A. ferrooxidans*) some peculiarities were observed. This hydrogenase is oxygen insensitive and no Ni-A state could be detected, only the Ni-B state is found. Interestingly, in this enzyme the Ni-B state is light sensitive and converts to a new redox state “Ni_B-L” with *g* values of 2.48, 2.23, and 2.17.¹⁵⁷ The EPR signals have been found for isolated enzyme as well as in whole cells, indicating that the redox states are not artifacts of the purification procedure and concomitant exposure to oxygen. The enzyme is further characterized by Ni-C and Ni-L states with *g* values similar to those of, e.g., *A. vinosum* hydrogenase, see Table 2. FTIR studies have shown that the isolated form of the enzyme is heterogeneous. Two species are identified, of which only one (small fraction) gives rise to EPR signals.¹⁵⁷ Further studies are needed to fully understand the electronic structure of the active site.

In the following sections, an overview is given of the investigations of these redox states by EPR and related spectroscopies, with emphasis on the elucidation of the electronic structure, composition of the active center, in particular the bridging ligand, and the catalytic mechanism. First, the discovery of the presence of nickel in these enzymes is discussed. The other sections are devoted to reviewing the spectroscopic properties of each individual redox state and their interpretation.

5.2. The Presence of Ni and Fe in the Active Site

The first EPR spectra of the Fe–S clusters in hydrogenase was reported in 1971,^{209–211} and the first EPR of the active center was recorded in 1982²¹² after Thauer et al. discovered nickel in purified hydrogenase 1 year earlier.²¹³ The latter measurement was performed on the enzyme of *D. gigas* in a state, which was isolated under aerobic conditions. The oxidized “unready” Ni-A signal dominated the spectrum and the Ni-B form was observed as a minority species. Early reviews are given in refs 52, 53, 140, and 214. Since the crystal structure of the enzyme was not known at that time, the exact composition of the active site was a matter of debate. A major breakthrough occurred when Thauer, Albracht, and, independently, Moura and co-workers decided to examine the presence of nickel by ⁶¹Ni (*I* = 3/2) isotope labeling.^{215–218} The studies were carried out on the hydrogenases from *Methanobacterium* (*M.*) *thermoautotrophicum* and *D. gigas* and revealed a rich hyperfine structure. The ⁶¹Ni hyperfine coupling constants *A*(*x,y,z*) = 21.0, 42.0, 75.9 MHz, elucidated for the Ni-A state of *M. thermoautotrophicum*, confirmed the presence of nickel as the central metal of this enzyme. Only after the publication of the first crystal structure in 1995,⁶³ the structure of the active site—including the presence of iron as a second metal of the bimetallic center—was revealed. Shortly afterward, EPR and ENDOR measurements of ⁵⁷Fe enriched hydrogenase confirmed the presence of iron close to nickel, but the observed coupling to the unpaired electron was found to be so small that the iron was assigned to be diamagnetic in all redox states of the metal center.²¹⁹ EPR signals typical for a nickel center, that is, that of [NiFe] hydrogenases, have also been observed

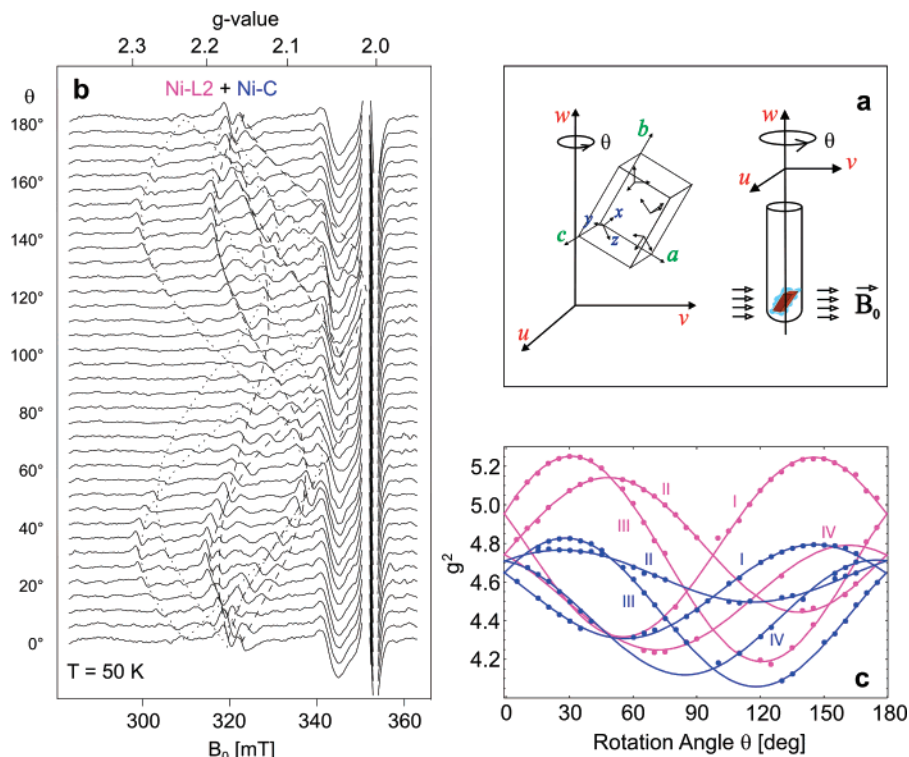


Figure 5. (a) Overview of the single-crystal EPR experiment, performed on the Ni-C and Ni-L states of *D. vulgaris* Miyazaki F hydrogenase.⁹⁴ EPR spectra are recorded as a function of the orientation of the crystal in the magnetic field; a set of spectra is shown in panel b. Analysis of the EPR spectra (Ni-C and Ni-L2 are simultaneously detected) gives information on the magnitude and axes directions of the complete g tensor with respect to the crystallographic axes (c). For further details see text and ref 94.

later in other catalytic [NiFe] hydrogenases^{85,187,205–208} (see above). In *R. eutropha* the membrane-bound, the regulatory, and the NAD-reducing hydrogenase have been investigated.^{50,220–222} In contrast to the other enzymes, it is proposed from EXAFS spectroscopy for the latter two enzymes that a more significant structural change happens upon reduction, which is still under debate.^{156,164,168,223} Concomitantly, FTIR measurements indicate the presence of more than three inorganic diatomic ligands in the active site for the NAD-reducing hydrogenase,^{156,158,224,225} which can even cleave hydrogen in the presence of oxygen.²²⁶ In recent chemical analyses, the presence of four cyanide groups has been corroborated.²²⁵ One of the extra cyanides is bound to iron and one to nickel. In the oxidized state the nickel is thus 6-coordinate.^{156,222} Activation removes the bridging ligand and leads to catalytically active 5-coordinate Ni^{2+} .¹⁵⁸

After the initial use of ^{61}Ni to prove the presence of nickel in the active site, this isotope has not been used for a long time to extract more detailed information in terms of electronic structure. Only recently, the investigation of the ^{61}Ni hyperfine coupling constants have been determined for the EPR-detectable states in *D. vulgaris* Miyazaki hydrogenase.²²⁷ It was found that for Ni-A, Ni-B, and Ni-C the largest ^{61}Ni hyperfine coupling is similar and is oriented along the g_z axis, whereas the other components show some differences. All three sets are fully compatible with a formal Ni^{III} oxidation state, with the unpaired electron in the $3d_{z^2}$ orbital as also shown by DFT calculations.²²⁸ Only the Ni-L2 state shows markedly different signals and the largest splitting is observed along g_x . This difference is, however, mainly attributed to a change of the isotropic hyperfine coupling, which may be the result of a small admixture of the $3d_{x^2-y^2}$ orbital into the wavefunction of the unpaired electron.¹⁸⁰

5.3. The Oxidized (As-Isolated) States

Under aerobic, oxidizing conditions the [NiFe] hydrogenases are inactive and are “parked” in a resting state. For the catalytically active hydrogenases a mixture of two redox states exists, they are called Ni-A and Ni-B. Both states have also been observed in intact cells,^{157,229} albeit with slightly different EPR spectra (g values). The Ni-A and Ni-B states have the same oxidation level, but they are characterized by different g tensors in the EPR spectrum. The g values are typically 2.32, 2.24, and 2.01 for Ni-A and 2.33, 2.16, and 2.01 for Ni-B and show remarkably little spread in [NiFe] hydrogenases of different origin. This shows that the active site must be structurally and electronically very similar in these “catalytic” hydrogenases. For the noncatalytic, regulatory [NiFe] hydrogenase of *R. eutropha* no EPR signal is observed in the oxidized state, indicating that this protein cannot reach the typical Ni-A and Ni-B states and is EPR-silent under oxidizing conditions.^{49,50,230,231}

5.3.1. g Tensor Analysis and the Ligand Field

By using single-crystal EPR spectroscopy, the complete g tensor, including directions of the principal axes can be determined with respect to the crystallographic axes, and thus to the geometry of the active site. An overview is given in Figure 5. If the orientation of the crystal with respect to the direction of the magnetic field is changed, the EPR spectrum changes as well. By analyzing the orientation dependence of the EPR signals, the principal directions of the g tensor can in principle be elucidated with respect to the directions of the crystallographic axes. By combining this information with the crystal structure, the orientation of the g tensor axes with respect to the geometry of the active site is found. The g tensor directions, which can only be retrieved by perform-

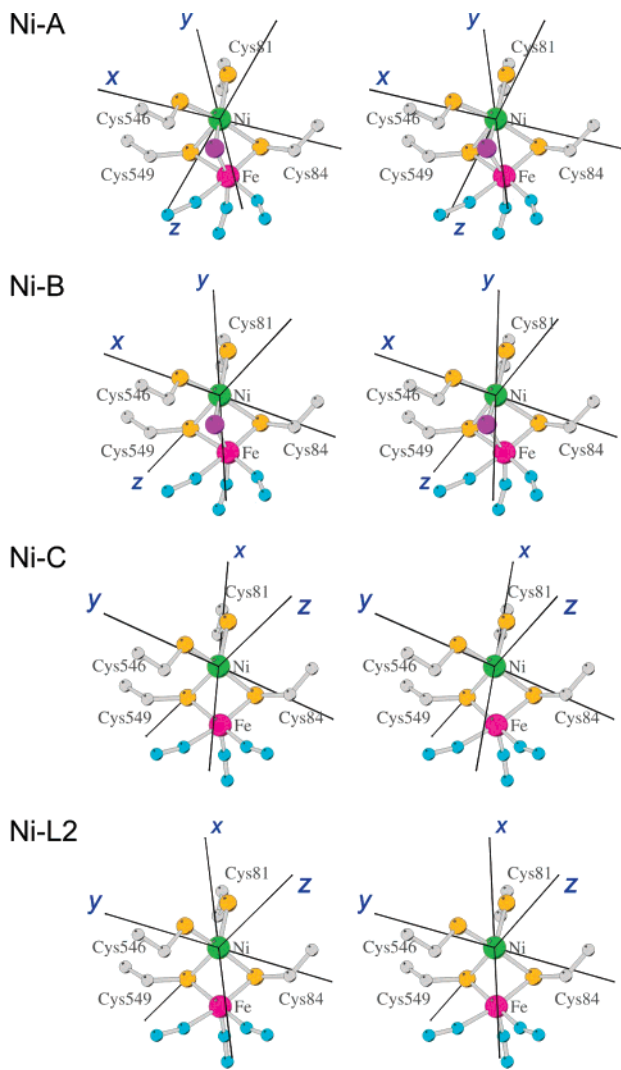


Figure 6. Stereoview of the directions of the principal axes of the g tensor with respect to the geometry of the active site, for the cases of Ni-A, Ni-B, Ni-C, and Ni-L2 in *D. vulgaris* Miyazaki F [NiFe] hydrogenase. Data taken from ref 94.

ing experiments on single crystals, give important information on the part of the wavefunction of the unpaired electron on nickel and the ligand field, of which an overview has been given in a recent contribution.¹⁸⁰ For single crystals of *D. vulgaris* Miyazaki F hydrogenase, it was found that the g_z axis for both the Ni-A and Ni-B states is parallel to the direction from nickel to the axial sulfur, see Figure 6,^{187,188} thus confirming a five-coordinate square pyramidal ligand field environment, compatible with earlier published X-ray structures.^{63,66} In this situation, the nickel atom is formally in the trivalent Ni^{III} state and carries seven d-electrons, of which the unpaired electron is in a $3d_{z^2}$ orbital. Theoretically, the g values are described by eq 1–3 in Appendix II.

A striking difference between Ni-A and Ni-B is the center g value, $g_y = 2.24$ for Ni-A and $g_y = 2.16$ for Ni-B. The difference is observed in the Ni-A and Ni-B states of many hydrogenases. By examining eq 2 (Appendix II) for g_y , this difference between Ni-A and Ni-B may be caused by a different energy of the d_{xz} orbital, which seems to be destabilized in the case of Ni-A. On a molecular level, the reason for this has not yet been determined, however, it might either be related to the presence of an additional oxygen at a cysteine located along the g_x direction (see Figure 6) or an out-of-plane reorientation of the equatorial cysteine ligands

along the g_x direction, which would destabilize the d_{xz} orbital for Ni-A.

In recent work by Ogata et al., using Na_2S to prepare the Ni-A state⁷⁴ a new redox state has been observed in *D. vulgaris* Miyazaki F hydrogenase with g values of 2.00, 2.14, and 2.29. It was noted that this signal appears at the expense of Ni-B.⁷⁴ The Na_2S treatment left the Ni-A signal virtually unchanged. Oxidation with O_2 converted the new signal into Ni-A. The new redox state disappears after dialysis to remove the excess Na_2S , but Ni-A remains stable and no reappearance of Ni-B was observed. Moreover, it was suggested that the new redox state undergoes electron transfer with the [3Fe-4S] cluster upon addition of traces of O_2 .⁷⁴ At present the composition of the active site in this new redox state, called Ni-B*, is not clear,⁷⁴ but from the g values, it is suspected that it also concerns a square pyramidal ligand field, possibly with a sulfur bridge between Ni and Fe.

5.3.2. Hyperfine Interactions

When the unpaired electron is delocalized over the active site, the magnetic interaction between the electron spin and the nuclear spins of nearby nuclei with $I > 0$, that is, the hyperfine interaction can be measured to determine the ligand-based part of the wavefunction of the unpaired electron. Several EPR related techniques, like ENDOR and ESEEM are designed for this purpose. A description of these methods is given in Appendix I.

⁶¹Ni. In principle, the hyperfine and quadrupole coupling constants of ⁶¹Ni can be used to examine the direct electronic environment of nickel and, indirectly, to obtain information about the identity of the ligands to nickel, which up to the time of this review is still under debate for Ni-A. ⁶¹Ni hyperfine coupling constants for *D. vulgaris* Miyazaki F hydrogenase are now available from EPR²²⁷ and for the Ni-B state from ELDOR-detected NMR measurements.²³² The latter also yield the nuclear quadrupole coupling constants and thus the electric field gradient at the nickel.

⁵⁷Fe. ENDOR measurements of ⁵⁷Fe enriched hydrogenase did not result in the observation of large ⁵⁷Fe hyperfine coupling constants in both the Ni-A and Ni-B states.²¹⁹ Couplings of about 1 MHz were observed for Ni-A, and for Ni-B (and Ni-C) virtually no signal was observed. The iron was therefore assigned to be diamagnetic in all redox states, most likely it is in the Fe²⁺ low-spin state.²¹⁹

³³S, ⁷⁷Se. Ligand hyperfine interactions have been studied for several ligand atoms, mainly protons and nitrogen, but also ³³S²³³ and ⁷⁷Se.^{234–236} In the case of ³³S enrichment, a large hyperfine interaction is observed along the g_y component of the Ni-B state. This coupling was assigned to one coordinated sulfur atom.²³³ By comparison with DFT calculations, this likely concerns the cysteine sulfur in the axial position of the square pyramid (see section 5.8). The observed hyperfine interactions for ⁷⁷Se in [NiFeSe] hydrogenase in the oxidized states of *D. baculatum* are small, they concern an atom in the equatorial (xy) plane of the square pyramid as confirmed by both X-ray structure analysis⁴¹ and comparison with hyperfine data derived from DFT calculations.²³⁷ The observed coupling constants for both ³³S and ⁷⁷Se are thus compatible with the picture of the spin density being in the $3d_{z^2}$ orbital in the ground states for both Ni-A and Ni-B.^{233–237}

¹⁷O. Hyperfine interactions can also be used to establish the identity of ligands, such as the bridging ligand between nickel and iron, which changes upon activation of the

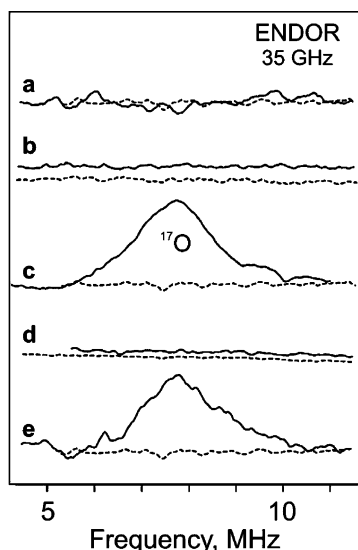


Figure 7. 35 GHz ^{17}O CW ENDOR of *D. gigas* [NiFe] hydrogenase in H_2^{16}O (dashed) and in H_2^{17}O (solid). (a) Ni-A, exchanged into H_2^{17}O . (b) Ni-C in H_2^{17}O , generated by H_2 -reduction of the Ni-A samples from panel a. (c) Ni-A in H_2^{17}O after one reduction/reoxidation cycle, (Ni-A \rightarrow Ni-C \rightarrow Ni-A). (d) Ni-C, generated by H_2 -reduction of the Ni-A samples from panel c. (e) Ni-A in H_2^{17}O after two reduction/reoxidation cycles, (Ni-A \rightarrow Ni-C \rightarrow Ni-A \rightarrow Ni-C \rightarrow Ni-A). Conditions: $g = 2.31$ (Ni-A) or 2.19 (Ni-C); $T = 2$ K. Spectra are reproduced from ref 90 with permission. (Copyright 2002 American Chemical Society.)

enzyme. For example, ENDOR experiments on *D. gigas* hydrogenase using H_2^{17}O revealed large and anisotropic ^{17}O hyperfine coupling constants for Ni-A, which show that the bridging ligand is oxygen-based, and that it can only be exchanged to ^{17}O after first completely removing it by reduction followed by a reoxidation step.⁹⁰ The experiment is shown in Figure 7. Trace (a) contains the spectrum in H_2^{16}O , (b) after exchange to H_2^{17}O , (c) after one reduction–oxidation cycle, (d) the reduced enzyme, and (e) again oxidized. For Ni-B, such a study has unfortunately not been performed yet. The X-ray structural data on the vast majority of hydrogenases indicate that the bridging ligand is also oxygen-based, and experiments with ^{17}O using molecular $^{17}\text{O}_2$ already showed an increase in EPR line width for both the Ni-A and Ni-B states.⁸⁹

H. Investigation by ENDOR spectroscopy of the Ni-A state revealed ^1H hyperfine couplings ranging from 0 to 12.8 MHz.²³⁸ None of the protons were found to be exchangeable. The large hyperfine coupling constants result from the β - CH_2 protons of the axial cysteine of the square pyramid,^{239,240} again confirming the $3d_{z^2}$ ground state. For the Ni-B state, ENDOR and HYSCORE spectroscopy—first on frozen solutions of *A. vinosum* and *D. vulgaris* Miyazaki F^{239,241} and later on single crystals—in combination with DFT calculations²⁴⁰ revealed additionally a ^1H hyperfine coupling constant for an exchangeable proton in the equatorial (xy) plane that could only be assigned to the bridging ligand, and this ligand was thus assigned as an OH^- in Ni-B.²⁴⁰ By careful analysis of the orientation dependence of the single-crystal data, one out of two possible conformations for the OH^- in the bridging position was favored, where the proton is found in the xy plane (see refs 239 and 240).

The g values of the Ni-A state were also found to be most compatible with the presence of an OH^- ligand.^{242,243} A reanalysis of the recent X-ray structure for Ni-A by Soderhjelm et al., which originally contained a bridging ligand

proposed by Volbeda et al. to be a species with two non-hydrogen atoms, for example, OOH^- ,⁷¹ was most compatible with the presence of OH^- for Ni-A.²⁴⁴ Another proton hyperfine interaction has been observed by high-resolution EPR spectroscopy on *A. vinosum* hydrogenase.²⁴⁵ In this respect, it is interesting to note that recent electrochemical data, using a procedure with Na_2S to obtain Ni-A, identified a μ -sulfido bridged species in *D. vulgaris* Miyazaki F,⁹² for which no EPR or ^1H ENDOR data are available yet. In summary, the identity of the third bridging ligand in Ni-A (OH^- or OOH^-) has not been clarified yet. This is, however, important for understanding this oxygen-inhibited state of the enzyme.

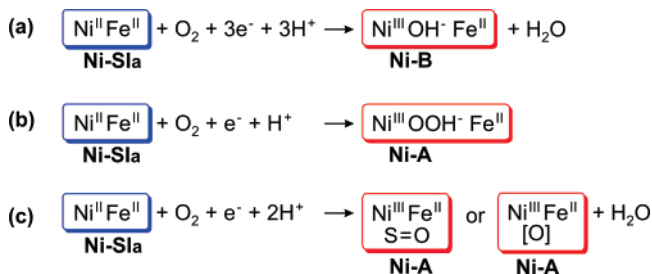
$^{14}\text{N}/^{15}\text{N}$. Nitrogen hyperfine interactions have been observed as well, stemming from a histidine which is hydrogen bonded to the axial cysteine in the catalytic hydrogenases. For *D. gigas* hydrogenase in the Ni-A²⁴⁶ state and *D. vulgaris* Miyazaki F hydrogenase in the Ni-B state,²⁴⁷ ^{14}N hyperfine and quadrupole coupling constants have been obtained from ESEEM spectroscopy. In both cases, virtually the same coupling constants were derived and were interpreted as resulting from a highly conserved histidine forming a weak $\text{N}-\text{H}\cdots\text{S}$ bond to the axial cysteine. The H-bond is probably placed to fine-tune the electronic structure of the [NiFe] center. Two [NiFe] hydrogenases from *M. thermoautotrophicum* have also been investigated, of which only one, the F₄₂₀ reducing hydrogenase, showed characteristic signals of a nitrogen coupling.²⁴⁸

5.3.3. Activation and Inactivation Studies

Activation studies in combination with, for example, FTIR spectroscopy^{85,86} and electrochemistry²⁴⁹ have shown that the Ni-B state is rapidly activated, at room temperature within seconds, whereas the Ni-A state is only activated in minutes. Moreover, the Ni-A/Ni-SU redox couple has been investigated by redox titrations monitored by EPR and the midpoint potential was found to depend on the pH (for *D. gigas*, -150 mV at pH 7.0 and -220 mV at pH 8.5^{250,251}). The pH dependence of -60 mV/pH unit indicates that the one-electron reduction of the active site is accompanied by a protonation of the enzyme. The midpoint potential of the [3Fe–4S] cluster is about -70 mV.²⁵² For *A. vinosum* hydrogenase, it has been shown that the Ni-A \rightarrow Ni-SU reduction is reversible, but the Ni-B \rightarrow Ni-SIr reduction strongly depends on pH and temperature. At pH 6.0 and 2 °C the reduction was completely irreversible, at pH 8 and 30 °C both reduction steps were reversible.¹⁴³ Recently, also for *A. vinosum* hydrogenase, it has been demonstrated that the Ni-A state does not directly react with hydrogen and first has to undergo a conformational change.¹⁶⁰ The ready state, however, activates after a lag phase of about 6 seconds and can react with substoichiometric amounts of H_2 . One has to be careful, however, to generalize these results to [NiFe] hydrogenases of other organisms.²⁵³ For *M. formicium* hydrogenase, the midpoint potential for activation lies at -300 mV.²⁵⁴ For the [NiFe] hydrogenase of *D. desulfuricans*, the midpoint potential for the $\text{Ni}^{\text{III}}(\text{Ni-B})/\text{Ni}^{\text{II}}$ couple was determined to be -170 mV, that of reduction of Ni-C at -360 mV, and that of reduction of the [3Fe–4S] cluster at -75 mV.²⁵⁵ Other enzymes that have been studied by EPR and electrochemistry which showed similar results are *D. salexigens*,⁸³ *D. desulfuricans* strain Norway,²⁵⁶ *D. gigas*,^{257–259} and *M. thermoautotrophicum* (strain Marburg).²⁶⁰

The above studies reveal that the activation of the Ni-B state proceeds readily, albeit with a thermal activation barrier

Scheme 2



for some enzymes, whereas the Ni-A state most probably does not directly react with hydrogen, but first has to undergo an as yet unknown conformational change. From the similarity of the midpoint potential of the [4Fe–4S] clusters, it is very likely that the electrons of the turned-over hydrogen travel from the [NiFe] center to the [4Fe–4S] clusters.

The inactivation of activated enzyme has also been investigated. Initially, it was found that even in as-isolated preparations of *A. vinosum* hydrogenase, a “defect” inactive form exists, which is independent of the relative ratio of Ni-A and Ni-B. This form can, however, be repaired by a chemical procedure.²⁶¹ By using O_2 or CO the protein can be inactivated.¹⁵⁹ In the case of O_2 , the *A. vinosum* enzyme became inactivated in 158 ms and then resided in the Ni-B state.¹⁵⁹ For *D. gigas* hydrogenase, oxidative titrations and simulations thereof have shown that the active Ni-C state is two electrons more reduced than the Ni-A and Ni-B states.^{262,263}

It is striking that after inactivation of the active enzyme by O_2 , the [NiFe] center resides mostly in the Ni-B state, not Ni-A. It seems as if the as-yet unknown conformational change, which was necessary to activate Ni-A, is also required in the reverse direction to obtain the Ni-A state again after inactivation. Whether this happens at the oxidation level of the Ni-B or of the Ni-SIr state (i.e., the EPR-silent one-electron-more-reduced equivalent to Ni-B, “Ni-B silent”, or “silent-ready” state), or with which kinetics and temperature behavior this process is associated, is still unclear. It is an important result, however, for the inhibition of the enzyme by O_2 (vide infra), since it indicates that O_2 itself does inactivate the enzyme, but only to the Ni-B state, which is easily activated again. To further inhibit the enzyme, most likely, a conformational change has to occur. In this respect, from electrochemistry data, injection of O_2 predominantly under reducing conditions (0 mV, H_2 present) yields the Ni-B state in the *A. vinosum* enzyme. At higher potentials (>200 mV, under N_2) more than 80% of the enzyme converts into the Ni-A state.^{98,99} On the basis of these results and the available EPR and structural data, Armstrong and co-workers suggested^{98,99,264} that when electrons are abundant, reduction of O_2 proceeds on a fast time scale by four-electron reduction into two water molecules (one effectively retained as OH^-). However, when electrons are not abundant O_2 reacts only to peroxide, thus creating a powerful and potentially damaging oxidant to attack the active site producing Ni-A and other products with oxidized cysteines (S=O and or S–OH groups) (see Scheme 2). On the basis of the recent investigations of the Ni-A state this intermediate may carry a peroxide or hydroperoxide ligand in the bridge between Ni and Fe.^{74,80} A hydroxide ligand has also been suggested on the basis of spectroscopic and theoretical studies.^{241,243,244} In both X-ray structures an oxidation of cysteine sulfurs is also evident.^{74,80} These results are of great importance for understanding the inhibition of the enzyme by molecular oxygen which

currently limits the use of hydrogenases for a biotechnology that combines light-induced water oxidation (producing oxygen) and hydrogen production by hydrogenases.

5.3.4. The Fe–S Clusters

In the Ni-A and Ni-B state, the oxidized $[\text{3Fe–4S}]^{2+}$ cluster is also paramagnetic, the [4Fe–4S] clusters are diamagnetic. The $[\text{3Fe–4S}]^{2+}$ cluster carries a spin $S = 1/2$ and interacts magnetically with the electron spin on the [NiFe] center.^{265,266} The $[\text{3Fe–4S}]^{2+}$ cluster is characterized by a narrow, radical-like signal with g values of 2.0113, 2.0176, and 2.0261, and the principal direction of the g tensor has been obtained by single-crystal studies at W-band (95 GHz) for the enzyme of *D. vulgaris* Miyazaki F.²⁶⁷ It has been demonstrated that the $[\text{3Fe–4S}]^{2+}$ cluster exists in two forms that are characterized by different relaxation times.²⁶⁷ By performing ESEEM and HYSCORE measurements, a nitrogen in the coordination sphere of the $[\text{3Fe–4S}]^{2+}$ cluster has been identified.²⁶⁷

The $[\text{3Fe–4S}]^{2+}$ cluster was also investigated by ENDOR spectroscopy and ^{57}Fe labeling in the enzyme from *D. gigas*. The observed signals could be best understood by assuming a model in which the cluster would have a bimodal distribution.²⁶⁸ It was observed that the iron with the largest spin density has different properties in both forms.²⁶⁸

With PELDOR spectroscopy, the strength of the dipolar spin–spin interaction between the weakly coupled [NiFe] and $[\text{3Fe–4S}]^{2+}$ centers can be measured, which allows the determination of the effective distance between the two clusters. The spin–spin interactions have been obtained for *D. vulgaris* Miyazaki F hydrogenase.^{269,270} In the interpretation the spin density distribution over the $[\text{3Fe–4S}]^{2+}$ cluster had to be considered.

It is not immediately clear why a [3Fe–4S] cluster instead of a [4Fe–4S] is actually present in the enzyme. Especially the midpoint potentials do not seem to be well adjusted to those of the electron transport chain and the [NiFe] center.⁹⁶ It may be that the [3Fe–4S] cluster with its rather positive potential plays a role in effectively trapping electrons from the active site rendering the reaction between H_2 and the ready enzyme irreversible.²⁷¹ Furthermore, it has been speculated that the [3Fe–4S] cluster protects the enzyme against oxidative damage in nature. A mutant of *D. fructosovorans* in which the [3Fe–4S] cluster was changed to a [4Fe–4S] cluster became highly sensitive toward O_2 .⁷⁷

5.4. The Active Intermediate State

5.4.1. g Tensor Analysis and the Ligand Field

Upon activation of the enzyme by H_2 and a sufficiently long incubation time, a new paramagnetic redox state can be observed. It is characterized by g values of 2.01, 2.15, and 2.20 and named Ni-C (see Figure 4), with remarkably little variation among the catalytic [NiFe] hydrogenases of different origin. Also the regulatory hydrogenase has a Ni-C redox state.^{93,230} The Ni-C state is an active state, which is of key importance in the catalytic turnover of molecular hydrogen. Since one of the g values (2.01) is very close to the free electron g value ($g_e = 2.0023$), this redox state is most probably characterized by a $3d_{z^2}$ ground state. An investigation by X-ray crystallography has not revealed substantial electron density at the position of the bridging ligand between nickel and iron.⁷² However, studies by single-crystal EPR spectroscopy⁹⁴ showed that the c_∞ axis of the $3d_{z^2}$ orbital is approximately parallel to the bond direction

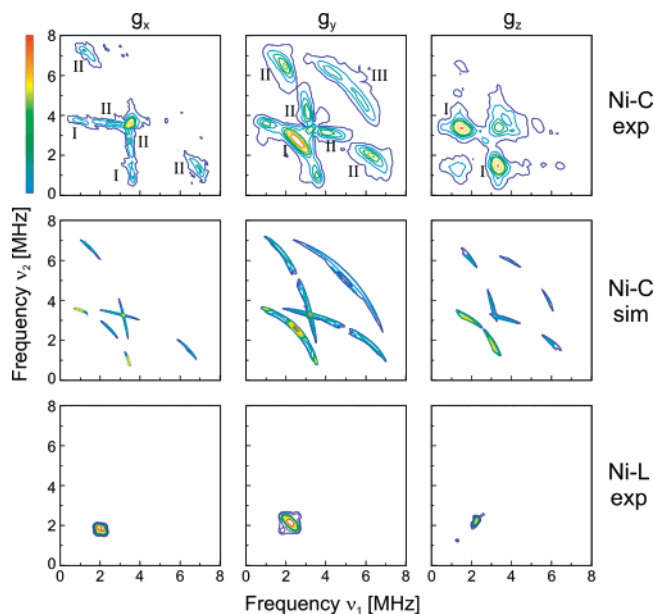


Figure 8. Top: orientation selected HYSCORE spectra at X-band recorded at the three canonical orientations (g_x , g_y , g_z) for the Ni-C state in the regulatory hydrogenase of *R. eutropha* in $^2\text{H}_2\text{O}$ activated with $^2\text{H}_2$. All observed ridges in the spectrum stem from the hydride bridging ligand ($^2\text{H}^-$), located in the xy plane of the square pyramid (cf. Scheme 3). Middle: simulations of the experimental spectra. Bottom: HYSCORE spectra of the Ni-L1 state. As is seen in the spectra, the strong couplings have disappeared, indicating a photodissociation of the hydride bridge upon illumination. Data are adapted from ref 93.

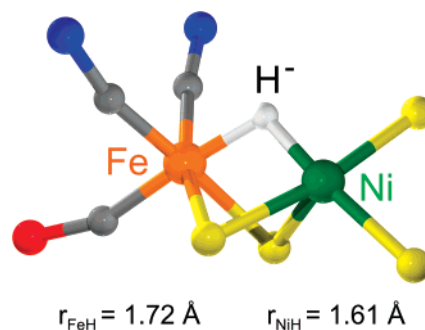
from nickel to the axial sulfur, as was the case for the oxidized states Ni-A and Ni-B, see Figure 6. It also strongly indicates that the ligand field is still square pyramidal and that the bridging position, found to be empty in the crystal structure, is likely occupied by a light atom, which cannot be observed in the X-ray experiment, that is, by a hydrogen species. The presence of a hydrogen species in the bridging position will be discussed further in the next section. The nickel atom is then still characterized as being five coordinate.

5.4.2. Hyperfine Interactions

^1H . Pioneering work in the group of Hoffman using ENDOR spectroscopy has revealed an exceptionally strong ^1H hyperfine interaction of an exchangeable proton with an effective coupling of 16.8 MHz.¹⁶³ In this work, another exchangeable proton was detected with an effective hyperfine coupling constant of about 4.4 MHz. Also two nonexchangeable $\beta\text{-CH}_2$ protons have been observed which are dominantly isotropically coupled and belong to the cysteine associated with the axial direction of the square pyramid.⁹⁵ A simple analysis of the dipolar coupling yields a Ni-H distance of 1.63 Å in very good agreement with a DFT calculation ($r_{\text{NiH}} = 1.61$ Å, $r_{\text{FeH}} = 1.72$ Å) that also reproduced the tensor magnitude and orientation of the bridging hydride quite well.⁹³

The hyperfine coupling tensor components of the strongly coupled proton have later been more completely determined by ENDOR and in particular HYSCORE spectroscopy for the regulatory hydrogenase of *R. eutropha*⁹³ and the catalytically active hydrogenase of *D. vulgaris* Miyazaki F.⁹⁵ An overview of the HYSCORE spectra of *R. eutropha* hydrogenase in D_2O recorded at the three canonical orientations and corresponding simulations is shown in Figure 8, where

Scheme 3



hyperfine coupling constants have been determined from the shape of the cross-ridges that show an unusual anisotropy. The dipolar coupling turned out to be so large that the ridges could only stem from a proton close to the spin center (Ni). The signals were assigned to a formal hydride. The analysis of the data shows that the H^- occupies the bridging position between Ni and Fe. Because of its small isotropic hyperfine interaction, it resides in the equatorial plane of the $3d_{x^2-y^2}$ orbital at nickel and in the base plane of the square pyramid. A schematic overview of the active site in the Ni-C state is given in Scheme 3. The Ni-C active site is indeed two electrons more reduced than that of Ni-A and Ni-B, but the valence state of nickel remains formally Ni^{III} with a coordinated hydride. The Ni^{III} valence state is in agreement with results from EXAFS spectroscopy¹⁶⁵ and EPR investigations of synthetic model systems.^{272–275} A formal assignment as Ni^{I} would lead to a $3d_{x^2-y^2}$ ground state with the lobes of the $3d_{x^2-y^2}$ orbital pointing toward the hydrogen, which is incompatible with both EPR measurements of single crystals⁹⁴ and ENDOR measurements of frozen solutions.⁹⁵

^{61}Ni . ^{61}Ni hyperfine coupling constants have been measured for *D. vulgaris* Miyazaki F hydrogenase.²²⁷ The largest coupling is found along the g_z canonical orientation ($A_z = -75$ MHz), thus confirming that the electronic ground state of Ni-C is similar to that of the oxidized Ni-A and Ni-B states.

^{14}N . The ^{14}N hyperfine and quadrupole coupling constants observed for the oxidized states have also been detected in the Ni-C state (*D. gigas* enzyme),²⁴⁶ indicating that the hydrogen bond of histidine to the axial sulfur is still present. In the regulatory hydrogenase of *R. eutropha*, which does not display a Ni-A or Ni-B EPR spectrum, no ^{14}N signals are observed. The amino acid sequence of this protein does not contain a histidine that forms a hydrogen bond to the axial sulfur. However, introduction of a histidine at this position (Gln \rightarrow His) by site directed mutagenesis restores the hydrogen bond and gives rise to essentially identical ESEEM spectra as those observed for the catalytic hydrogenases.²³⁰

5.4.3. The Fe–S Clusters

In catalytically active reduced hydrogenases, the proximal $[\text{4Fe-4S}]$ cluster is also reduced and gives rise to a paramagnetic state. The Ni-C state interacts strongly with this $[\text{4Fe-4S}]^+$ cluster, whose interaction is so large that the spectrum broadens and even splits at low temperatures (see Figure 4), as has been observed for *D. gigas*,^{250,276} *A. vinosum*,¹⁴⁶ *M. thermoautotrophicum*,¹⁴⁶ and *D. vulgaris* Miyazaki F⁹⁵ hydrogenase. The observed splitting has been advantageously used to determine the magnitude of the spin–

spin interaction between the two metal centers.^{277–279} At higher temperatures, the spin relaxation of the $[4\text{Fe}-4\text{S}]^+$ cluster becomes so fast, that the spin–spin coupling is averaged out. The coupling is absent over the whole temperature range in the regulatory hydrogenase of *R. eutropha*, for which the proximal $[4\text{Fe}-4\text{S}]$ cluster remains in the oxidized diamagnetic state,⁹³ and an unsplit Ni-C signal is observed at low temperatures.

Using redox titrations, the midpoint potential of the $[4\text{Fe}-4\text{S}]$ cluster has been estimated for *D. gigas* hydrogenase. It was found to be pH dependent and amounted to -270 mV at pH 7.0 for the appearance and -390 mV for the disappearance.¹⁴⁵ From the relative ratio of “split” to “unsplit” Ni-C, the midpoint potential of the proximal $[4\text{Fe}-4\text{S}]$ cluster was found to be about -350 mV and changed by -60 mV per pH unit.¹⁴⁵ Thus, by carefully setting the potential, it is possible to optimize the amount of unsplit Ni-C and perform ENDOR and HYSCORE measurements at low temperature.^{95,280} The midpoint potential for the $[4\text{Fe}-4\text{S}]$ cluster in the regulatory hydrogenase of *R. eutropha* is obviously lower, because no split Ni-C signals are observed at any temperature.

5.5. Inhibition of the Enzyme

5.5.1. Inhibition by O_2

A major concern in practical applications of hydrogenases for the production of hydrogen is oxygen sensitivity. Oxygen inactivates the enzyme, and in some cases even causes irreversible damage. Oxygen sensitivity studies have recently been investigated using site directed mutagenesis by which certain amino acids are exchanged near a putative gas channel, which is used by hydrogen to travel from the protein surface to the active site.²³¹ In these studies, the width of the gas channel was changed which indeed affected the oxygen tolerance. $[\text{NiFe}]$ hydrogenases vary with respect to their oxygen sensitivity depending on the origin of the enzyme. For example, the extremophile *Aquifex aeolicus* contains three $[\text{NiFe}]$ hydrogenases, two membrane-bound and one soluble,²⁸¹ they have all been found to be thermostable and oxygen tolerant.²⁸² The membrane-bound, soluble, and regulatory hydrogenases of *R. eutropha* are oxygen tolerant as well. Most other enzymes are not oxygen tolerant to varying degrees. Moreover, as was stated before, only when introduction of O_2 is accompanied by a conformational change of the $[\text{NiFe}]$ center, the enzyme is strongly inhibited. For these reasons, from the point of view of EPR spectroscopy, it is difficult at present to make general statements about how O_2 may be bound, how it inhibits the enzyme, or how oxygen inhibition may be prevented (for example, does it block the gas access channel for H_2 , the width of which may vary between enzymes of different origin). On the basis of X-ray crystallography, however, a diatomic bridging ligand, most probably OOH^- was proposed for Ni-A, with the possibility of additional modifications at the cysteines,^{71,74} indicating that O_2 may undergo a reaction, possibly not a specific one, near the active site, see Scheme 2. As already mentioned, this reaction depends on the abundance of electrons; Ni-A is formed only at high potentials (> 200 mV under N_2).^{98,99}

5.5.2. Inhibition by CO

In the case of CO inhibition for *A. vinosum* hydrogenase, two EPR signals were observed, only one was light-

sensitive.¹⁴⁸ Concerning the EPR-silent Ni-CO (silent), it was found that the CO directly binds to the active site, preferably to the Ni-SIA state; the paramagnetic Ni-CO (active) species is formed on a much slower time scale.¹⁵⁹ The EPR-detectable Ni-CO (active) state has g values of 2.02, 2.07, and 2.12 and an isotropic ^{13}C (^{13}CO) hyperfine interaction of 85 MHz.^{89,149} The obtained results were analyzed by combining them with results from DFT calculations, where it was found that the g values and the observed ^{13}C hyperfine coupling of ^{13}CO inhibited enzyme were most compatible with an axially bound CO and a formal Ni^{I} redox state. The Ni-CO (active) state likely has an empty bridging position.²⁸³ In a recent work using X-ray crystallography on the CO inhibited form, the CO has indeed been found in an axial coordination position to nickel, but binds under an angle of 160 degrees,⁷³ which is compatible with DFT calculations.²⁸³ Interestingly, the Ni-CO (active) state also shows a split signal at low temperature (see Figure 4) and is light sensitive.⁸⁹ Upon illumination the CO is reversibly dissociated.⁷³

5.5.3. Other Inhibitory Agents

It is known that the enzyme can be inhibited by copper and mercury salts.^{284,285} Other, less common chemicals can be used for inhibition as well. For example, for *T. roseopersicina* hydrogenase, it was found that the Ni-C signal disappears upon addition of acetylene. Such an effect was not observed for *D. baculatum* hydrogenase, whereas both enzymes are irreversibly inhibited by iodoacetamide.²⁸⁶

5.6. Light Sensitivity of the Enzyme

The Ni-C state is light sensitive and can be converted under illumination and at low temperature to another state, which is called Ni-L, see Figure 9 (top). Depending on the source of the enzyme, the temperature and the illumination time, up to three different Ni-L states may be observed in catalytic $[\text{NiFe}]$ hydrogenases, which are usually called Ni-L1, Ni-L2, and Ni-L3. The g values vary slightly depending on which species is studied. For *A. vinosum* hydrogenase, they amount typically to 2.30, 2.12, and 2.05 for Ni-L1 and 2.27, 2.12, and 2.05 for Ni-L2¹⁴⁶ (see also Figure 4). For Ni-L3, only two g values are known, 2.41 and 2.16; the third could not be determined. When the temperature is raised, typically to about 170 K, the Ni-L states convert back to Ni-C as is shown in Figure 9c.^{147,163}

The action spectrum associated with the Ni-C to Ni-L2 conversion is shown in Figure 9b. It displays a broad band that spans the entire visible range. Structure was observed in the spectrum, which has local maxima at 590, 700, and 850 nm. The two maxima at 590 and 700 nm are close to maxima observed in the UV–vis spectrum of the reduced enzyme. This correlation indicates that the Ni-C to Ni-L conversion may be triggered by absorption of white light by the $[\text{NiFe}]$ center itself, either via a ligand-to-metal charge transfer or d–d transitions.²⁸⁷ This is in-line with the MCD spectrum of the Ni(III) form of hydrogenase from *M. thermoautotrophicum*, which shows a signal assigned to a nickel d–d transition between 550 and 700 nm.²⁸⁸

The g_z value of the Ni-L states is significantly shifted away from the free electron g value, it is typically 2.05. This g value indicates that the wavefunction of the unpaired electron on nickel cannot be described anymore by a pure $3d_z^2$ orbital. Most likely, the $3d_{x^2-y^2}$ orbital mixes with $3d_z^2$.¹⁸¹ However, single-crystal EPR experiments have shown that the direction

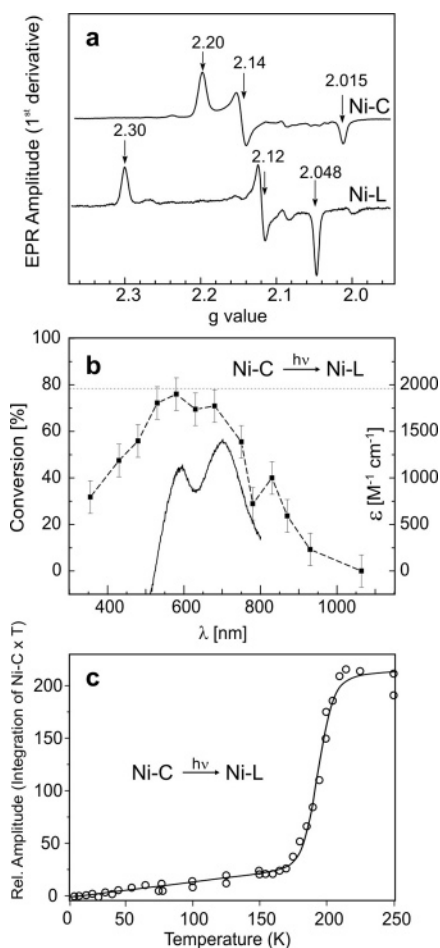


Figure 9. (a) EPR spectra of the Ni-C and Ni-L2 states in *D. vulgaris* Miyazaki F [NiFe] hydrogenase. (b) The action spectrum (dashed line) associated with the Ni-C to Ni-L2 conversion. The observed structure in the action spectrum seems to be correlated with weak structural features observed in the UV-vis spectrum of the reduced state (shown as solid curve). Data taken from ref 287. (c) Temperature dependence of the annealing process from Ni-L2 back to Ni-C. Data reproduced from ref 163.

of the principal axis that corresponds to the lowest g value (2.05) is still parallel to the direction that connects nickel and the axial sulfur (see Figure 6). The wavefunction is therefore still best described by a $3d_{z^2}$ orbital and a small admixture of $3d_{x^2-y^2}$ orbital. It also suggests that the formal redox state of Ni-L is closer to Ni^{III} than to Ni^I, which is in-line with XAS measurements that show that Ni-L is only slightly more reduced than Ni-C and that the observed edge shift is not compatible with a formal Ni^I redox state.¹⁶⁵

Most notably, the hydride signals observed in HYSORE spectra for Ni-C are absent in Ni-L (see Figure 8, bottom). The only signal which remains is an unstructured signal at the free deuterium Zeeman frequency (2 MHz). This suggests that the hydride (or in the case of the experiment shown in Figure 8, $^2\text{H}^-$) is dissociated from the [NiFe] center, most likely as a proton, and binds to a nearby base so that it can reoccupy the bridging position upon annealing. In this respect, a difference has been observed between [NiFe] and [NiFeSe] hydrogenases. For the [NiFeSe] hydrogenase of *D. baculatum* a different line narrowing upon D₂O exchange was detected in the EPR spectrum than that in the [NiFe] hydrogenase, possibly pointing to subtle differences in the composition of the active site with respect to the location of a hydride species.²⁸⁹

5.7. EPR-Silent States

The EPR-silent states of [NiFe] hydrogenases are Ni^{II} (d^8) states, which can adopt a low-spin or high-spin electronic configuration.²⁹⁰ They have been proposed to exist in high-spin ($S = 1$) states by XAS spectroscopy.¹⁶⁶ The high-spin or low-spin character of the “EPR silent” Ni^{II} states is determined by the energy splitting of the $d_{x^2-y^2}$ and d_{z^2} orbitals. When these orbitals are near-degenerate, the high-spin ground state is favored and both orbitals carry one electron. A distortion which most efficiently brings the $d_{x^2-y^2}$ orbital down in energy is one toward a trigonal bipyramid. Whether or not the orbitals come close enough together that the high-spin state becomes the ground state is an open question that could be addressed by high-field EPR spectroscopy experiments in the future.

5.8. Other Hydrogenases Containing Nickel

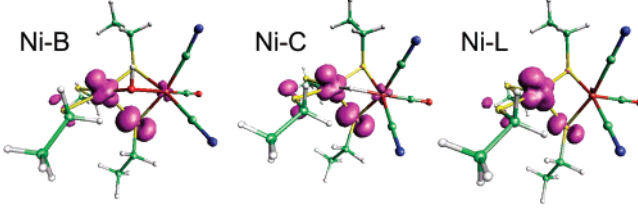
A sulfhydrogenase has been investigated from *Pyrococcus* (*P.*) *furiosus*.^{291,292} Though the enzyme was found to contain nickel, no characteristic Ni-A, Ni-B, or Ni-C signals were observed, as in the NAD-reducing hydrogenase from *R. eutropha*.¹⁵⁸ The g values of [1.92, 1.95, 2.02], [1.89, 1.93, 2.07], and [1.98, 2.25] were all assigned to Fe-S clusters. The results indicate that a [NiFe] center typical for standard hydrogenases is not present in this enzyme and that the Fe-S clusters may play a crucial role here. Essentially the same observations have been made for the hydrogenase from the thermophile *T. stetteri*,²⁹³ *A. aeolicus*,²⁸¹ and *T. litoralis*,²⁹⁴ but for the reduced state of a membrane bound hydrogenase in *P. furiosus*, a Ni-C signal was observed.²⁹⁵ For the enzyme of *A. ferrooxidans*¹⁵⁷ a Ni-C state has been observed as well. This enzyme also displays a Ni-B state with slightly changed g values, but little more information is known about the exact coordination or functional role of nickel in these enzymes.

5.9. DFT Calculations and Electronic Structure

The spectroscopic investigation of the above-discussed redox states gives information about the electronic structures of all intermediates. To extract information about the electronic structure in a quantitative manner, quantum chemical calculations are required. Because of the large size of the [NiFe] center, these studies mainly concern density functional theory (DFT) calculations, which allow the description of larger systems than *ab initio* methods. DFT calculations have as a limitation that one has to be careful with the interpretation of the results in terms of the underlying physics which is somewhat obscured in DFT.²⁹⁶

In early work by Hall et al.,²⁹⁷ models for the reaction intermediates were proposed and compared with experiments based on the vibrational frequencies of the inorganic CN⁻ and CO ligands. In their work, the site of hydrogen splitting was proposed to be iron and one terminal cysteine was proposed to be protonated in the Ni-SIr state.²⁹⁷

DFT calculations with emphasis on reproducing the EPR g values and hyperfine coupling constants were first presented by Stein et al.²⁹⁸ The g values of 2.21, 2.17, and 1.98 were calculated for Ni-B within the zeroth-order regular approach (ZORA) using a model in which none of the cysteine sulfur atoms were protonated and an OH⁻ ligand was present in the bridging position between Ni and Fe. Considering the accuracy of the DFT method for the computation of g values,²⁹⁹ the agreement can be considered

Table 3. Calculated Spin Density Distribution of Model Systems for the [NiFe] Center That Represent the Ni-B, Ni-C, and Ni-L States^a


	Ni-B (X = OH ⁻)	Ni-C (X = H ⁻)	Ni-L (X = vacant)
Ni	0.52	0.51	0.76
Fe	-0.002	0.01	-0.08
S (axial)	0.34	0.29	0.16
S (terminal)	0.06	0.10	0.09
X	0.01	-0.001	

^a Data taken from ref 228. X = third bridging ligand, see Figure 1. Above the respective columns the spin density plots for the three states are shown. For details see refs 283 and 300. Calculated hyperfine tensor values for all states can be found in ref 283 (Supplementary Material).

very satisfying. For Ni-C a hydride bridge was proposed and g values of 2.20, 2.14, and 2.01 were calculated.^{237,298,300} For the Ni-L state an empty bridge was proposed (calculated g values are 2.26, 2.10, 2.05²⁸³) and for Ni-CO (active), a CO terminally bound to the empty coordination position of Ni gave best agreement with the experimental g values.²⁸³ At that time a μ -oxo bridge was proposed for Ni-A,²⁹⁸ though recent experiments have shown that the bridge is most probably also protonated for Ni-A,^{241,301} thus suggesting a hydroxo or hydroperoxo bridge.

In similar work on the enzyme of *D. fructosovorans*, the experimental g values of Ni-A and Ni-B were investigated by DFT calculations.²⁴³ In this study, the effect of the environment was investigated by including more amino acids in the model for the calculation. For both Ni-A and Ni-B at that time, it was concluded that the bridging ligand is likely an OH⁻, and that the difference may be caused by a different protonation state of, for example, the nickel-coordinating sulfur atoms of the cysteines. The effect of the environment on the g values can change the g_x value by typically 0.05,²⁴³ indicating that the overall structure is primarily determined by the direct ligands to Ni and that it is further fine-tuned by surrounding amino acids.

Amara et al. performed QM/MM calculations³⁰² and included even more of the protein environment. They compared their calculations with data available from FTIR spectroscopy and noted the special role of the terminal cysteine near the H₂ channel (Cys-530 for *D. gigas*). Moreover, they conclude that the redox activity mainly occurs at nickel and the terminal S ligands and that iron is not involved.³⁰² Their proposed mechanism includes a μ -oxo bridge for Ni-A, a hydride bridge for Ni-C, and two hydride species for Ni-R.³⁰²

The spin density distribution for the Ni-A, Ni-B, and Ni-C states confirm the 3d_z² character of the wavefunction of the unpaired electron.²³⁷ An overview is given in Table 3. The table also includes data for the Ni-L2 state. In total, for the Ni-C state 51% spin density was found on Ni and 29% on the cysteine of the axial sulfur (Cys-549 for *D. vulgaris* Miyazaki F), which gives rise to hyperfine splitting in the EPR spectrum of ³³S enriched [NiFe] hydrogenase.²³³ The terminal cysteine near the gas channel (Cys-546) carries about 10% spin density and the remaining 5% is distributed

over the other atoms. The spin density at the iron was found to be small (about 1%), indicating the presence of a low-spin Fe(II). Essentially the same spin density distribution was found for the [NiFeSe] hydrogenase of *D. baculatum* in the Ni-C state.²³⁷ A similar picture is obtained for the Ni-B state. The spin density at the bridging OH⁻ was found to be small (Table 3). In the case of Ni-L2, larger shifts of the spin density are observed: the spin density at Ni increases and that at the axial sulfur (Cys-549 for *D. vulgaris* Miyazaki F) decreases. The calculated spin densities may vary up to about 10% depending on the method of calculation (e.g., with respect to the choice of functional). The z -axis of the 3d_z² orbital is almost parallel to the bond direction from nickel toward the axial sulfur atom (Cys-549 for *D. vulgaris* Miyazaki F and Cys 533 for *D. gigas*).

The DFT calculations also allow for a critical comparison with EPR data from single crystals. In principle, both methods independently yield the directions of the principal axes of g and hyperfine tensors. For the Ni-B,^{188,240} Ni-C⁹⁴ and Ni-L2^{94,95} states, the experimentally found principal directions of the g tensor and ¹H hyperfine tensors are reproduced by the respective models of the calculations (OH⁻ bridge for Ni-B, H⁻ bridge for Ni-C, empty bridge for Ni-L2), giving experimental confirmation that the models used in the calculation contain the correct features. For example, in the case of the OH⁻ bridge for Ni-B, two conformations are possible, but only one conformation was compatible with experimental data.²⁴⁰ For Ni-A, even though no exchangeable protons have been observed,²³⁸ it is possible to exchange a proton by a reduction–oxidation cycle. The observed dipolar coupling constant for the “exchangeable” proton is compatible with a proton that belongs to the bridging ligand^{241,301} and analysis as to its exact position is underway. In the Ni-C state, the hyperfine tensor of the observed hydride bridge, including the direction of the principal axes, was satisfactorily reproduced by the calculations.⁹⁵ The ¹³C hyperfine coupling of added isotopically labeled ¹³CO in the Ni-CO(active) state was best reproduced by a terminally bound CO ligand,²⁸³ in agreement with earlier crystallographic data.⁷³ A collection of hyperfine data of the various nuclei in the different states of [NiFe] hydrogenase can be found in ref 283.

Concerning the EPR-silent states, for which obviously no EPR or ENDOR data are available, a DFT study has been performed by Bruschi et al.³⁰³ It was found that the low spin ($S = 0$) and high spin ($S = 1$) states for both Ni-SI and Ni-R are very close in energy to an extent that their order becomes method dependent, especially with respect to the amount of Hartree–Fock exchange included in the calculation.³⁰³ In their model, the Ni-R state maintains a hydride bridge, like in Ni-C, and their Ni-SI state model concerned a site with an empty bridge and a protonated terminal cysteine (Cys-65 for *D. gigas*).

In conclusion, one can say that DFT calculations are very helpful, if not essential, to understand the electronic structure. The structural models used in these calculations have to be critically tested, though, by evaluating spectroscopic properties like g values, hyperfine coupling constants, or FTIR frequencies besides the total energies, to gain confidence in the proposed models and to establish a connection with the experiment. By considering both the accuracies of experiment and calculation, one can try to find structural models or partial features (e.g., an OH⁻ bridge for Ni-B) that describe the observed experimental data the best. On the basis of such comparisons, an attempt can be made to understand the catalytic cycle, which will be described below.

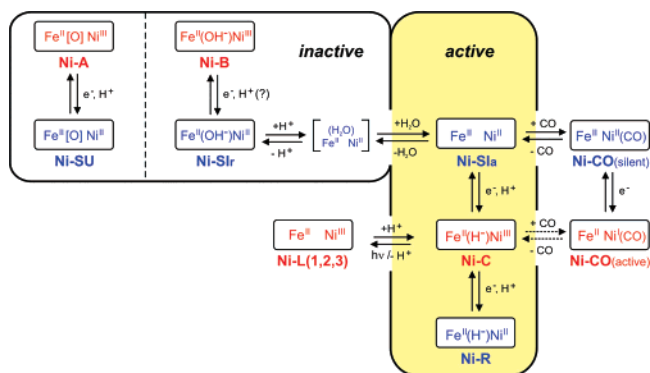


Figure 10. Schematic overview of [NiFe] hydrogenase activation/deactivation, catalytic cycle as well as the inhibition by CO and the light sensitivity. The figure only includes structural features of the intermediates directly determined from crystallographic and spectroscopic experiments and no transient species. For the various states the formal oxidation numbers for Ni and Fe are given and the third bridging ligand between them (X in Figure 1) is specified. For Ni-A, the identity of the bridging ligand [O] is still unknown. The EPR-detectable states are given in red; the EPR-silent states are given in blue. The species involved in the catalytic cycle are placed in a yellow box. Note that the redox transitions in the catalytic cycle can also be driven by molecular hydrogen ($\pm\text{H}_2$). The exact mechanism and the transient species involved are not yet known; for a recent proposal cf. to ref 271. The redox states of the three Fe–S clusters are not shown, for details see text and refs 140, 160, and 227. For other nomenclatures used for the various states in the literature see Figure 2 (caption).

5.10. The Catalytic Cycle

In the preceding sections the spectroscopic characterization of the intermediate states in the reaction cycle of [NiFe] hydrogenases has been described. In Figure 10, the transitions between the different states are given. The intermediates shown here are based on the spectroscopic data and redox titration, accompanied by proton transfer. Short-lived species that might occur in the reaction sequence are not displayed. In the following these species and their interconversion are discussed. In this process the enzyme shuttles between formal Ni^{III} and Ni^{II} states as indicated. Ni^{III} has a d_{z^2} ground state ($S = 1/2$).⁹⁴ Whether the EPR-silent Ni^{II} states are high-spin ($S = 1$) or low-spin ($S = 0$) is still an open question. By DFT calculations, the singlet and triplet states of the Ni^{II} were found to be close in energy³⁰⁴ and spin crossover was proposed to be possible at room temperature. The iron (Fe^{II}) is not redox active, and it is always low spin ($S = 0$, diamagnetic).

In the unready oxidized Ni-A state the bridging ligand, denoted as [O], is either assumed to be OH⁻^{241,243} but could also be an OOH⁻,^{71,74,80} where only one oxygen bridges the metals. Probably, the ligand is retained in Ni-SU but little information is available about the composition of the active site in this state. The inactive ready oxidized state Ni-B has been conclusively shown to contain an OH⁻ bridge; the metal redox states could also be clarified.^{94,240} After one-electron reduction the Ni-SI state is formed which is in acid–base equilibrium, Ni-SIr \rightleftharpoons Ni-SIa. It has been proposed^{85,271} that in this process first the bridging ligand (OH⁻) is protonated and forms H₂O. In *A. vinosum* hydrogenase an inactive state could be trapped at low temperature (2 °C),¹⁴³ which most probably still carries the water ligand close to the active site and hinders the reaction with H₂. This state is also not binding CO. Since the state has not been observed in other hydrogenases so far,^{86,88} it is shown in brackets in the scheme

(Figure 10). At ambient temperatures the water is removed and a highly active state, Ni-SIa, is formed. The process of reductive enzyme activation described here can also be initiated by dihydrogen. The underlying mechanism has not been elucidated yet in detail (for a proposal see ref 271).

The states involved in the catalytic cycle are believed to be Ni-SIa, Ni-C and Ni-R, which are interconverted by one electron/one proton equilibria. This information has been inferred by George et al.¹⁵⁹ and Kurkin et al.¹⁶⁰ on the basis of redox titrations and kinetic assays. The above states are also active in H/D exchange.⁸⁶ The Ni is probably the site of H₂ binding since the gas channel ends close to the Ni open-coordination site, the binding of the inhibitor CO is at Ni and the putative OOH⁻ ligand in the inactive Ni-A state is also blocking this site. In the actual catalytic process the approaching H₂ is attached to the Ni followed by base-assisted heterolytic cleavage of the H₂ molecule leading to a bridging hydride species. One of the candidates for acting as a base is the terminal cysteine (Cys530 in *D. gigas*³⁰³) that has a high-temperature factor in crystallographic studies indicating conformational flexibility and a possible role in proton transfer. Alternatively, a water molecule bound to the iron has been proposed to act as base.²⁸³ Concomitant electron transfer to the proximal Fe–S cluster then leads to the Ni-C state, which has been shown to carry a hydride bridge between Ni^{III} and Fe^{II}.^{93–95} This stable state is EPR active and is a central intermediate in the catalytic cycle. The observed two spectroscopic forms of Ni-C (split and unsplit)⁸⁵ have been attributed to its interaction with the proximal [4Fe–4S]⁺²⁺ cluster which can be either reduced or oxidized. Further reduction of Ni-C by another H₂ molecule leads to the Ni-R state which still carries the hydride.^{80,85,141} This state can occur in different subforms. It has been suggested that these forms correspond to different protonation states of Ni-R,^{85,305} but they may also be related to different spin states of the Ni^{II} and/or different conformations of the active site.^{80,88} A proposal for the mechanistic details of the reaction with H₂ in the actual catalytic cycle has recently been made in ref 271 which is based on earlier experiments.¹⁶⁰

The Ni-L states (Ni-L1 and Ni-L2) are redox states of the [NiFe] hydrogenase that are created upon illumination of Ni-C at different temperatures. The ligand field of these states is most compatible with that of a formal Ni^{III} ground state and a wavefunction of a mixed $d_{z^2}/d_{x^2-y^2}$ character (EPR active, $S = 1/2$). In Ni-L, the bridging hydride is (reversibly) transferred as a proton to a nearby base.^{93,227} It has been suggested^{80,306} that Ni-L-like states could occur as transients in the catalytic cycle. Furthermore, CO-inhibited states exist that are formed by reaction with CO from either the Ni-SIa or Ni-C states (cf. Figure 10). They are EPR-silent and EPR-active, respectively. The latter has been described as a Ni^I-CO species that upon illumination yields the Ni-L state. A discussion of the redox states of the Fe–S clusters during activation and the catalytic cycle is given in reference 140.

With all data available from the methods described in this chapter, attempts have been made to establish a chemical working model for the actual enzymatic reaction cycle of the [NiFe] hydrogenase. The first group to propose a model was Siegbahn et al.^{307,308} Others who proposed mechanisms are Hall et al.,²⁹⁷ De Gioia et al.,^{304,309} Stein and Lubitz,²⁸³ de Lacey et al.⁶⁵ and Teixeira et al.²⁷⁶ An overview of the similarities and differences of these mechanisms are given in recent reviews^{100,303} (see also de Lacey et al. in this issue).

6. Magnetic Resonance Studies of [FeFe] Hydrogenases

The H-cluster in [FeFe] hydrogenases can be present in several redox states. Only two of these, that is, H_{ox} and H_{red} , play a role in the catalytic cycle. Both of these can be characterized with IR and Mössbauer spectroscopy but only H_{ox} is paramagnetic. Therefore, the amount of information on the H-cluster which can be extracted with EPR spectroscopy is somewhat limited. Nevertheless, by studying the hyperfine interactions of the ^{57}Fe nuclei of the cluster-core as well as the ^{14}N and ^{13}C nuclei in the ligands important indications can be obtained on the unpaired spin distribution and electronic structure of the H-cluster. It turns out that the CO inhibited state of the enzyme, $H_{ox}\text{-CO}$, which is also paramagnetic, yields additional information on the redistribution of spin density in the H-cluster upon binding a substrate in the exchangeable site at Fe_d . In the following sections several important questions on the H-cluster (H_{ox} and $H_{ox}\text{-CO}$) will be addressed using advanced EPR spectroscopic methods: (i) The spin density distribution over the $[4\text{Fe-4S}]_H$ and $[2\text{Fe}]_H$ subclusters; (ii) the oxidation states of the individual iron atoms in the $[2\text{Fe}]_H$ subcluster; (iii) the effect of CO inhibition on the electronic structure; (iv) identification of a nitrogen in the bridging dithiol ligand; (v) the light sensitivity of the CO inhibited state $H_{ox}\text{-CO}$.

6.1. Overview of EPR Spectra in Various Redox States of the Enzyme

In contrast to the enzymes of *C. pasteurianum* and *M. elsdenii*, which are purified under strict anaerobic conditions,^{104,109} the hydrogenases from *D. desulfuricans* and *D. vulgaris* Hildenborough can be isolated aerobically.^{55,111,310} But in this case the enzyme is inactive (H_{ox}^{air}) and needs to be activated under reducing conditions (e.g., by H_2 or artificial reductants). The reductive activation (using mediated electrochemistry) of [FeFe]-hydrogenase from *D. vulgaris* Hildenborough has been investigated by Patil et al. and Pierik et al. using CW EPR spectroscopy^{117,150} and by Pereira et al. using Mössbauer spectroscopy.¹⁵¹ The key EPR spectra obtained during this procedure are depicted in Figure 11. In the as-isolated state an almost "isotropic" EPR signal at $g = 2.02$ is observed (trace a). This signal is often seen in preparations of enzymes containing $[4\text{Fe-4S}]$ centers. It is thought to be due to traces of an oxidized F cluster which has lost one Fe atom and is assigned to an $[3\text{Fe-4S}]^+$ cluster. The H-cluster itself is in an EPR-silent state. At a potential in the range from 0 to +200 mV (NHE) an $S = 1/2$ rhombic signal appears (trace b) characterized by a maximum g value $g_{max} = 2.06$ (for *D. vulgaris* Hildenborough the g tensor principal values are 2.06, 1.96, and 1.89) with its maximum intensity reached at about -160 mV. This signal is believed to belong to the H-cluster. Its g values are similar to characteristic values of a reduced $[4\text{Fe-4S}]$ cluster. Therefore, it was concluded that this signal is due to reduction of the $[4\text{Fe-4S}]_H$ subcluster. Also the Mössbauer data¹⁵¹ suggest that the first reduction equivalent initially is localized on the cubane. This redox state of the H-cluster is considered to be a transition state and will therefore be denoted as " H_{trans} ". Upon further lowering the redox potential, this rhombic signal is replaced by another rhombic signal (trace c) with g tensor principal values of 2.10, 2.04, and 2.00. This is a characteristic signal, observed in all [FeFe] hydrogenases, and was assigned to the "oxidized" form of the H-cluster (H_{ox}). It differs fundamentally from EPR spectra

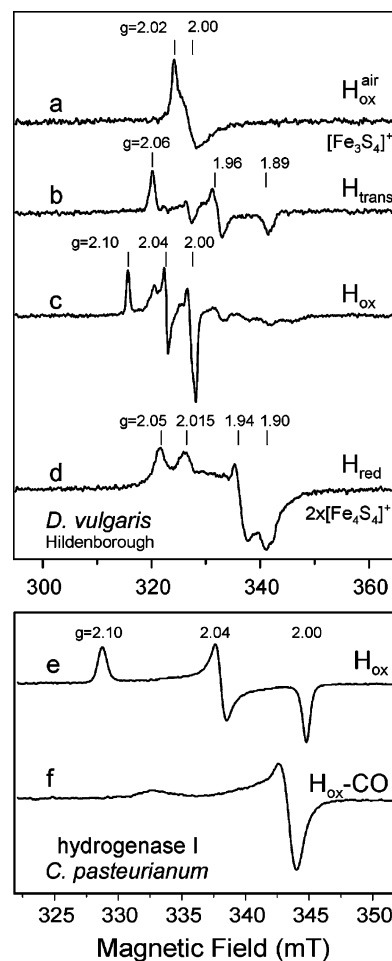


Figure 11. EPR spectra of [FeFe] hydrogenase from *D. vulgaris* Hildenborough (a–d) under different redox conditions. (Reprinted with permission from reference 117. Copyright 1988 American Society for Biochemistry and Molecular Biology, Inc.) (a) as isolated protein; (b) rhombic signal at -160 mV (H_{trans}); (c) rhombic signal at -255 mV (H_{ox}); (d) fully reduced enzyme under H_2 (H_{red}); EPR spectra from oxidized (e) and CO inhibited (f) [FeFe] hydrogenase I from *Clostridium pasteurianum* (*C.p.I.*). Figure was adapted from ref 152. (Reprinted with permission from ref 152. Copyright 2000 American Chemical Society.)

from ferredoxin type clusters $[4\text{Fe-4S}]$. The intensity of this signal is maximized at a potential of about -300 mV. Below -320 mV, the signal rapidly vanishes. Upon complete reduction of the H-cluster an EPR-silent state is obtained (H_{red}). However, another quite complex EPR signal is obtained (trace d) with its maximum intensity at -350 mV. This signal is assigned to the two reduced F-clusters (i.e., ferredoxin type $[4\text{Fe-4S}]^+$ clusters) which are dipolar-coupled. As reported by van Dijk et al., the reductive activation can be reversed only under special conditions, that is, the application of a two electron oxidant in the presence of iron and EDTA.³¹¹ In Table 4 the paramagnetic species observed in four different [FeFe] hydrogenases are summarized together with their g values. In the following the various states will be characterized in more detail.

6.2. The Oxidized (As Isolated) State

In air, as isolated, the H-cluster (H_{ox}^{air} or H_{inact}) of the hydrogenase from *D. vulgaris* Hildenborough (and *D. desulfuricans*) is "over-oxidized". It is in an inactive state. The cubane $[4\text{Fe-4S}]_H$ subcluster is oxidized and EPR silent. Because of the strong ligands the irons in the binuclear

Table 4. g-Values of Different Oxidation and Coordination States of the H-Cluster Obtained for the Various [FeFe] Hydrogenases from Different Organisms^a

state	g-component	<i>D.d./D.v.H.</i>	<i>C.p.I</i>	<i>C.p.II</i>	<i>M. elsdenii</i>
H_{trans}	g_1	2.06		(2.06) ^b	
	g_2	1.96		(1.96) ^b	
	g_3	1.89		(1.89) ^b	
H_{ox}	g_1	2.10	2.10	2.08	2.10
	g_2	2.04	2.04	2.03	2.04
	g_3	2.00	2.00	2.00	2.00
$H_{\text{ox-CO}}$	g_1	2.00	2.01	2.03	
	g_2	2.00	2.01	2.02	
	g_3	2.06	2.07	2.00	
H_{L2}	g_1	2.22	2.26		
	g_2	2.13	2.12		
	g_3	2.05	1.89		

^a *D.d.* = *D. desulfuricans*,^{135,312,313} *D.v.H.* = *D. vulgaris* Hildenborough,¹¹⁷ *C.p.I* = hydrogenase I from *C. pasteurianum*,³¹⁴ *C.p.II* = hydrogenase II from *C. pasteurianum*,¹⁷⁶ *M. elsdenii* = *Megasphaera elsdenii*.¹⁰⁸ ^b Note that the as-isolated reduced form of *C.p.II* shows a spectrum of an oxidized F-cluster identical to the H_{trans} spectrum of *D.d.*

subcluster $[2\text{Fe}]_{\text{H}}$ are in a low-spin coordination with oxidation states either Fe(II) or Fe(III). The Mössbauer data favor Fe(III), but Fe(II) cannot be excluded.¹⁵¹ The redox configuration of the $H_{\text{ox}}^{\text{air}}$ state can therefore be indicated as $[\text{Fe}(\text{II})\text{Fe}(\text{II})]_{\text{H}}[4\text{Fe-4S}]_{\text{H}}^{2+}$ or $[\text{Fe}(\text{III})\text{Fe}(\text{III})]_{\text{H}}[4\text{Fe-4S}]_{\text{H}}^{2+}$. According to the X-ray structure¹²¹ and IR studies¹²⁷ the bridging CO is present in this state and the open coordination site is occupied by H_2O or OH^- . The F-clusters in the protein are all oxidized, and EPR silent.

6.3. The Intermediate States

At a potential of about -200 mV an EPR-active state is formed (H_{trans}) assumed to be singly reduced as compared to $H_{\text{ox}}^{\text{air}}$ but with the reduction equivalent located on the $[4\text{Fe-4S}]_{\text{H}}$ subcluster. The redox configuration is therefore $[\text{Fe}(\text{II})\text{Fe}(\text{II})]_{\text{H}}[4\text{Fe-4S}]_{\text{H}}^+$ or $[\text{Fe}(\text{III})\text{Fe}(\text{III})]_{\text{H}}[4\text{Fe-4S}]_{\text{H}}^+$. No crystal structure is known from this state but it is assumed that the open coordination site is still occupied by the oxygen species (H_2O or OH^-). The IR data¹²⁷ indicate that the bridging CO is still present.

Upon further lowering the redox potential (-300 mV) another rhombic EPR species is formed. It is assumed that through (or in conjunction with) a conformational change the reduction equivalent shifts from the cubane to the binuclear cluster. In this process the coordinating ligand on the distal iron is removed. Spectroelectrochemical studies suggest that this conformational change is accompanied by an “irreversible” two electron reduction process.¹²⁷ It is not clear however which group near the H-cluster is participating in this process. The resulting H_{ox} state is observed in all hydrogenases (see Table 4) and is regarded as the physiological oxidized intermediate in the catalytic cycle. The redox state is given as $[\text{Fe}(\text{II})\text{Fe}(\text{I})]_{\text{H}}[4\text{Fe-4S}]_{\text{H}}^{2+}$ or $\text{Fe}(\text{III})\text{Fe}(\text{II})]_{\text{H}}[4\text{Fe-4S}]_{\text{H}}^{2+}$.

Early Mössbauer and ENDOR studies on the ^{57}Fe enriched hydrogenase I of *C. pasteurianum* in the H_{ox} state indicated ^{57}Fe hf couplings of around 9.5 and 17 MHz¹³⁶ (see Figure 12). A Mössbauer investigation of ^{57}Fe -enriched hydrogenase II¹³⁹ also showed two ^{57}Fe hf couplings in the H_{ox} state of about 7.5 and 18 MHz. The weak hf couplings were assigned to the iron nuclei of the $[4\text{Fe-4S}]_{\text{H}}$ subcluster, whereas the large hf coupling was suggested to belong to the proximal iron nucleus (Fe_p) of the $[2\text{Fe}]_{\text{H}}$ subcluster (see Table 5).

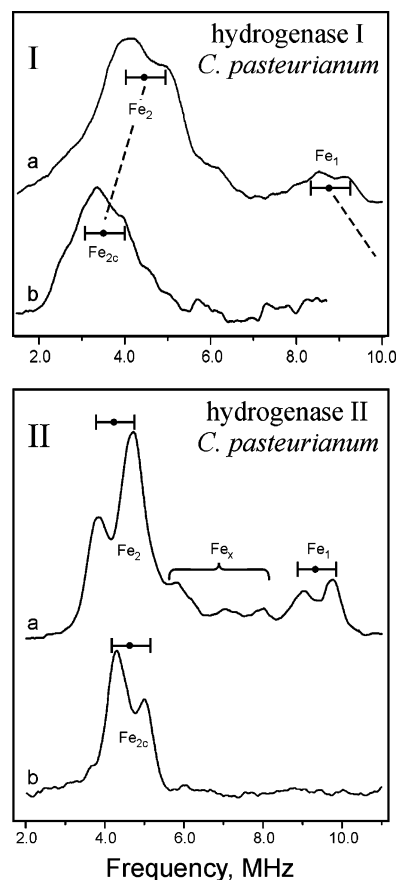


Figure 12. (I) X-band CW ENDOR (low-frequency range) of the hydrogenase I from *Clostridium pasteurianum* enriched in ^{57}Fe in the H_{ox} state (a) and in the CO inhibited state (b). Figure taken from reference 314. (Reprinted with permission from ref 314. Copyright 1986 American Society for Biochemistry and Molecular Biology, Inc.) (II): X-band CW ENDOR (low-frequency range) of the hydrogenase II from *Clostridium pasteurianum* enriched in ^{57}Fe in the H_{ox} state (a) and in the CO inhibited state (b). Reprinted with permission from ref 137. Copyright 1987 American Society for Biochemistry and Molecular Biology, Inc.

Table 5. ^{57}Fe Hyperfine Couplings [MHz] Determined for the [FeFe] Hydrogenases I and II from *Clostridium pasteurianum* (*C.p.I* and *C.p.II*) in the H_{ox} and $H_{\text{ox-CO}}$ State. For the Latter State Also the ^{13}C Couplings from the Externally Bound CO Are Listed

	H_{ox}		$H_{\text{ox-CO}}$		
	A1 (4Fe)	A2 (2Fe)	A2 (4Fe)	A1 (2Fe)	A (^{13}C)
<i>C.p.I</i> ^a	9.5	17	32.5	5.8	21
<i>C.p.II</i> ^b	7	18	30	10	34
<i>C.p.II</i> ^c	7.5, -7.5	18	25.3, -28.3	9.5	

^a From CW ENDOR (ref 314). ^b From CW ENDOR (ref 137). ^c From Mössbauer spectroscopy (ref 139).

Recent Q-band Davies ENDOR experiments on the ^{57}Fe -labeled H-cluster of *D. desulfuricans*^{312,313} offer a slightly different picture of the unpaired spin distribution over the active site. Two distinct almost isotropic ^{57}Fe hf couplings around 12 MHz were found (see Figure 13).^{312,313} A line-width comparison between the X-band EPR spectrum obtained from ^{57}Fe enriched and of the native H_{ox} showed, however, that six iron nuclei with couplings around 12 MHz each must be taken into account to explain the line broadening caused by the “unresolved” ^{57}Fe hyperfine interaction. Therefore, it must be concluded that all six iron atoms are interacting with the unpaired electron. The two stronger

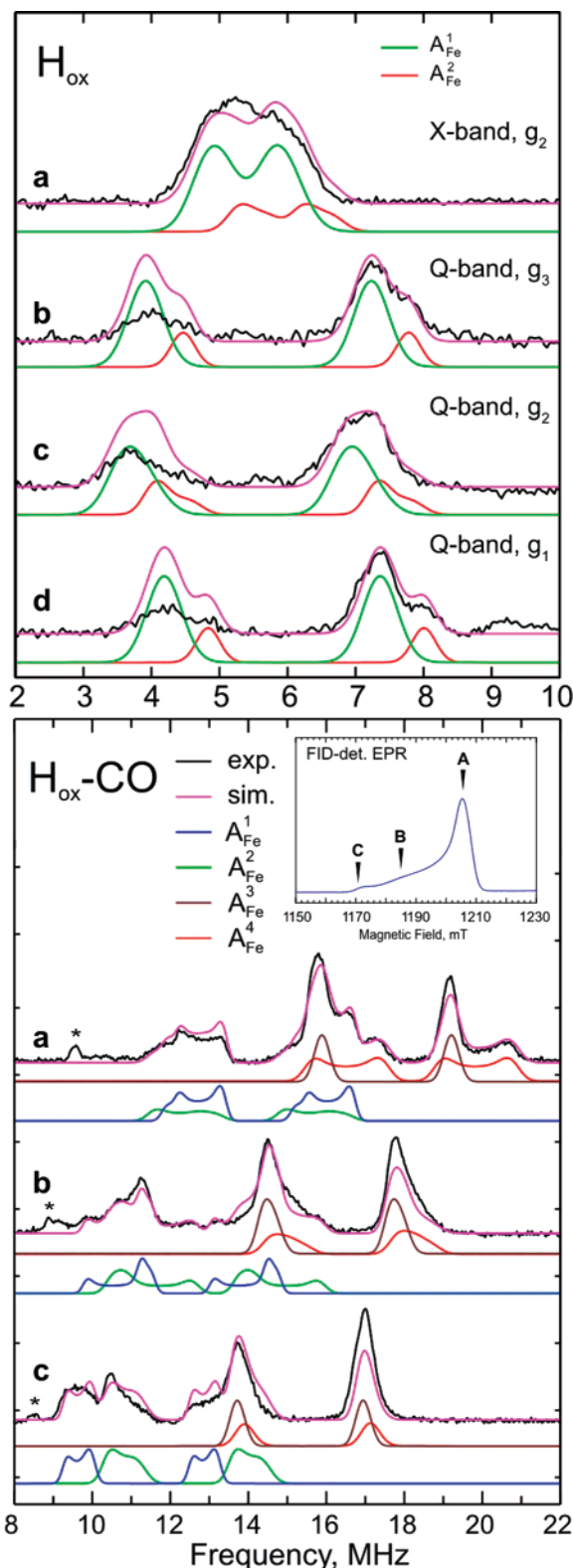


Figure 13. Top: The X-band (a) and Q-band (b–d) pulse ENDOR spectra of ^{57}Fe -enriched [FeFe] hydrogenase from *D. desulfuricans* in the H_{ox} state. The black curves represent experimental data. The magenta curves are the simulations of the ENDOR spectra using the two parameter sets presented in Table 6. Figures adapted from ref 312. Bottom: Q-band pulse ENDOR spectra of the ^{57}Fe -enriched [FeFe]-hydrogenase from *D. desulfuricans* in the $\text{H}_{\text{ox-CO}}$ state. The black lines represent the experimental data. The magenta lines represent simulations of the ENDOR spectra. The colored solid lines below each experimental spectrum, are the components of the simulation corresponding to four individual ^{57}Fe hyperfine couplings originating from the $[\text{4Fe-4S}]_{\text{H}}$ -subcluster (see Table 6).

Table 6. ^{57}Fe Hyperfine Couplings [MHz] Determined for [FeFe] Hydrogenases

		Pulse ENDOR ^a			Mössbauer spectroscopy ^b		
		$\text{H}_{\text{ox-CO}}$			$\text{H}_{\text{ox-CO}}$		
		A_x	A_y	A_z	A_x	A_y	A_z
[4Fe-4S] _H	A1	27.8	21.8	30.3			
(first pair)	A2	26.7	23.8	30.2	31.5	29.45	27.94
[4Fe-4S] _H	A3	-35.4	-35.0	-30.4	-32.19	-38.35	-30.95
(second pair)	A4	-34.5	-38.4	-30.7			
[2Fe] _H Fe _p	A5	5.3	4.5	2.2		-6.85	
[2Fe] _H Fe _d	A6	2.1	2.1	-1.7		0	
		A_x	H_{ox} A_y	A_z	H_{ox} A_{iso}		
[4Fe-4S] _H	A1,2				8.5		
(first pair)		11.2	10.4	11.6			
[4Fe-4S] _H	A3,4				-8.5		
(second pair)							
[2Fe] _H Fe _p	A5	12.3	11.4	12.9	0		
[2Fe] _H Fe _d	A6				-16.4		

^a Pulse ENDOR data for *D. desulfuricans* from refs 312 and 313; errors 0.1–0.3 MHz. ^b Mössbauer data for *D. vulgaris* Hildenborough from ref 151; errors ~1 MHz.

couplings (A_5 and A_6 in Table 6) were assigned to the $[\text{2Fe}]_{\text{H}}$ subcluster while the four weaker couplings (A_1 to A_4 in Table 6) were attributed to the cubane cluster $[\text{4Fe-4S}]_{\text{H}}$. Table 6 also lists the fitted ^{57}Fe hfc values for *D. desulfuricans* (obtained from pulse ENDOR) together with those found for *D. vulgaris* Hildenborough using Mössbauer spectroscopy.¹⁵¹ The obtained hfc values for *D. desulfuricans* are different from those found for *C. pasteurianum*. While in *D. desulfuricans* both irons of the $[\text{2Fe}]$ cluster seem to participate in the obtained hyperfine pattern the coupling detected in *C. pasteurianum* was assigned to one of the irons of the binuclear subcluster (presumably Fe_d). It should be realized that the interpretation of the Mössbauer spectra of [FeFe] hydrogenases is complicated because the two F-clusters in the protein (i.e., eight iron nuclei) are giving rise to fully overlapping spectra with that of the H-cluster. This complication is not present for the EPR spectra. In addition, also the quadrupole parameters of the ^{57}Fe excited state ($I_{\text{ex}} = 3/2$) have to be fitted. Therefore the interpretation of the obtained coupling parameters from Mössbauer spectroscopy is difficult. The interpretation of the ^{57}Fe ($I = 1/2$) ENDOR spectra, however, is more straightforward since only $I = 1/2$ doublet patterns have to be fitted. Therefore, the ^{57}Fe ENDOR analyses allow a higher accuracy in the obtained parameters. We assume that also in the case of *C. pasteurianum* hydrogenases both irons in the $[\text{2Fe}]_{\text{H}}$ subcluster are carrying spin density in H_{ox} .

Early ESEEM and ENDOR measurements focused on ^{14}N hyperfine and quadrupole interactions^{129,130} and revealed signals which can be assigned to the nitrogens in the CN^- ligands.¹³¹ Recent HYSORE measurements on the H_{ox} state³¹² confirm that the nitrogens in both CN^- ligands have similar hyperfine and quadrupole couplings. These findings support the conclusion that substantial spin density is present on both irons in the $[\text{2Fe}]_{\text{H}}$ subcluster. In the same work a third nitrogen coupling has been detected which may belong to the bridging DTN ligand (cf. Figure 1b, Scheme 1).

6.4. The H_2 -Reduced State

After reduction of the hydrogenase from *D. vulgaris* Hildenborough the EPR signal of the H-cluster disappears, indicating a one-electron reduction step. The Mössbauer

data,¹⁵¹ however, show that the cubane subcluster is still oxidized. The H_{red} state must therefore have a redox configuration $[\text{Fe(I)Fe(I)}]_{\text{H}}[4\text{Fe}-4\text{S}]_{\text{H}}^{2+}$ or $[\text{Fe(II)Fe(II)}]_{\text{H}}[4\text{Fe}-4\text{S}]_{\text{H}}^{2+}$. IR studies indicate that the signature of the bridging CO is lost.⁴⁰ This also holds for the *D. desulfuricans* enzyme.^{121,127} The crystal structure of the latter enzyme, reduced under 6 bar H_2 , suggests that the Fe_d atom has three diatomic ligands, two of which were ascribed to end-on bound CO groups. The bond between the formerly bridging CO and Fe_p seems to be absent.¹²¹ In the completely reduced state both F-clusters are reduced and give rise to the characteristic dipolar coupled EPR spectrum (see Figure 11).

When the H_{red} state of *D. desulfuricans* is incubated under argon for 10 to 30 min the enzyme apparently becomes active in proton reduction and transforms to the H_{ox} state.¹⁰² In most preparations, however, the dipolar coupled EPR spectrum of the reduced F-clusters does not completely disappear^{131,135} indicating an incomplete (nonstoichiometric) conversion.

6.5. The CO-Inhibited State

The active enzyme is very sensitive to inhibition by CO. In this state the open site at Fe_d is coordinated by the extrinsic CO ligand. This species is characterized by an axial EPR spectrum¹¹⁶ ($g_{\perp} = 2.006$, $g_{\parallel} = 2.065$) (see Figure 11f). The inhibited state can be obtained by incubation of the enzyme in the H_{ox} state under CO (0.4 atm) for 5 min. Also from the H_{red} state the enzyme can be inhibited, but for hydrogenase I of *C. pasteurianum* after 5 min of CO treatment only 50% of the hydrogenase is contributing to the axial EPR signal. The rest of the spectrum indicates only a partial oxidation of the F-clusters, while the other 50% of the H-clusters are still EPR silent.¹⁵² This confirms that the CO inhibition is competitive with proton reduction (H_2 formation), because this process will leave the H-cluster in the oxidized state with its open coordination site which is then subsequently blocked by the extrinsic CO.

In a CW ENDOR study by Telser et al.³¹⁴ the H_{ox} -CO state of hydrogenase I of *C. pasteurianum* was investigated using ^{57}Fe -enriched protein as well as ^{13}C -labeled CO gas. The inhibition by CO turned out to have a profound effect on the ^{57}Fe hf couplings observed for H_{ox} (see above). The lowest value ($A_1 = 9.5$ MHz) dropped to $A_1^{\text{CO}} = 5.8$ MHz while the largest one ($A_2 = 17$ MHz) increased to $A_2^{\text{CO}} = 31\text{--}34$ MHz (see Figure 12 top). The ^{13}C hfc of the extrinsic CO was found to be 21 MHz. The ^{57}Fe and ^{13}C hfc values are in the same range as found for a series of $\text{Fe}_x(\text{CO})_y$ complexes.^{315,316} Similar results ($A_1 = 7$ MHz, $A_1^{\text{CO}} = 10$ MHz, $A_2 = 18$ MHz, $A_2^{\text{CO}} = 30$ MHz) were obtained for the ^{57}Fe hfc of hydrogenase II from *C. pasteurianum*¹³⁷ (see Figure 12 bottom). The ^{13}C coupling of the H_{ox} -CO state, however, was found to be around 34 MHz, which is 50% larger than that recorded for hydrogenase I from *C. pasteurianum*. The comparison of the hfc values of the two hydrogenases from *C. pasteurianum* is summarized in Table 5. Mössbauer studies¹⁷⁶ largely confirmed the observed ^{57}Fe couplings. The Mössbauer study by Popescu and Münck¹³⁹ also listed ^{57}Fe hf couplings of the CO inhibited state for hydrogenase II from *C. pasteurianum*: hfc constants were found in the range of 25–28 and 9.5 MHz. In this case, the large couplings were assigned to the cubane subcluster $[4\text{Fe}-4\text{S}]_{\text{H}}$ (according to the intensities of the lines and the isomeric shift) and the small coupling to the Fe_p nucleus of the binuclear subcluster. This behavior points to large changes in the electronic structure of the H-cluster upon binding of the external CO ligand.

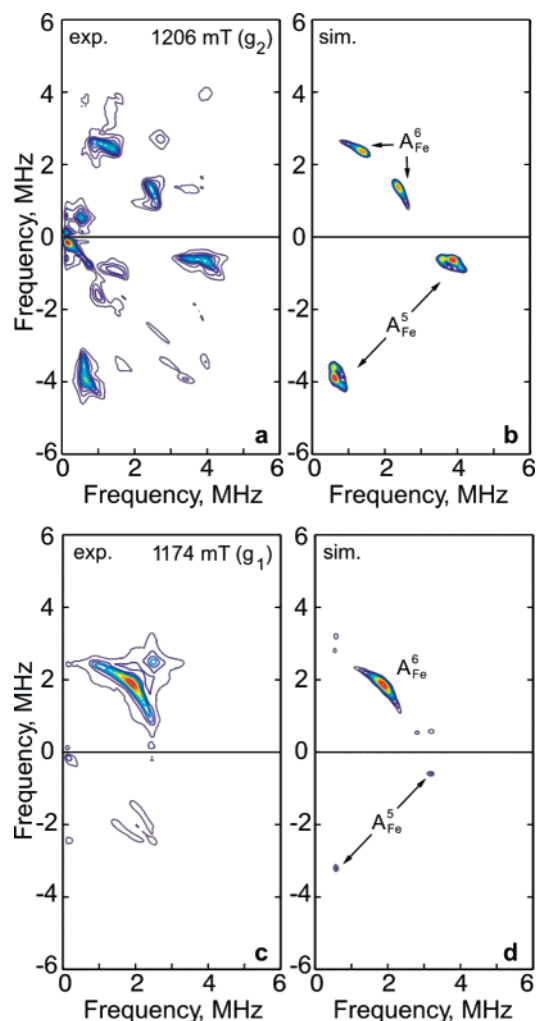


Figure 14. Q-band HYSCORE spectra of [FeFe]-hydrogenase from *D. desulfuricans* at $T = 20$ K in the H_{ox} -CO state at different magnetic fields: (a) 1206 mT (g_2) and (c) 1174.0 mT (close to g_1) and simulated spectra (b,d) using parameters A_5 and A_6 from Table 6. Figure taken from reference 312.

The distal iron atom in the binuclear subcluster $[2\text{Fe}]_{\text{H}}$ was suggested to be diamagnetic and carrying no spin density. Later, Pereira et al.¹⁵¹ used Mössbauer spectroscopy for the investigation of the [FeFe] hydrogenase from *D. vulgaris* (Hildenborough). For this H-cluster hfc values were found to be similar to the ones of hydrogenase II from *C. pasteurianum* determined by Popescu and Münck. The observed hfc values of ^{57}Fe and ^{13}C are summarized in Table 5.

The most recent EPR investigations on the ^{57}Fe labeled H-cluster of *D. desulfuricans* using Q-band pulse ENDOR and ESEEM techniques^{312,313} offer a more differentiated picture of the unpaired spin distribution over the active site. The increased magnetic field (1.2 T at Q-band vs 0.35 T at X-band) leads to a larger nuclear Zeeman interaction ($\nu(^{57}\text{Fe}) = 4$ MHz) and thus to a significant improvement of the spectral resolution of the ^{57}Fe hyperfine interactions.

The Q-band Davies ENDOR study on the H_{ox} -CO state revealed unique ^{57}Fe hf couplings of all four iron atoms in the $[4\text{Fe}-4\text{S}]^{2+}$ subcluster (Figure 13). Furthermore, triple resonance experiments confirmed the opposite signs of the hf couplings originating from the two Fe(II)Fe(III) pairs in the cubane. The hf couplings from the two irons in the $[2\text{Fe}]_{\text{H}}$ subcluster were not detected in Q-band ENDOR. However, Q-band HYSCORE spectra (see Figure 14) revealed clear spectral features that could be assigned to two relatively small

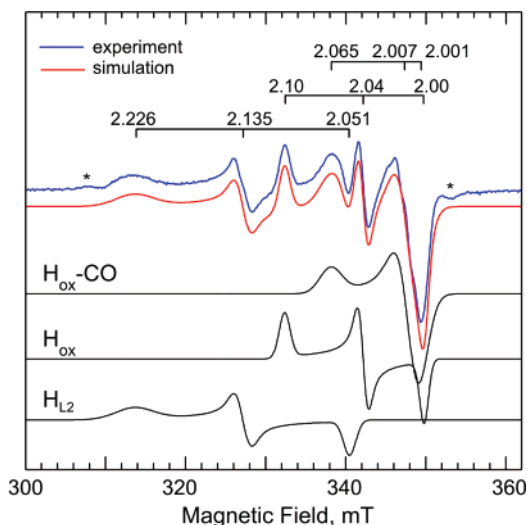


Figure 15. Paramagnetic species obtained from the H_{ox} -CO state from *D. desulfuricans* ATCC-7757 upon photodissociation using laser illumination (531 nm, 8.5 mJ/pulse) for 2 h, $T = 40$ K. Figure taken from reference 312.

^{57}Fe hf couplings from the binuclear subcluster $[2\text{Fe}]_H$. While for the *C. pasteurianum* hydrogenases it seems that only one iron nucleus (presumably Fe_p) contributes to the observed hf interactions, for *D. desulfuricans* hydrogenase both iron nuclei in the $[2\text{Fe}]_H$ subcluster clearly show a hf interaction. Again it should be realized that the Mössbauer analysis^{139,151} of the H_{ox} -CO state might not have resolved all couplings, that is, the smallest hyperfine interaction in the H_{ox} -CO state, so that also in *C. pasteurianum* hydrogenase both iron nuclei in the $[2\text{Fe}]_H$ subcluster may carry spin density. It also should be pointed out that a substantial ^{13}C hyperfine interaction is observed from the inhibiting ^{13}C ligand in the H_{ox} - ^{13}C CO state.³¹⁴ This also points to a nonzero spin density at the distal iron atom.

6.6. Light Sensitivity of the CO-Inhibited State

From IR investigations it is known that upon light excitation at temperatures between 20 and 70 K the external CO ligand can be reversibly removed. After illumination with white light for 1 h, a substantial amount of the H-cluster is converted into a state H_{L1} of which the EPR spectrum is identical to that of the H_{ox} state (see Figure 15). The H_{ox} -CO state can be recovered by annealing the sample (in the dark) above 150 K, thereby restoring the axial EPR spectrum.^{40,118,135} During illumination an additional state of the H-cluster can be obtained. This state (H_{L2}) is characterized by a broad rhombic EPR spectrum with g -tensor principal values of 2.221, 2.132, and 2.048 for *D. desulfuricans*¹³⁵ and 2.26, 2.12, and 1.89 for hydrogenase I from *C. pasteurianum*.¹³⁸ The species generated from H_{ox} -CO from *D. desulfuricans* are depicted in Figure 15. FTIR studies on both hydrogenase I from *C. pasteurianum* and *D. desulfuricans* hydrogenase show that for the (H_{L2})-state the signature of the bridging CO is lost. This indicates a complete dissociation of this CO ligand or a conversion to terminal coordination.^{127,134} Since no IR vibration indicative of an additional terminal CO has been found, the CO association must be considerably weaker than a “regular” CO bound to the metal or it is completely absent. Albracht et al.¹³⁵ have recently shown that the H-cluster of *D. desulfuricans* is very light sensitive in general at room temperature in the H_{ox} and H_{red} states. Under ambient light conditions the enzyme can be severely damaged during reductive activation and incubation

under argon. One H-cluster may lose its CO ligands under irradiation and be irreversibly inactivated. Other H-clusters will pick up the dissociated CO ligands and become inhibited. This explains the occurrence of the H_{ox} -CO EPR signal in preparations of hydrogenases which never were exposed to CO. The enzyme is, however, light stable when in the H_{ox}^{air} or H_{ox} -CO state, although the latter state is affected by light as well (as was already discussed above). A detailed FTIR study on H_{ox} -CO in which the extrinsic CO ligand was labeled with ^{13}C showed that all three CO ligands associated with Fe_d can be exchanged under illumination at room temperature.¹²⁷ Inhibition by O_2 is believed to be irreversible. Thin film electrochemical studies by Vincent et al.²⁶⁴ show that the activity of the enzyme is strongly reduced after exposure to oxygen. Binding of oxygen to the free coordination site (in the H_{ox} and H_{red} state) may oxidize the binuclear iron cluster to Fe(III) causing the loss of the CO and CN^- ligands, thereby destroying the H-cluster.

6.7. Electronic Structure of the H-Cluster

6.7.1. Origin of the ^{57}Fe Hyperfine Couplings in the H-Cluster

As explained in Appendix III, the $[4\text{Fe}-4\text{S}]_H$ subcluster is formally diamagnetic because of the strong antiferromagnetic coupling between the two valence delocalized $S = 9/2$ Fe(II)Fe(III) pairs. Therefore no ^{57}Fe hyperfine couplings are expected from this subcluster. Because of the additional spin-exchange interaction between the corner Fe(II/III) atom of the cubane and the proximal Fe atom, Fe_p , of the binuclear subcluster, the symmetry within the cubane cluster is broken. Therefore, higher spin states are mixed into the singlet ground state of the $[4\text{Fe}-4\text{S}]_H$ subcluster and effective ^{57}Fe hyperfine interactions are induced. This mixing effect strongly depends on the relative magnitudes of the inter-subcluster spin-exchange interaction and the spin-exchange interaction within the cubane (see Appendix III). The theory also predicts that the ^{57}Fe hyperfine interactions from the two Fe(II)Fe(III) pairs are opposite. This has been confirmed by the Mössbauer studies on the H-clusters of hydrogenase II from *C. pasteurianum*,¹³⁹ the hydrogenase from *D. vulgaris* Hildenborough,¹⁵¹ and the pulsed ENDOR study on the hydrogenase from *D. desulfuricans*.^{312,313} The difference in the contribution of the $[4\text{Fe}-4\text{S}]_H$ subcluster to the observed hfc pattern between the H_{ox} and H_{ox} -CO state is caused by the difference in the inter-subcluster exchange interaction “ j ” of these states. The H_{ox} -CO state is characterized by a strong j interaction (see Figure 16) leading to an enhanced hf contribution from the cubane and a reduced contribution from the binuclear cluster. In the H_{ox} state, this exchange interaction is much reduced so that the contribution from the binuclear cluster becomes much stronger while the mixing effect in the cubane cluster is reduced. In both states the proximal Fe (Fe_p) must be carrying “intrinsic” spin density to account for the j interaction. This has consequences for the electronic structure of the intermediates and the catalytic function of the enzyme (*vide infra*). The spin delocalization within the $[2\text{Fe}]_H$ subcluster is assumed to result from orbital overlap through the bridging ligands and a direct metal–metal bond.³¹⁷

6.7.2. Redox States of the Iron Atoms in the Binuclear Cluster

Concerning the possible redox states of the binuclear iron cluster in the various catalytic states there is still some debate. Popescu and Münck¹³⁹ have concluded (based on the isomeric shift) that the $[4\text{Fe}-4\text{S}]_H$ subcluster remains in the

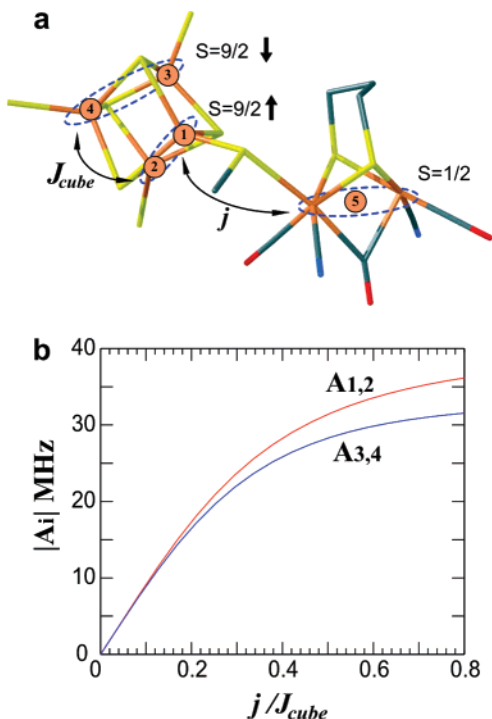


Figure 16. (a) Scheme of exchange interactions within the H-cluster of [FeFe] hydrogenase (adapted from ref 317). Two valence-delocalized Fe(II)Fe(III) pairs in the cubane subcluster, having a total spin of $S_{\text{pair}} = 9/2$ each, are antiferromagnetically coupled by the HDVV exchange interaction J_{cube} . This results in a diamagnetic ground state $S = 0$. Coupling of the fifth spin $S_{\text{H}} = 1/2$ of the binuclear cluster to the closest iron of the “cubane” admixes the first excited state $S = 1$ of the cubane into the ground state, and gives rise to effective spin density on the irons of the cubane. (b) Dependence of the ^{57}Fe hfc's on the strength of the exchange interactions j and J_{cube} according to eq 7 (Appendix III) assuming an isotropic hyperfine coupling of $a = -22$ MHz (adapted from ref 139).

[2+] state in the H_{ox} , $\text{H}_{\text{ox}}\text{-CO}$, and H_{red} species. In the same work the authors proposed an $[\text{Fe}_p(\text{II})\text{Fe}_d(\text{III})]$ oxidation state of the binuclear cluster in the H_{ox} and $\text{H}_{\text{ox}}\text{-CO}$ states in which the magnetic spin is located on the distal iron (Fe_d). However, the possibility of a $\text{Fe}_p(\text{II})\text{Fe}_d(\text{I})$ configuration was not completely excluded. On the other hand, DFT calculations on model systems^{318,319} are in favor of the latter possibility. This would mean that the $[\text{2Fe}]_{\text{H}}$ subcluster in the fully oxidized, inactive state ($\text{H}_{\text{ox}}^{\text{irr}}$) is described as $\text{Fe}_p(\text{II})\text{Fe}_d(\text{II})$, in the oxidized active state (H_{ox}) as $\text{Fe}_p(\text{II})\text{Fe}_d(\text{I})$, and in the reduced, active state (H_{red}) as $\text{Fe}_p(\text{I})\text{Fe}_d(\text{I})$ species. Inorganic model systems of the binuclear subcluster have been prepared³²⁰ which show that in the completely reduced state the $\text{Fe}(\text{I})\text{Fe}(\text{I})$ arrangement is very stable. These findings have also been confirmed by later quantum chemical calculations.³²¹ De Lacey et al.¹²⁶ argue in their early IR study on the H_{ox} and $\text{H}_{\text{ox}}\text{-CO}$ state that, based on the relative frequency of the CO ligand stretch vibrations, the distal iron has a lower oxidation state than the proximal one. More recent IR studies¹²⁷ including all states for the H-cluster indicate, however, that the CO-stretch vibration of the ligand bound to the proximal iron is not changing its frequency between the oxidized and the reduced state of the H-cluster showing that the oxidation state of Fe_p remains the same. Therefore it must be concluded that Fe_p is already in its lowest oxidation state. At the same time the ENDOR and ESEEM results^{312,313} indicate that the proximal iron is formally paramagnetic in the H_{ox} and $\text{H}_{\text{ox}}\text{-CO}$ state. This condition can only be fulfilled

if Fe_p remains Fe(I) in these two states. The H_{ox} state is then characterized by a $[\text{Fe}_d(\text{II})\text{Fe}_p(\text{I})]$ configuration, while H_{red} is in the fully reduced $[\text{Fe}_d(\text{I})\text{Fe}_p(\text{I})]$ state. The recent ENDOR and ESEEM experiments, in combination with the IR data seem to support the earlier conclusions based on DFT calculations and model system studies in that H_{red} is characterized by the most reduced Fe species. The pulse EPR spectroscopic data,^{312,313} the IR spectroscopic data,¹²⁷ and the most recent DFT calculations on the whole H-cluster by Fiedler and Brunold,³¹⁷ however, do not give a consistent picture on the possible spin and valence delocalization within the $[\text{2Fe}]_{\text{H}}$ cluster in the H_{ox} and $\text{H}_{\text{ox}}\text{-CO}$ states. The most recent IR data seem to indicate that the Fe(I) valence remains localized on Fe_p , while both pulse EPR and DFT data suggest that in one of the states a strong delocalization occurs. According to the observed ^{57}Fe and ^{14}N hyperfine interactions the H_{ox} state would be characterized by a strong delocalization over both iron atoms and the $\text{H}_{\text{ox}}\text{-CO}$ state by a localization of the spin on $\text{Fe}_p(\text{I})$. On the other hand the DFT calculations suggest that in the $\text{H}_{\text{ox}}\text{-CO}$ state a delocalization occurs over both iron atoms while in the H_{ox} state the spin is localized on $\text{Fe}_d(\text{I})$. The DFT calculations and pulse EPR experiments agree, however, on the point that binding of the external CO significantly shifts the spin density toward the $[\text{4Fe-4S}]_{\text{H}}$ cluster.

6.8. Possible Mechanisms for the Catalytic Cycle

The fact that only one of the redox states in the catalytic cycle (H_{ox}) is EPR active makes it difficult to use the information on the magnetic interactions within the H-cluster to derive a clear-cut picture of the reaction mechanism. From the observed ^{57}Fe hyperfine interactions it is, however, apparent that the iron atoms in the binuclear subcluster $[\text{2Fe}]_{\text{H}}$ and the cubane subcluster $[\text{4Fe-4S}]_{\text{H}}$ are in strong electronic contact, thus facilitating electron transport to and from the F-clusters in the protein. As was already discussed in the previous sections the ^{57}Fe hyperfine pattern for the H_{ox} state suggests an almost equal spin distribution over the two iron atoms of the binuclear subcluster.^{135,312,313} Upon binding of the external CO ($\text{H}_{\text{ox}}\text{-CO}$ state) the observed spin density is shifted toward the proximal iron and the cubane subcluster, but again the IR data show that the formal oxidation state of the Fe_p is not changed, that is, it remains Fe(I). On the other hand recent DFT calculations³¹⁷ on the H_{ox} state favor a valence localized $\text{Fe}(\text{I})\text{Fe}(\text{II})$ pair in which the unpaired electron is located on the distal Fe while the $\text{H}_{\text{ox}}\text{-CO}$ state is characterized by a valence delocalized Fe-Fe pair. The authors state that although the effect of the cubane subcluster was fully included in the geometry optimized structure the calculated ^{57}Fe hyperfine values deviate substantially from the experimental ones. The calculated couplings were also strongly dependent on the protonation state of the linking cysteine sulfur bond. Apparently, the electronic structure of the H-cluster is very sensitive to slight changes in the geometry so that accurate predictions of hyperfine couplings and spin distributions may have to wait for even more advanced quantum chemical calculations. Nevertheless, various DFT calculations of the H-cluster and its possible transition states (e.g., involving the binding of molecular hydrogen) offer very useful insights in the possible scenarios of the catalytic cycle.

The overall consensus oxidation/reduction reaction scheme is depicted in Figure 17 where it is assumed that electron and proton transport will take place in (almost) simultaneous steps. Several studies involve the stability of the hydride

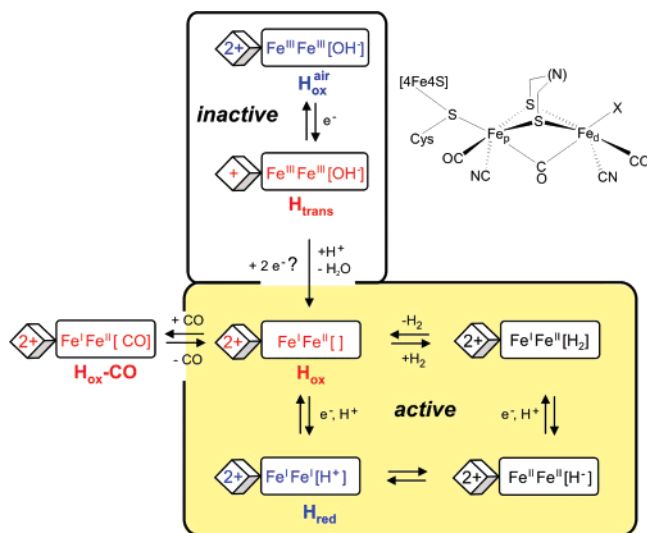


Figure 17. General scheme of redox states of the H-cluster and the proposed catalytic cycle for [FeFe] hydrogenase. For the various states the oxidation numbers of the 2 Fe ions in the binuclear subcluster are given together with the oxidation level of the cubane cluster. The ligand X occupying the sixth coordination site at Fe_d are given for all states. The EPR-active states are given in red, the EPR-silent states in blue, and transient states in black. The species involved in the catalytic cycle are placed in a yellow box. For further details see text.

intermediate in which a hydride is attached to the Fe(II)Fe(II) subcluster either bound terminally to the distal iron^{290,318,319} or in a bridging position between the two irons.^{322–325} It turns out that both configurations are feasible but the bridging configuration is thermodynamically more stable. This would suggest that the hydrogen splitting and proton reduction will occur in the bridging position. At the same time, however, it has been demonstrated by Hall et al.³²⁶ that the amine group in the proposed DTN bridging ligand would provide an excellent proton acceptor in the catalytic cycle. In addition the crystal structure provides a proton pathway through the protein leading to the DTN bridging ligand.¹²¹ If the hydride would bind in the bridging position the dithiolate sulfur ligands could act as proton acceptors but it would also require the bridging CO ligand to flip over to the terminal position on the distal iron. Thermodynamically this rearrangement would be feasible but it is not clear if the active site provides sufficient flexibility to allow such a ligand exchange process at high rates (i.e., compatible with the high turnover rates of the enzyme). Furthermore, it is not clear if the proton reduction (H₂ production) and H₂ oxidation (uptake) reaction will follow the same mechanism. Recent kinetic studies on the H₂ uptake reaction suggest that two molecules H₂ bind to the enzyme while only one of these is split.³²⁷ Strictly speaking, the structure of H_{red} with the bridging CO shifted to the terminal position at Fe_d, could accommodate two additional Fe ligands (e.g., H₂) to complete a sixfold coordination of each iron center. One of the H₂ molecules could thus bind at Fe_p (low affinity site) to activate the binuclear cluster, while the second H₂ might subsequently bind to Fe_d (high affinity) where it is heterolytically split. The activation step may involve the oxidation of Fe_p(I) to Fe_p(II) followed by H₂ binding and subsequent oxidation of Fe_d(I) to Fe_d(II). In the final step the second H₂ could bind and the proton be accepted by the DTN ligand amine, whereas the hydride reduces the Fe_p(II)Fe_d(II) unit to Fe_p(I)Fe_d(I) while releasing the proton. Experimental strategies to elucidate the catalytic mechanism

could involve (i) the creation of protein mutants (e.g., restricting the proton transport) which will stabilize additional intermediates, (ii) time-resolved FTIR measurements on proteins immobilized on an electrode, (iii) study of artificial H-clusters and model complexes. In addition, more sophisticated DFT calculations may shed light on the effect of the cubane subcluster in electron transport and the possible CO ligand rearrangement during the catalytic cycle.

7. Concluding Remarks

Paramagnetic metal sites occur in the [NiFe] and [FeFe] hydrogenases. Therefore, EPR is playing a central role in the identification and structural characterization of these enzymes. This technique has been used to identify nickel as a constituent of the active site of [NiFe] hydrogenase, to identify some of the iron-sulfur clusters and their interaction with the active center, to determine midpoint potentials for the redox transitions of this enzyme, to identify the valence and spin states of the metal ions, and to clarify their coordination geometry in the various steps of the reaction cycle. The method can only be employed to study “EPR-active” states. The combined use of spectroscopic and theoretical methods proved to be particularly fruitful in hydrogenase research to obtain reliable structures of reaction intermediates. Such experimental data are mainly derived from EPR and FTIR studies. For the identification of the substrate (H₂) binding site, X-ray crystallography of single crystals does not suffice, since the protons are not resolved in the electron density. Fortunately, hydrogen has a large magnetic moment and a nuclear spin of 1/2, so that detection by magnetic resonance methods is possible. In paramagnetic systems like the [NiFe] and [FeFe] hydrogenase, interaction of the metal center with hydrogen ($I = 1/2$) or deuterium ($I = 1$) leads to electron–nuclear hyperfine splitting in the spectra. This is only rarely detectable directly by CW EPR but can be resolved by pulse techniques, for example, HYSCORE, or double resonance methods like ENDOR. For [NiFe] hydrogenases, this allowed identification of the binding site of the substrate hydrogen and its respective products (e.g., the bridging hydride in Ni-C) in the active site. The generation of Ni-L from Ni-C by low-temperature illumination is accompanied by photodissociation of the hydride, which is important for understanding hydrogenase function. The detection of a hydroxide ligand in the bridging position in the oxidized active state using ¹⁷O and ¹H ENDOR and HYSCORE helped to understand the activation and deactivation mechanism of the enzyme. The Ni-A state is currently a focal point of interest to study oxygen sensitivity and inhibition of the enzyme that is related to either changing the geometric or electronic structure of the active site or the gas channel.

For the [FeFe] hydrogenases EPR was also instrumental to identify the various paramagnetic species in the reaction cycle. The spin distribution in the H-cluster was determined from analysis of the ⁵⁷Fe hyperfine couplings in the respectively labeled enzyme. Inhibition and light sensitivity has also been studied in detail and information has been obtained on the additional iron–sulfur clusters. The question of the presence of nitrogen in the unusual bridging dithiolate ligand has been approached by ESEEM techniques, and ⁵⁷Fe ENDOR was instrumental in combination with other methods like FTIR and Mössbauer spectroscopy to determine the formal oxidation states of the iron ions in the H-cluster. With respect to the actual hydrogen conversion mechanism less information is available for [FeFe] than for [NiFe] hydrogenase at present. In one possible scenario the hetero-

lytic H₂ splitting takes place at the distal iron with the nitrogen in the dithiolate bridge acting as base for the proton. In another scenario the two metals serve as the primary binding site, a hydride bridge is formed, and, for example, a thiolate sulfur acts as base, which is similar to the mechanism for the [NiFe] hydrogenase. The problem here is that the active reduced intermediates are EPR-silent so that different methods must be employed for a structural characterization.

To better understand hydrogenase structure and function it is useful to compare the two types of enzymes, in particular their active sites. [NiFe] and [FeFe] hydrogenases are not related evolutionary; they have a different protein structure and require different genes for their biosynthesis. However, they share some astonishing similarities and fulfill a very similar task. The bimetallic centers carry CN⁻ and CO ligands at the iron and have a Me₂S₂ butterfly shaped core. This common motif is found for all classes of hydrogenases and might indicate a functional role in dihydrogen activation. The metal–metal distances lie in the range 2.5–2.9 Å (indicating a metal–metal bond), bridges are provided by two cysteine thiolates (NiFe) and a bidentate di(thiolato-methyl)amine or a 1,3-propanedithiolate ligand (FeFe). A third bridging ligand is present between the metals that is released and replaced by a hydride in the catalytic cycle of [NiFe] hydrogenase. In case of [FeFe] hydrogenase the involvement of this bridging position (e.g., in hydride binding) is still unclear. Both enzymes have metals with square pyramidal geometries and an open site to coordinate dihydrogen. Both enzymes catalyze the H/D exchange reaction between H₂ gas and D₂O showing that the H₂ splitting is heterolytic. This is not found for hydrogen conversion using heavy metal catalysts like Pt or Pd in chemical processes, where the splitting is homolytic. Obviously, in the case of hydrogenase the metal renders the dihydrogen ligand sufficiently acidic (at pK_a = 7) to be deprotonated, probably by a nearby nitrogen or sulfur base, leaving a hydride at the metal center.

The catalytic activity is inhibited in both enzymes by CO and O₂. In the case of [FeFe] hydrogenase the inhibition by dioxygen is (often) rapid and irreversible and leads to destruction of the enzyme, whereas for [NiFe] hydrogenase oxygen inhibition is (partially) reversible, even oxygen tolerant species like *Ralstonia eutropha* have been found. These differences in oxygen sensitivity are not yet fully understood. They may be related to the type, coordination sphere, and geometry of the active site metal; the size and type of the hydrogen access channel has also been discussed to play a role in the inhibition process.

In the catalytic process at least two redox states occur, an oxidized one (Ni^{III}Fe^{II} and Fe^{II}Fe^I) and a reduced one (Ni^{II}Fe^{II} and Fe^IFe^I). The former mixed valence states (present in Ni-C and H_{ox}, respectively) are paramagnetic with an *S* = 1/2 ground state and a metal in a low-spin d⁷ electron configuration (Ni^{III} and Fe^I); they give similar rhombic EPR spectra. Considering the further ligand sphere, it is remarkable that the 5-coordinated active centers also have the same total charge. However, there are also striking differences between the two classes of enzymes. First of all, in [NiFe] hydrogenase one iron is replaced by nickel with some differences in the direct coordination sphere (number of thiolates ligands). In [FeFe] hydrogenase a bridging CO is present between the two metals that is not found for [NiFe] hydrogenase, and a bridging hydride has not been definitely detected in the [FeFe] enzyme.

In industrial processes heavy metals are widely used as catalysts for hydrogen conversion. In hydrogenases, nature

has used the more abundant first row transition metals Ni and Fe instead; here the ligand sphere has obviously been tailored accordingly to adjust the electronic structure of the metals for optimum performance of these enzymes. The CO/CN⁻ ligands are known to stabilize Fe in a low (more electron-rich) oxidation state, furthermore the strong ligand field will result in a low spin state (*S* = 0). The thiolates are non-innocent ligands leading to a significant electron spin (and charge) delocalization. This has been detected for the different states, for example, for [NiFe] hydrogenase, where only ~50% of the spin is at the Ni. In this way the system avoids larger shifts of spin and charge density in the catalytic cycle, which reduces the reorganization energy. The redox active metal (Ni or Fe) changes oxidation state *formally* by only ± 1 in the whole catalytic cycle; effectively this change in charge will even be much smaller.

Another important question concerns the significance of the protein surrounding. It keeps the active site and the other cofactors in the right place for the enzymatic reaction, it provides direct ligands for the active center, channels for educts and products (H₂, H⁺), it hosts the protein's electron transport chain and even participates in it, and provides attachment sites for the secondary electron acceptors/donors. Very little is known to date about the molecular details of these processes, which is partially due to the nondeveloped molecular genetics for many systems. In addition, the protein might actively be involved in the various steps of the whole mechanism by providing just the right electrostatic local environment and the appropriate dynamical modes for the specific task of hydrogen splitting or production to occur with high rates. Another important aspect that requires further studies is hydrogenase maturation, including the generation of the unusual active sites.

In view of the high complexity of the biological systems the question arises if it will be possible in the foreseeable future to obtain good hydrogenase activity in biomimetic or bioinspired synthetic systems. This is certainly not an easy task since it requires more than just the clever construction of a catalytic metal center, namely the inclusion of a smart matrix mimicking the protein surrounding. The creation of such functional catalytic machines presents one of the main challenges for the synthetic bioinorganic/bioorganic chemist in future years.

8. List of Abbreviations

CW	continuous wave
DEER	double electron–electron resonance
DFT	density functional theory
ENDOR	electron nuclear double resonance
EPR	electron paramagnetic resonance
ESE	electron spin echo
ESEEM	electron spin echo envelope modulation
EXAFS	extended X-ray absorption fine structure
FID	free induction decay
FTIR	fourier transform infrared
hf	hyperfine
hfc	hyperfine coupling
HYSCORE	hyperfine sublevel correlation (spectroscopy)
MBH	membrane bound hydrogenase
NMR	nuclear magnetic resonance
PELDOR	pulsed electron–electron double resonance
RH	regulatory hydrogenase
SH	soluble hydrogenase
TRIPLE	electron–nuclear–nuclear triple resonance
XANES	X-ray absorption near edge spectroscopy
XAS	X-ray absorption spectroscopy
ZORA	zeroth-order regular approximation

9. Acknowledgments

We would like to acknowledge the many important contributions of our collaborators whose names appear in the respective references. We are grateful to B. Plaschkes and B. Deckers for their help in preparing the text and the figures. The authors are also indebted to M. Flores, M.-E. Pandelia, and A. Silakov (all MPI Mülheim) for helpful discussions and critically reading the manuscript. The work was supported by the Deutsche Forschungsgemeinschaft, the Max Planck Society, the BMBF (Bio-H₂), and the European Union (SOLAR-H).

10. Appendix I. Advanced EPR Methods Used in Hydrogenase Research

In this section a short overview is given of the general pulsed EPR methods used in most of the studies cited in this review. The appendix is intended to describe the strengths of each method and give the reader a feeling for how these techniques can be efficiently employed. A more in-depth and detailed explanation of these methods, including references to original articles, is given in the literature, for example, in the book of Schweiger and Jeschke.¹⁹³

10.1. FID-Detected EPR

In this technique, one 90° pulse is applied to the spin system, to transfer the magnetization from the *z*-axis (parallel to the magnetic field) into the *xy* plane. As the spins, which are aligned immediately after the microwave pulse, start to dephase because of inhomogeneities of the internal field felt by the electron spins, the net magnetization decreases with a time constant T_m , the phase memory time. The decay, indicated in yellow in Figure 18 is called the free-induction decay (FID). This method is rarely used to obtain information about the system, because for a certain time directly after the microwave pulse, signal detection is impossible, and during this dead-time of the spectrometer most of the magnetization usually decays. Moreover, unlike in NMR spectroscopy, the spectral width of the EPR signal is too large for a complete excitation with one microwave pulse. In practice, the experiment has therefore to be performed by measuring the FID, and stepwise incrementing the magnetic field over the spectral range of the EPR signal. FID-detected EPR can be useful for systems in which spin-spin (T_2) relaxation lies in the order of the dead-time of the spectrometer, under conditions where the ESE-detected EPR sequence fails. The FID signal moreover is sensitive to the microwave power.^{328,329}

10.2. ESE-Detected EPR

ESE-detected EPR can be viewed as an extension of the FID-detected EPR method. After the 90° pulse and the first dephasing (FID) have taken place, a second pulse is applied to the system. This is a 180° pulse, which inverts the time evolution of the spin system, such that spin rephasing takes place. After a time, equal to the separation of both pulses, rephasing is complete and all spins are aligned again. Thereafter, the dephasing proceeds again. The phenomenon of spin rephasing, followed by dephasing, is called an echo, for this particular pulse sequence the Hahn echo, first described in 1950.³³⁰ It has the advantage that for pulse separations longer than the dead-time of the spectrometer, the complete echo can be recorded.

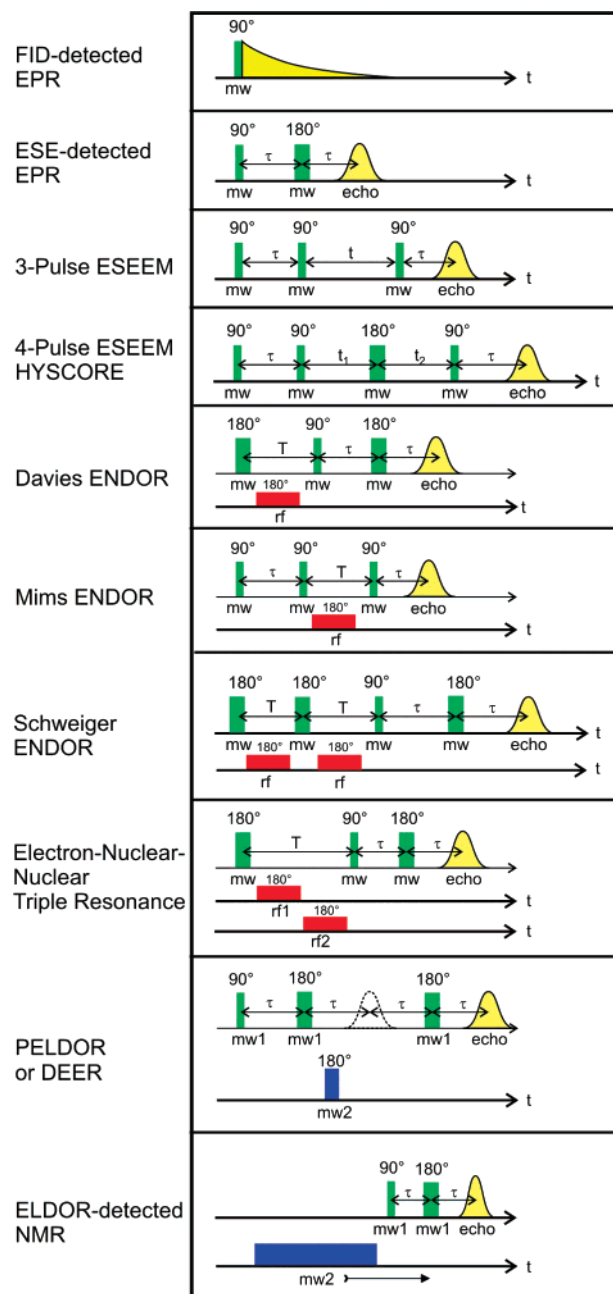


Figure 18. Schematic overview of pulse sequences employed for EPR, ESEEM, ENDOR, and ELDOR methods employed in hydrogenase research.

The ESE-detected EPR experiment is performed by keeping the microwave frequency fixed, stepwise incrementing the magnetic field, and monitoring the intensity of the echo. At magnetic fields for which the resonance condition $h\nu = g\mu_B\mathbf{B}$ (h , Planck constant; ν , microwave frequency; μ_B , Bohr magneton; \mathbf{B} , magnetic field; and g , effective g value) is fulfilled an echo appears. By this technique, an EPR spectrum (in absorption) is recorded and information can be obtained about the g values of the system, which are characteristic for the electronic structure of the paramagnetic center. When nuclei with a large hyperfine interaction (i.e., the magnetic coupling between the spin of the unpaired electron and the spin of the nucleus) are present, additional structure appears in the EPR spectrum, from which these interactions can be determined. Once the hyperfine interaction is known, information can be obtained, for example, about the effective distance between the electron spin and

the nuclear spin and about the electronic structure (spin density distribution).

10.3. Three-Pulse Electron Spin Echo Envelope Modulation (ESEEM) Spectroscopy

When nuclei with small hyperfine interactions are present that are not resolved in the EPR spectrum, it may be possible to detect these couplings by electron spin echo envelope modulation (ESEEM) spectroscopy. When the hyperfine interaction is smaller than the inhomogeneous line width of the EPR spectrum, and the nuclear frequencies are sufficiently small, the microwave pulses become nonselective with respect to the nuclear sublevels. This results in a coherent superposition of states, which evolves during the times in between and after the microwave pulses. When the time t between the second and third pulse is stepwise increased, while keeping ν and \mathbf{B} constant and monitoring the height of the echo, modulations can be observed whose frequencies are equal to nuclear transition frequencies. Once the nuclear transition frequencies are known, or the variation thereof over the field range spanned by the EPR spectrum, hyperfine and (for nuclei with $I > 1/2$) quadrupole coupling constants can be elucidated, which in turn give information on the electronic structure near the atom which carries the nuclear spin. ESEEM spectra are usually presented as Fourier transform spectra, in which the time axis t is converted to a frequency axis, which facilitates determination of the frequencies present in the modulation pattern. ESEEM spectroscopy works particularly well when the nuclear transition frequencies in one of the electron-spin-manifolds are close to 0 MHz (cancellation condition). The technique has for example been used in hydrogenase research to detect the $^{14}\text{N}/^{15}\text{N}$ hfcs and nqcs of amino acids that are weakly coupled to the active site, for example, histidine. The technique was pioneered by Mims³³¹ and has been used in the hydrogenase field, for example, to detect a weakly coupled histidyl nitrogen near the [NiFe] center.²⁴⁶

10.4. Four-Pulse ESEEM (HYSCORE)

The four pulse variant of ESEEM spectroscopy is called hyperfine sublevel correlation (HYSCORE) spectroscopy. The difference with the former pulse sequence is that now two time intervals, t_1 and t_2 , are independently incremented, thus creating a two-dimensional modulation pattern. After double Fourier transformation, a spectrum similar to a two-dimensional NMR spectrum is obtained, in which nuclear frequencies that stem from the same nucleus can be correlated and grouped together. The technique is very useful for strongly coupled nuclei, for which the signals will appear in a different part of the spectrum than those of the weakly coupled nuclei, and for disentangling convoluted 3-pulse ESEEM spectra with contributions from many nuclei. HYSCORE spectroscopy was pioneered by Höfer et al.¹⁹⁵ It has been used to experimentally identify the presence of a hydride bridge in the Ni-C state of [NiFe] hydrogenases.⁹³

10.5. Pulse Electron–Nuclear Double Resonance (ENDOR) Spectroscopy

In electron nuclear double resonance (ENDOR) spectroscopy, originally introduced by Feher¹⁹² in 1956, an RF pulse is introduced to the system, with the aim to directly excite a nuclear spin transition. The experiment is performed at fixed microwave frequency and magnetic field, and the echo

intensity is recorded as a function of the frequency of the RF radiation. Two basic variants of the ENDOR pulse sequence exist, called Davies ENDOR³⁴² and Mims ENDOR.³³² The two pulse sequences differ slightly in the order in which the pulses are applied to the system, as can be seen in Figure 18. Davies ENDOR is usually used to detect nuclear frequencies of nuclei with a strong coupling to the unpaired electron, whereas Mims ENDOR is more suited to detect the nuclear transitions of more weakly coupled nuclei further away from the electron spin. Mims ENDOR unfortunately suffers from a “blind spot” dependence, in that frequencies for which $\sin(\omega\tau) = 0$, with τ the time between the first and second pulse, cannot be detected. The Davies ENDOR sequence has been extended by Schweiger and co-workers,³³³ by splitting the RF pulse and applying an additional strong microwave pulse between the two RF pulses. For systems with a long spin–lattice relaxation time, this leads to an improvement by a factor of 2 in signal intensity as compared to Davies ENDOR. The frequencies obtained from ENDOR spectroscopy are essentially the same as those obtained from ESEEM spectroscopy. ENDOR spectroscopy, however, is complementary to ESEEM spectroscopy, in that the technique becomes more sensitive as the nuclear transition frequencies increase and become appreciably far away from 0 MHz. When ENDOR spectra are recorded at many magnetic field values that span the range of the powder-type EPR spectrum, a selection of orientations becomes possible in the powder-type EPR allowing the elucidation of hyperfine and quadrupole tensors (like in ESEEM spectroscopy). ENDOR spectroscopy has initially been applied to [NiFe] hydrogenases in the Hoffman group to identify ^1H couplings of protons in and near the [NiFe] active site.^{163,238}

10.6. Pulse Electron–Nuclear–Nuclear Triple Resonance

The electron–nuclear–nuclear triple resonance experiment (TRIPLE) is the two-dimensional equivalent to ENDOR spectroscopy, in the same way as HYSCORE is the 2D variant of ESEEM spectroscopy. In the TRIPLE experiment,³³⁴ two RF pulses are applied whose frequencies are independently incremented, and the echo intensity is recorded. Whenever an RF frequency is resonant with a nuclear transition a slight change of the echo intensity can be observed. In the two-dimensional TRIPLE spectrum, again nuclear transitions that belong to the same nucleus can be determined. Another advantage of TRIPLE spectroscopy is that it can be used to determine the relative and sometimes even the absolute sign of the hyperfine interaction. The latter property cannot be determined by any of the other spectroscopies discussed so far.

10.7. Pulse Electron–Electron Double Resonance (PELDOR/DEER) Spectroscopy

ELDOR, electron–electron double resonance spectroscopy, is useful when two or more weakly interacting paramagnetic centers are present. When the relative orientations and dynamical properties of the two centers are constant over the duration of the experiment, microwave pulses can be applied with the aim to determine the magnetic coupling between the two centers. The experiment is performed by monitoring the echo of one of the two unpaired electrons via a three pulse sequence (see Figure 18). When a fourth pulse of different frequency is applied to flip the spin of the

unpaired electron of the other center, the effective magnetic field felt by the first electron changes. The microwave pulse is then moved in time with respect to the pulses applied to the “observer electron spin” and a modulation of the echo intensity can be observed. The modulation frequency is essentially determined by the magnetic coupling between the two centers, which in turn give information about the distance and relative orientations of the spin distributions in both centers. Pulse ELDOR was introduced in 1959.³³⁵ It has for example been used to measure the distance between the [NiFe] center and the [3Fe–4S] cluster in [NiFe] hydrogenases.²⁶⁹

10.8. ELDOR-Detected NMR

Electron–electron double resonance detected NMR spectroscopy was originally introduced as a pulse sequence in which a weak Gaussian pulse appears to induce EPR transitions.¹⁹⁶ In the three-pulse ELDOR-detected NMR experiments described here, three rectangular pulses are applied. The aim of the experiment is to determine the nuclear transition frequencies of very strongly coupled nuclei, for example the central metal of the paramagnetic site (provided it carries a nuclear spin). Two pulses are used to drive EPR allowed transitions and to create a normal two-pulse echo, as was used in the ESE-detected EPR experiment. Additionally, a strong and nonselective microwave pulse is applied to drive EPR forbidden transitions. The frequency of this pulse is scanned, and the echo height is again monitored. When the frequency is such that an EPR forbidden transition is induced a small change of the echo intensity is observed. The frequency difference of the microwaves driving the EPR allowed and EPR forbidden transitions is equal to a nuclear transition frequency. The method seems to work well for fast relaxing nuclei, such as the central metal ⁶¹Ni in [NiFe] hydrogenase,²³² but does not have the same resolution as, for example, that obtained in ENDOR and ESEEM spectroscopy.

11. Appendix II. Crystal Field Considerations for Ni^{III} and Ni^I in a Square Pyramidal Crystal Field

In the crystal structures of [NiFe] hydrogenases, the nickel atom is surrounded by five ligands, four sulfur atoms from cysteines, and an additional bridging ligand, as shown schematically in Figure 19a. The base plane is formed by three sulfur atoms and an oxygen, the axial (*z*) direction is given by the direction from nickel to the sulfur of the fourth cysteine. In such a square-pyramidal ligand field, the splitting of d orbitals is given according to the energy scheme shown in Figure 19b.³³⁶

The unpaired electron is in a 3d_{z²} orbital for a Ni^{III} and a 3d_{x²-y²} orbital for Ni^I. For Ni^{III}, the formal redox state of nickel in the case of Ni-A, Ni-B, Ni-C, and Ni-L, DFT calculations are able to essentially reproduce the electronic wavefunction of hydrogenase even on a simplified model of Ni^{III}(SH⁻)₄(OH⁻), with the main spin density being about evenly distributed in the 3d_{z²} orbital of Ni and the 3p_z orbital of the apical (axial) sulfur.

By single-crystal EPR measurements, the directions of the *g* tensor with respect to the geometry of the active site are determined. The principal axis that corresponds to the *smallest* principal value (*g_z*) is invariably found for all redox states to be along the *z*-axis of the square pyramid, which is in-line with eq 3, where it can indeed be seen that the *g_z*

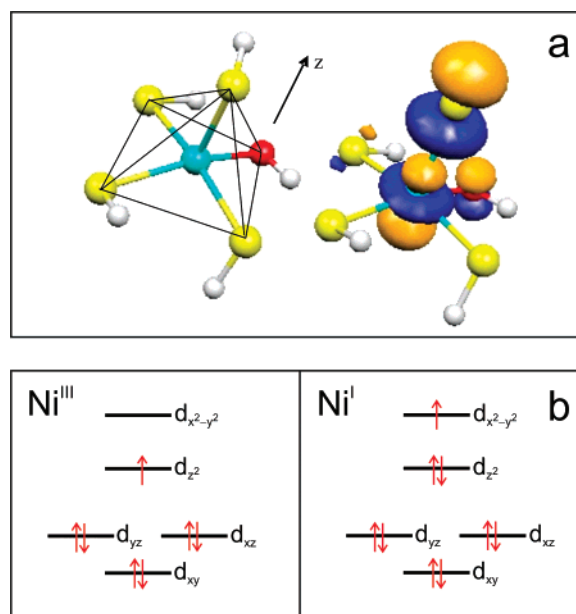


Figure 19. (a) Schematic representation of the square pyramidal crystal field of Ni (left) and contour plot of the singly occupied orbital from a DFT calculation (B3LYP functional, spin-unrestricted formalism, split-valence basis set) in a Ni^{III}(SH⁻)₄(OH⁻) model system. The *z* direction is indicated by an arrow. (b) d-Orbital energy levels for a Ni^{III} (left) and Ni^I (right) ion in a square pyramidal crystal field.

value remains equal to *g_e*. Thus the EPR active redox states in [NiFe] hydrogenases (A, B, C, L) are best classified as Ni^{III} states. For a formal Ni^{III} species, the *g* values would be

$$g_x = g_e - \rho_S(\text{Ni}) \frac{6\lambda}{E(d_{z^2}) - E(d_{yz})} \quad (1)$$

$$g_y = g_e - \rho_S(\text{Ni}) \frac{6\lambda}{E(d_{z^2}) - E(d_{xz})} \quad (2)$$

$$g_z = g_e \quad (3)$$

where *g_e* is the free electron *g* value (2.0023), $\rho_S(\text{Ni})$ the spin density at Ni, and λ is the spin-orbit coupling parameter of Ni. Note that for Ni λ is negative.

For a formal Ni^I redox state, the equations for the *g* values are

$$g_x = g_e - \rho_S(\text{Ni}) \frac{2\lambda}{E(d_{x^2-y^2}) - E(d_{yz})} \quad (4)$$

$$g_y = g_e - \rho_S(\text{Ni}) \frac{2\lambda}{E(d_{x^2-y^2}) - E(d_{xz})} \quad (5)$$

$$g_z = g_e - \rho_S(\text{Ni}) \frac{6\lambda}{E(d_{x^2-y^2}) - E(d_{xy})} \quad (6)$$

It can be seen (under the assumption that the d_{xy}, d_{xz}, and d_{yz} orbitals have similar energy) that for a Ni^I the *largest* *g* value would be expected along the *z*-axis, which is not in line with the single crystal EPR measurements.⁹⁴

12. Appendix III. The Spin Exchange Model of the H-cluster in [FeFe] Hydrogenase

To explain the experimental observation of the ⁵⁷Fe *h* couplings from the formally diamagnetic [4Fe–4S]_H sub-

cluster in the H_{ox} and H_{ox} -CO states, a spin exchange model has been developed. As pointed out above, the $[4Fe-4S]_H$ subunit of the H-cluster remains in the $2+$ state. The ground state of the cluster comprises two valence-delocalized pairs, with spin $S_{1,2} = S_{3,4} = 1/2$ (see Figure 16). The two pairs are antiferromagnetically coupled by Heisenberg–Dirac–Van-Vleck (HDVV) exchange, J_{cube} , which yields a diamagnetic ground state ($S_{cube} = 0$) and a triplet first excited state ($S_{cube} = 1$).³³⁷ According to experimental studies on $[4Fe-4S]^{2+}$ clusters the value of J_{cube} was estimated to be about 200 cm^{-1} .³³⁸ Therefore no ^{57}Fe hf couplings are expected from the $[4Fe-4S]_H$ subunit of the H-cluster. However, an additional exchange coupling exists between the Fe_p in the $[2Fe]_H$ subcluster (with spin $S_5 = 1/2$; see Figure 16) and one of the irons of the “diamagnetic” $[4Fe-4S]_H$ subunit. This interaction mixes the $S = 1$ excited-state of the cubane subcluster into the electronic ground state thus giving rise to an induced spin density resulting in the observation of ^{57}Fe hyperfine couplings from the $[4Fe-4S]_H$ subcluster (Figure 16b). This phenomenon has been observed in several multi-iron cluster proteins.^{337–339}

Bominaar and co-workers³³⁷ have developed an electronic model that explains the experimentally observed ^{57}Fe hf interactions of all iron nuclei in the $S = 5/2$ state of the siroheme exchange coupled to the $[4Fe-4S]^{2+}$ chromophore in oxidized *Escherichia coli* sulfite reductase. Later Belinsky³³⁹ has reviewed this model and adopted a simplified version to describe the $S = 1/2$ state of NO-complexed sulfite reductase. Xia et al.³³⁸ used this theory to explain the observed ^{57}Fe hf couplings from the $[4Fe-4S]^{2+}$ found in the Ni-activated R-subunit of carbon monoxide dehydrogenase from *Clostridium thermoaceticum*. Application of this theory to the active [FeFe] hydrogenase by Popescu and Münck successfully explains the observation of the ^{57}Fe hf couplings from the $[4Fe-4S]_H$ subcluster in the H_{ox} and H_{ox} -CO state.¹³⁹ In the electronic model the coupling of the additional spin ($S_5 = 1/2$) mixes the excited $S_{cube} = 1$ state of the “cubane” via coupling constant j into the ground state $S_{cube} = 0$ of the cubane (see Figure 16a). This gives rise to isotropic ^{57}Fe hf couplings of the $[4Fe-4S]_H$ whose values depend on the j/J_{cube} ratio. The calculations based on the work of Belinsky,³³⁹ result in the following expression for the hf constants:³³⁸

$$A_{1,2(3,4)} = \left\{ \frac{[1 - (1-x)\Gamma]}{6} + (-) \frac{33}{2} \frac{x}{\Gamma} \right\} a \quad (7)$$

where $\Gamma = [1 - 2x + 100x^2]^{1/2}$, $x = j/4J_{cube}$ and a is the intrinsic hyperfine interaction of the individual iron sites, considered to be isotropic in this approximation. Figure 16b shows the dependence of the isotropic part of the ^{57}Fe hfc of the cubane on the j/J_{cube} ratio. The analysis of the hf interaction of the valence-delocalized pairs in $[3Fe-4S]^0$, $[4Fe-4S]^{2+,3+}$ clusters suggests that $a = -22 \text{ MHz}$.³⁴⁰ The theory predicts that the signs of the hfc for the two Fe(II)-Fe(III) pairs are opposite.

13. References

- Hoffmann, P. *Tomorrow's Energy. Hydrogen, Fuel Cells, and the Prospects for a Cleaner Planet*; The MIT Press: Cambridge, 2002.
- Sperling, D. C. J. *The Hydrogen Energy Transition: Moving Toward the Post Petroleum Age in Transportation*; Elsevier Academic Press: San Diego, CA, 2004.
- Rifkin, J. *The Hydrogen Economy*; Tarcher/Putnam: New York, 2002.
- Coontz, R. H. B. *Science* **2004**, *305*, 957.
- Olah, G. A.; Goepfert, A.; Prakash, G. K. S. *Beyond Oil and Gas: The Methanol Economy*; Wiley-VCH: Weinheim, Germany, 2006.
- Collings, A. F.; Critchley, Ch. *Artificial Photosynthesis: From Basic Biology to Industrial Application*; Wiley-VCH Verlag GmbH: Weinheim, Germany, 2005.
- Cammack, R.; Frey, M.; Robson, R. *Hydrogen as a fuel: Learning from Nature*; Taylor & Francis: London and New York, 2001.
- Romm, J. J. *Der Wasserstoff-Boom*; Wiley-VCH Verlag GmbH: Weinheim, Germany, 2006.
- Pace, R. J. In *Artificial Photosynthesis: From Basic Biology to Industrial Application*; Collings, A. F., Critchley, Ch., Eds.; Wiley-VCH Verlag GmbH: Weinheim, Germany, 2005; Chapter 2, p 13.
- Blankenship, R. E. *Molecular Mechanisms of Photosynthesis*; Blackwell Science Ltd.: Oxford, 2002.
- Photosystem II, The Light-Driven Water: Plastoquinone Oxidoreductase*; Wydrzynski, T. J., Satoh, K., Eds.; Advances in Photosynthesis and Respiration, Vol 22.; Springer: Dordrecht, The Netherlands, 2005.
- Yano, J.; Kern, J.; Sauer, K.; Latimer, M. J.; Pushkar, Y.; Bieseadka, J.; Loll, B.; Saenger, W.; Messinger, J.; Zouni, A.; Yachandra, V. K. *Science* **2006**, *314*, 821.
- Vignais, P. M.; Billoud, B.; Meyer, J. *FEMS Microbiol. Rev.* **2001**, *25*, 455.
- Miyake, J.; Igarashi, Y.; Rögner, M. *Biohydrogen III*; Elsevier: Amsterdam, The Netherlands, 2004.
- Cammack, R. In *Hydrogen as a Fuel*; Cammack, R., Frey, M., Robson, R., Eds.; Taylor & Francis: London, 2001; Chapter 8, p 159.
- Rao, K. K.; Cammack, R. In *Hydrogen as a Fuel*; Cammack, R., Frey, M., Robson, R., Eds.; Taylor & Francis: London, 2001; Chapter 10, p 201.
- Ghirardi, M. L.; King, P.; Kosourov, S.; Forestier, M.; Zhang, L.; Seibert, M. In *Artificial Photosynthesis*; Collings, A. F., Critchley, Ch., Eds.; Wiley-VCH Verlag GmbH: Weinheim, Germany, 2005; Chapter 11, p 213.
- Melis, A. In *Artificial Photosynthesis*; Collings, A. F., Critchley, Ch., Eds.; Wiley-VCH Verlag GmbH: Weinheim, Germany, 2005; p 229.
- Happe, T.; Hemschemeier, A.; Winkler, M.; Kaminski, A. *Trends Plant Sci.* **2002**, *7*, 246.
- Melis, A.; Happe, T. *Photosynth. Res.* **2004**, *80*, 401.
- Esper, B.; Badura, A.; Rögner, M. *Trends Plant Sci.* **2006**, *11*, 543.
- Schütz, K.; Happe, T.; Troshina, O.; Lindahl, P. A.; Leitao, E.; Oliveira, O.; Tamagnini, P. *Planta* **2004**, *218*, 350.
- Elam, C. C.; Padró, C. E. G.; Sandrock, G.; Luzzi, A.; Lindblad, P.; Hagen, E. F. *Int. J. Hydrogen Energy* **2003**, *28*, 601.
- Kraatz, H.-B.; Metzler-Nolte, N. *Concepts and Models in Bioinorganic Chemistry*; Wiley-VCH: Weinheim, 2006.
- Harrop, T. C.; Mascharak, P. K. In *Concepts and Models in Bioinorganic Chemistry*; Kraatz, H.-B., Metzler-Nolte, N., Eds.; Wiley-VCH Verlag GmbH: Weinheim, Germany, 2006; Chapter 14, p 309.
- Morris, R. H. In *Concepts and Models in Bioinorganic Chemistry*; Kraatz, H.-B., Metzler-Nolte, N., Eds.; Wiley-VCH Verlag GmbH: Weinheim, Germany, 2006; Chapter 15, p 331.
- Darensbourg, M. Y.; Lyon, E. J.; Smees, J. J. *Coord. Chem. Rev.* **2000**, *206*, 533.
- Marr, A. C.; Spencer, D. J. E.; Schröder, M. *Coord. Chem. Rev.* **2001**, *219–221*, 1055.
- Rauchfuss, T. B. *Inorg. Chem.* **2004**, *43*, 14.
- Bouwman, E.; Reedijk, J. *Coord. Chem. Rev.* **2005**, *249*, 1555.
- Liu, X. M.; Ibrahim, S. K.; Tard, C.; Pickett, C. J. *Coord. Chem. Rev.* **2005**, *249*, 1641.
- Evans, D. J.; Pickett, C. J. *Chem. Soc. Rev.* **2003**, *32*, 268.
- Tard, C.; Liu, X. M.; Ibrahim, S. K.; Bruschi, M.; De Gioia, L.; Davies, S. C.; Yang, X.; Wang, L. S.; Sawers, G.; Pickett, C. J. *Nature* **2005**, *433*, 610.
- Sun, L. C.; Akermark, B.; Ott, S. *Coord. Chem. Rev.* **2005**, *249*, 1653.
- van der Vlugt, J. I.; Meyer, F. *Met. Ions. Life Sci.* **2007**, *5*, 181.
- Krasna, A. I. *Enzyme Microb. Technol.* **1979**, *1*, 165.
- Cammack, R.; Fernandez, V. M.; Hatchikian, E. C. *Meth. Enzymol.* **1994**, *243*, 43.
- Yagi, T.; Tsuda, M.; Inokuchi, H. *J. Biochem.* **1973**, *73*, 1069.
- Happe, R. P.; Roseboom, W.; Pierik, A. J.; Albracht, S. P. J.; Bagley, K. A. *Nature* **1997**, *385*, 126.
- Pierik, A. J.; Hulstein, M.; Hagen, W. R.; Albracht, S. P. J. *Eur. J. Biochem.* **1998**, *258*, 572.
- Garcin, E.; Venede, X.; Hatchikian, E. C.; Volbeda, A.; Frey, M.; Fontecilla-Camps, J. C. *Structure* **1999**, *7*, 557.
- Lyon, E. J.; Shima, S.; Boecher, R.; Thauer, R. K.; Grevels, F. W.; Bill, E.; Roseboom, W.; Albracht, S. P. J. *J. Am. Chem. Soc.* **2004**, *126*, 14239.

- (43) Shima, S.; Lyon, E. J.; Sordel-Klippert, M. S.; Kauss, M.; Kahnt, J.; Thauer, R. K.; Steinbach, K.; Xie, X. L.; Verdier, L.; Griesinger, C. *Angew. Chem., Int. Ed.* **2004**, *43*, 2547.
- (44) Lyon, E. J.; Shima, S.; Buurman, G.; Chowdhuri, S.; Batschauer, A.; Steinbach, K.; Thauer, R. K. *Eur. J. Biochem.* **2004**, *271*, 195.
- (45) Shima, S.; Lyon, E. J.; Thauer, R. K.; Mienert, B.; Bill, E. J. *Am. Chem. Soc.* **2005**, *127*, 10430.
- (46) Schwörer, B.; Fernandez, V. M.; Zirngibl, C.; Thauer, R. K. *Eur. J. Biochem.* **1993**, *212*, 255.
- (47) Wu, L. F.; Mandrand, M. A. *FEMS Microbiol. Rev.* **1993**, *104*, 243.
- (48) Friedrich, B.; Lenz, O. *Chem. Rev.*, in press.
- (49) Bernhard, M.; Buhrke, T.; Bleijlevens, B.; De Lacey, A. L.; Fernandez, V. M.; Albracht, S. P. J.; Friedrich, B. *J. Biol. Chem.* **2001**, *276*, 15592.
- (50) Pierik, A. J.; Schmelz, M.; Lenz, O.; Friedrich, B.; Albracht, S. P. J. *FEBS Lett.* **1998**, *438*, 231.
- (51) Bastian, N. R.; Wink, D. A.; Lawrence, P.; Wackett, L. P.; Livingston, D. J.; Jordan, L. M.; Fox, J.; Orme-Johnson, W. H.; Walsh, Ch. T. In *The Bioinorganic Chemistry of Nickel*; Lancaster, J. R., Ed.; 1988; Chapter 10, p 227.
- (52) Moura, J. J. G.; Teixeira, M.; Moura, I.; LeGall, J. In *The Bioinorganic Chemistry of Nickel*; Lancaster, C. R. D., Ed.; VCH Publishers: New York, 1988; Chapter 9, p 191.
- (53) Cammack, R.; Fernandez, V. M.; Schneider, K. In *The Bioinorganic Chemistry of Nickel*; Lancaster, J. R., Ed.; VCH New York: 1988; Chapter 8, p 167.
- (54) Cammack, R. *Nature* **1999**, *397*, 214.
- (55) Hatchikian, E. C.; Forget, N.; Fernandez, V. M.; Williams, R.; Cammack, R. *Eur. J. Biochem.* **1992**, *209*, 357.
- (56) Jones, A. K.; Sillery, E.; Albracht, S. P. J.; Armstrong, F. A. *Chem. Commun.* **2002**, 866.
- (57) Korbass, M.; Vogt, S.; Meyer-Klaucke, W.; Bill, E.; Lyon, E. J.; Thauer, R. K.; Shima, S. *J. Biol. Chem.* **2006**, *281*, 30804.
- (58) Pilak, O.; Mamat, B.; Vogt, S.; Hagemeyer, C. H.; Thauer, R. K.; Shima, S.; Vonnrhein, C.; Warkentin, E.; Ermler, U. *J. Mol. Biol.* **2006**, *358*, 798.
- (59) Thauer, R. K. Personal communication, 2007.
- (60) Montet, Y.; Amara, P.; Volbeda, A.; Vernede, X.; Hatchikian, E. C.; Field, M. J.; Frey, M.; Fontecilla-Camps, J. C. *Nat. Struct. Biol.* **1997**, *4*, 523.
- (61) Nicolet, Y.; Piras, C.; Legrand, P.; Hatchikian, C. E.; Fontecilla-Camps, J. C. *Struct. Fold. Des.* **1999**, *7*, 13.
- (62) Peters, J. W.; Lanzilotta, W. N.; Lemon, B. J.; Seefeldt, L. C. *Science* **1998**, *282*, 1853.
- (63) Volbeda, A.; Charon, M.-H.; Hatchikian, E. C.; Frey, M.; Fontecilla-Camps, J. C. *Nature* **1995**, *373*, 580.
- (64) Frey, M.; Fontecilla-Camps, J. C.; Volbeda, A. In *Handbook of Metalloproteins*; Messerschmidt, A., Huber, R., Poulos, T., Wieghardt, K., Eds.; John Wiley & Sons, Ltd.: Chichester, U.K., 2001; p 880.
- (65) De Lacey, A. L.; Fernandez, V. M.; Rousset, M. *Coord. Chem. Rev.* **2005**, *249*, 1596.
- (66) Higuchi, Y.; Yagi, T.; Yasuoka, N. *Structure* **1997**, *5*, 1671.
- (67) Lemon, B. J.; Peters, J. W. In *Handbook of Metalloproteins*; Messerschmidt, A., Huber, R., Poulos, T., Wieghardt, K., Eds.; Wiley: Weinheim, Germany, 2001; p 738.
- (68) Higuchi, Y.; Yasuoka, N.; Kakudo, M.; Katsube, Y.; Yagi, T.; Inokuchi, H. *J. Biol. Chem.* **1987**, *262*, 2823.
- (69) Niviere, V.; Hatchikian, C.; Cambillau, C.; Frey, M. *J. Mol. Biol.* **1987**, *195*, 969.
- (70) Volbeda, A.; Garcin, E.; Piras, C.; De Lacey, A. L.; Fernandez, V. M.; Hatchikian, E. C.; Frey, M.; Fontecilla-Camps, J. C. *J. Am. Chem. Soc.* **1996**, *118*, 12989.
- (71) Volbeda, A.; Martin, L.; Cavazza, C.; Matho, M.; Faber, B. W.; Roseboom, W.; Albracht, S. P. J.; Garcin, E.; Rousset, M.; Fontecilla-Camps, J. C. *J. Biol. Inorg. Chem.* **2005**, *10*, 239.
- (72) Higuchi, Y.; Ogata, H.; Miki, K.; Yasuoka, N.; Yagi, T. *Structure* **1999**, *7*, 549.
- (73) Ogata, H.; Mizoguchi, Y.; Mizuno, N.; Miki, K.; Adachi, S.; Yasuoka, N.; Yagi, T.; Yamauchi, O.; Hirota, S.; Higuchi, Y. *J. Am. Chem. Soc.* **2002**, *124*, 11628.
- (74) Ogata, H.; Hirota, S.; Nakahara, A.; Komori, H.; Shibata, N.; Kato, T.; Kano, K.; Higuchi, Y. *Structure* **2005**, *13*, 1635.
- (75) Matias, P. M.; Soares, C. M.; Saraiva, L. M.; Coelho, R.; Morais, J.; LeGall, J.; Carrando, M. A. *J. Biol. Inorg. Chem.* **2001**, *6*, 63.
- (76) Volbeda, A.; Montet, Y.; Vernede, X.; Hatchikian, E. C.; Fontecilla-Camps, J. C. *Int. J. Hydrogen Energy* **2002**, *27*, 1449.
- (77) Rousset, M.; Montet, Y.; Guigliarelli, B.; Forget, N.; Asso, M.; Bertrand, P.; Fontecilla-Camps, J. C.; Hatchikian, E. C. *Proc. Natl. Acad. Sci. U.S.A.* **1998**, *95*, 11625.
- (78) De Lacey, A. L.; Fernandez, V. M.; Rousset, M.; Cavazza, C.; Hatchikian, E. C. *J. Biol. Inorg. Chem.* **2003**, *8*, 129.
- (79) Volbeda, A.; Fontecilla-Camps, J. C. *Dalton Trans.* **2003**, 4030.
- (80) Volbeda, A.; Fontecilla-Camps, J. C. *Coord. Chem. Rev.* **2005**, *249*, 1609.
- (81) Frey, M. In *Nickel-iron hydrogenases: Structural and functional properties*; Springer-Verlag: Berlin, Heidelberg, 1998; Chapter 90, p 97.
- (82) Rieder, R.; Cammack, R.; Hall, D. O. *Eur. J. Biochem.* **1984**, *145*, 637.
- (83) Teixeira, M.; Moura, I.; Fauque, G.; Czechowski, M.; Berlier, Y.; Lespinat, P. A.; LeGall, J.; Xavier, A. V.; Moura, J. J. G. *Biochimie* **1986**, *68*, 75.
- (84) Teixeira, M.; Fauque, G.; Moura, I.; Lespinat, P. A.; Berlier, Y.; Prickril, B.; Peck, H. D.; Xavier, A. V.; LeGall, J.; Moura, J. J. G. *Eur. J. Biochem.* **1987**, *167*, 47.
- (85) Bleijlevens, B.; van Broekhuizen, F.; De Lacey, A. L.; Roseboom, W.; Fernandez, V. M.; Albracht, S. P. J. *J. Biol. Inorg. Chem.* **2004**, *9*, 743.
- (86) De Lacey, A. L.; Hatchikian, E. C.; Volbeda, A.; Frey, M.; Fontecilla-Camps, J. C.; Fernandez, V. M. *J. Am. Chem. Soc.* **1997**, *119*, 7181.
- (87) De Lacey, A. L.; Stadler, C.; Fernandez, V. M.; Hatchikian, E. C.; Fan, H.-J.; Li, S.; Hall, M. B. *J. Biol. Inorg. Chem.* **2002**, *7*, 318.
- (88) Fichtner, C.; Laurich, Ch.; Bothe, E.; Lubitz, W. *Biochemistry* **2006**, *45*, 9706.
- (89) van der Zwaan, J. W.; Coremans, J. M. C. C.; Bouwens, E. C. M.; Albracht, S. P. J. *Biochim. Biophys. Acta* **1990**, *1041*, 101.
- (90) Carepo, M.; Tierney, D. L.; Brondino, C. D.; Yang, T. C.; Pamplona, A.; Telsler, J.; Moura, I.; Moura, J. J. G.; Hoffman, B. M. *J. Am. Chem. Soc.* **2002**, *124*, 281.
- (91) Higuchi, Y.; Yagi, T. *Biochem. Biophys. Res. Commun.* **1999**, *255*, 295.
- (92) Vincent, K. A.; Belsey, N. A.; Lubitz, W.; Armstrong, F. A. *J. Am. Chem. Soc.* **2006**, *128*, 7448.
- (93) Brecht, M.; van Gastel, M.; Buhrke, T.; Friedrich, B.; Lubitz, W. *J. Am. Chem. Soc.* **2003**, *125*, 13075.
- (94) Foerster, S.; Stein, M.; Brecht, M.; Ogata, H.; Higuchi, Y.; Lubitz, W. *J. Am. Chem. Soc.* **2003**, *125*, 83.
- (95) Foerster, S.; van Gastel, M.; Brecht, M.; Lubitz, W. *J. Biol. Inorg. Chem.* **2005**, *10*, 51.
- (96) Page, C. C.; Moser, C. C.; Chen, X. X.; Dutton, P. L. *Nature* **1999**, *402*, 47.
- (97) Vincent, K. A.; Cracknell, J. A.; Parkin, A.; Armstrong, F. A. *Dalton Trans.* **2005**, 3397.
- (98) Lamle, S. E.; Albracht, S. P. J.; Armstrong, F. A. *J. Am. Chem. Soc.* **2004**, *126*, 14899.
- (99) Lamle, S. E.; Albracht, S. P. J.; Armstrong, F. A. *J. Am. Chem. Soc.* **2005**, *127*, 6595.
- (100) Lubitz, W.; van Gastel, M.; Gärtner, W. *Met. Ions. Life Sci.* **2007**, *2*, 279.
- (101) Adams, M. W. W.; Johnson, M. K.; Zambrano, I. C.; Mortenson, L. E. *Biochimie* **1986**, *68*, 35.
- (102) Adams, M. W. W. *Biochim. Biophys. Acta* **1990**, *1020*, 115.
- (103) Adams, M. W. W.; Mortenson, L. E. *J. Biol. Chem.* **1984**, *259*, 7045.
- (104) Chen, J. S.; Mortenson, L. E. *Biochim. Biophys. Acta* **1974**, *371*, 283.
- (105) Chen, J. S.; Blanchard, D. K. *Biochem. Biophys. Res. Commun.* **1978**, *84*, 1144.
- (106) Adams, M. W. W.; Mortenson, L. E. *Biochim. Biophys. Acta* **1984**, *766*, 51.
- (107) van Dijk, C.; Veeger, C. *Eur. J. Biochem.* **1981**, *114*, 209.
- (108) van Dijk, C.; Grande, H. J.; Mayhew, S. G.; Veeger, C. *Eur. J. Biochem.* **1980**, *107*, 251.
- (109) van Dijk, C.; Mayhew, S. G.; Grande, H. J.; Veeger, C. *Eur. J. Biochem.* **1979**, *102*, 317.
- (110) Filipiak, M.; Hagen, W. R.; Veeger, C. *Eur. J. Biochem.* **1989**, *185*, 547.
- (111) Hagen, W. R.; van Berkel-Arts, A.; Krüse-Wolters, K. M.; Voordouw, G.; Veeger, C. *FEBS Lett.* **1986**, *203*, 59.
- (112) van der Westen, H. M.; Mayhew, S. G.; Veeger, C. *FEBS Lett.* **1978**, *86*, 122.
- (113) Grande, H. J.; Dunham, W. R.; Averill, B.; van Dijk, C.; Sands, R. H. *Eur. J. Biochem.* **1983**, *136*, 201.
- (114) Grande, H. J.; van Berkel-Arts, A.; Breghe, J.; van Dijk, K.; Veeger, C. *Eur. J. Biochem.* **1983**, *131*, 81.
- (115) Huynh, B. H.; Czechowski, M. H.; Krüger, H. J.; DerVartanian, D. V.; Peck, H. D.; LeGall, J. *Proc. Natl. Acad. Sci. U.S.A.* **1984**, *81*, 3728.
- (116) Patil, D. S.; He, S. H.; DerVartanian, D. V.; LeGall, J.; Huynh, B. H.; Peck, H. D. *FEBS Lett.* **1988**, *228*, 85.
- (117) Patil, D. S.; Moura, J. J. G.; He, S. H.; Teixeira, M.; Prickril, B. C.; DerVartanian, D. V.; Peck, H. D.; LeGall, J.; Huynh, B. H. *J. Biol. Chem.* **1988**, *263*, 18732.
- (118) Patil, D. S.; Huynh, B. H.; He, S. H.; Peck, H. D.; DerVartanian, D. V.; LeGall, J. *J. Am. Chem. Soc.* **1988**, *110*, 8533.

- (119) Fauque, G.; Peck, H. D.; Moura, J. J. G.; Huynh, B. H.; Berlier, Y.; DerVartanian, D. V.; Teixeira, M.; Przybyla, A. E.; Lespinat, P. A.; Moura, I.; LeGall, J. *FEMS Microbiol. Rev.* **1988**, *54*, 299.
- (120) Glick, B. R.; Martin, W. G.; Martin, S. M. *Can. J. Microbiol.* **1980**, *26*, 1214.
- (121) Nicolet, Y.; De Lacey, A. L.; Venede, X.; Fernandez, V. M.; Hatchikian, E. C.; Fontecilla-Camps, J. C. *J. Am. Chem. Soc.* **2001**, *123*, 1596.
- (122) Nicolet, Y.; Cavazza, C.; Fontecilla-Camps, J. C. *J. Inorg. Biochem.* **2002**, *91*, 1.
- (123) Lemon, B. J.; Peters, J. W. *Biochemistry* **1999**, *38*, 12969.
- (124) Lemon, B. J.; Peters, J. W. *J. Am. Chem. Soc.* **2000**, *122*, 3793.
- (125) Peters, J. W.; Lanzilotta, W. N.; Lemon, B. J.; Seefeldt, L. C. *J. Inorg. Biochem.* **1999**, *74*, 44.
- (126) De Lacey, A. L.; Stadler, C.; Cavazza, C.; Hatchikian, E. C.; Fernandez, V. M. *J. Am. Chem. Soc.* **2000**, *122*, 11232.
- (127) Roseboom, W.; De Lacey, A. L.; Fernandez, V. M.; Hatchikian, C.; Albracht, S. P. J. *J. Biol. Inorg. Chem.* **2006**, *11*, 102.
- (128) Bagley, K. A.; Chen, J. Y.; Lemon, B. J.; Peters, J. W. *Abstr. Pap. ACS* **2002**, *224*, U645.
- (129) Thomann, H.; Bernardo, M.; Adams, M. W. W. *J. Am. Chem. Soc.* **1991**, *113*, 7044.
- (130) Williams, R.; Cammack, R.; Hatchikian, E. C. *J. Chem. Soc., Faraday Trans.* **1993**, *89*, 2869.
- (131) Van Dam, P. J.; Reijerse, E. J.; Hagen, W. R. *Eur. J. Biochem.* **1997**, *248*, 355.
- (132) Hatchikian, E. C.; Magro, V.; Forget, N.; Nicolet, Y.; Fontecilla-Camps, J. C. *J. Bacteriol.* **1999**, *181*, 2947.
- (133) Van der Spek, T. M.; Arendsen, A. F.; Happe, R. P.; Yun, S. Y.; Bagley, K. A.; Stufkens, D. J.; Hagen, W. R.; Albracht, S. P. J. *Eur. J. Biochem.* **1996**, *237*, 629.
- (134) Chen, Z. J.; Lemon, B. J.; Huang, S.; Swartz, D. J.; Peters, J. W.; Bagley, K. A. *Biochemistry* **2002**, *41*, 2036.
- (135) Albracht, S. P. J.; Roseboom, W.; Hatchikian, C. *J. Biol. Inorg. Chem.* **2006**, *11*, 88.
- (136) Wang, G.; Benceky, M. J.; Huynh, B. H.; Cline, J. F.; Adams, M. W. W.; Mortenson, L. E.; Hoffman, B. M.; Münck, E. *J. Biol. Chem.* **1984**, *259*, 4328.
- (137) Telser, J.; Benceky, M. J.; Adams, M. W. W.; Mortenson, L. E.; Hoffman, B. M. *J. Biol. Chem.* **1987**, *262*, 6589.
- (138) Kowal, A. T.; Adams, M. W. W.; Johnson, M. K. *J. Biol. Chem.* **1989**, *264*, 4342.
- (139) Popescu, C. V.; Münck, E. *J. Am. Chem. Soc.* **1999**, *121*, 7877.
- (140) Albracht, S. P. J. *Biochim. Biophys. Acta* **1994**, *1188*, 167.
- (141) Best, S. *Coord. Chem. Rev.* **2005**, *249*, 1536.
- (142) Fernandez, V. M.; Hatchikian, E. C.; Cammack, R. *Biochim. Biophys. Acta* **1985**, *832*, 69.
- (143) Coremans, J. M. C. C.; van der Zwaan, J. W.; Albracht, S. P. J. *Biochim. Biophys. Acta* **1992**, *1119*, 157.
- (144) Coremans, J. M. C. C.; van Garderen, C. J.; Albracht, S. P. J. *Biochim. Biophys. Acta* **1992**, *1119*, 148.
- (145) Cammack, R.; Patil, D. S.; Hatchikian, E. C.; Fernandez, V. M. *Biochim. Biophys. Acta* **1986**, *912*, 98.
- (146) van der Zwaan, J. W.; Albracht, S. P. J.; Fontijn, R. D.; Slater, E. C. *FEBS Lett.* **1985**, *2*, 271.
- (147) Medina, M.; Williams, R.; Cammack, R. *J. Chem. Soc., Faraday Trans.* **1994**, *90*, 2921.
- (148) van der Zwaan, J. W.; Albracht, S. P. J.; Fontijn, R. D.; Roelofs, Y. B. M. *Biochim. Biophys. Acta* **1986**, *872*, 208.
- (149) Happe, R. P.; Roseboom, W.; Albracht, S. P. J. *Eur. J. Biochem.* **1999**, *259*, 602.
- (150) Pierik, A. J.; Hagen, W. R.; Redeker, J. S.; Wolbert, R. B. G.; Boersma, M.; Verhagen, M. F. J. M.; Grande, H. J.; Veeger, C.; Mutsaers, P. H. A.; Sands, R. H.; Dunham, W. R. *Eur. J. Biochem.* **1992**, *209*, 63.
- (151) Pereira, A. S.; Tavares, P.; Moura, I.; Moura, J. J. G.; Huynh, B. H. *J. Am. Chem. Soc.* **2001**, *123*, 2771.
- (152) Bennett, B.; Lemon, B. J.; Peters, J. W. *Biochemistry* **2000**, *39*, 7455.
- (153) Bagley, K. A.; van Garderen, C. J.; Chen, M.; Duin, E. C.; Albracht, S. P. J.; Woodruff, W. H. *Biochemistry* **1994**, *33*, 9229.
- (154) Bagley, K. A.; Duin, E. C.; Roseboom, W.; Albracht, S. P. J.; Woodruff, W. H. *Biochemistry* **1995**, *34*, 5527.
- (155) Pierik, A. J.; Roseboom, W.; Happe, R. P.; Bagley, K. A.; Albracht, S. P. J. *J. Biol. Chem.* **1999**, *274*, 3331.
- (156) Burgdorf, T.; Löscher, S.; Liebisch, P.; Van der Linden, E.; Galander, M.; Lendzian, F.; Meyer-Klaucke, W.; Albracht, S. P. J.; Friedrich, B.; Dau, H.; Haumann, M. *J. Am. Chem. Soc.* **2005**, *127*, 576.
- (157) Schröder, O.; Bleijlevens, B.; de Jongh, T. E.; Chen, Z.; Li, T.; Fischer, J.; Förster, J.; Friedrich, C. G.; Bagley, K. A.; Albracht, S. P. J.; Lubitz, W. *J. Biol. Inorg. Chem.* **2007**, *12*, 212.
- (158) Van der Linden, E.; Burgdorf, T.; De Lacey, A. L.; Buhrke, T.; Scholte, M.; Fernandez, V. M.; Friedrich, B.; Albracht, S. P. J. *J. Biol. Inorg. Chem.* **2006**, *11*, 247.
- (159) George, S. J.; Kurkin, S.; Thorneley, R. N. F.; Albracht, S. P. J. *Biochemistry* **2004**, *43*, 6808.
- (160) Kurkin, S.; George, S. J.; Thorneley, R. N. F.; Albracht, S. P. J. *Biochemistry* **2004**, *43*, 6820.
- (161) Scott, R. A. In *Physical Methods in Bioinorganic Chemistry*; Que, L., Jr., Ed.; University Science Books: Sausalito, CA, 2000; Chapter 9, p 465.
- (162) Maroney, M. J. *J. Biol. Inorg. Chem.* **2001**, *6*, 452.
- (163) Whitehead, J. P.; Gurbiel, R. J.; Bagyinka, C.; Hoffman, B. M.; Maroney, M. J. *J. Am. Chem. Soc.* **1993**, *115*, 5629.
- (164) Gu, Z.; Dong, J.; Allan, C. B.; Choudhury, S. B.; Franco, R.; Moura, J. J. G.; Moura, I.; LeGall, J.; Przybyla, A. E.; Roseboom, W.; Albracht, S. P. J.; Axley, M. J.; Scott, R. A.; Maroney, M. J. *J. Am. Chem. Soc.* **1996**, *118*, 11155.
- (165) Davidson, G.; Choudhury, S. B.; Gu, Z.; Bose, K.; Roseboom, W.; Albracht, S. P. J.; Maroney, M. J. *Biochemistry* **2000**, *39*, 7468.
- (166) Wang, H.; Patil, D. S.; Gu, W.; Jacquamet, L.; Friedrich, S.; Funk, T.; Cramer, S. P. *J. Electron Spectrosc. Relat. Phenom.* **2001**, *114–116*, 855.
- (167) Gu, W. W.; Jacquamet, L.; Patil, D. S.; Wang, H. X.; Evans, D. J.; Smith, M. C.; Millar, M.; Koch, S.; Eichhorn, D. M.; Latimer, M.; Cramer, S. P. *J. Inorg. Biochem.* **2003**, *93*, 41.
- (168) Haumann, M.; Porthun, A.; Buhrke, T.; Liebisch, P.; Meyer-Klaucke, W.; Friedrich, B.; Dau, H. *Biochemistry* **2003**, *42*, 13786.
- (169) Münck, E. In *Physical Methods in Bioinorganic Chemistry*; Que, L., Jr., Ed.; University Science Books: Sausalito, CA, 2000; Chapter 6, p 287.
- (170) Gütlich, P. L. R. T. A. *Mössbauer Spectroscopy and Transition Metal Chemistry*; Springer-Verlag: Berlin, 1979.
- (171) Huynh, B. H.; Patil, D. S.; Moura, I.; Teixeira, M.; Moura, J. J. G.; DerVartanian, D. V.; Czechowski, M. H.; Prickril, B. C.; Peck, H. D.; LeGall, J. *J. Biol. Chem.* **1987**, *262*, 795.
- (172) Teixeira, M.; Moura, I.; Xavier, A. V.; Moura, J. J. G.; LeGall, J.; DerVartanian, D. V.; Peck, H. D.; Huynh, B. H. *J. Biol. Chem.* **1989**, *264*, 16435.
- (173) Teixeira, M.; Moura, I.; Fauque, G.; DerVartanian, D. V.; LeGall, J.; Peck, H. D.; Moura, J. J. G.; Huynh, B. H. *Eur. J. Biochem.* **1990**, *189*, 381.
- (174) Zaborosch, C.; Koster, M.; Bill, E.; Schneider, K.; Schlegel, H. G.; Trautwein, A. X. *Biomaterials* **1995**, *8*, 149.
- (175) Sureus, K. K.; Chen, M.; van der Zwaan, J. W.; Rusnak, F. M.; Kolk, M.; Duin, E. C.; Albracht, S. P. J.; Münck, E. *Biochemistry* **1994**, *33*, 4980.
- (176) Rusnak, F. M.; Adams, M. W. W.; Mortenson, L. E.; Münck, E. *J. Biol. Chem.* **1987**, *262*, 38.
- (177) Pierik, A. J.; Hagen, W. R.; Dunham, W. R.; Sands, R. H. *Eur. J. Biochem.* **1992**, *206*, 705.
- (178) Münck, E.; Popescu, C. V. *Hyperfine Interact.* **2000**, *126*, 59.
- (179) Semin, B. K.; Davletshina, L. N.; Novakova, A. A.; Kiseleva, T.; Lanchinskaya, V. Y.; Aleksandrov, A. Y.; Seifulina, N.; Ivanov, I. I.; Seibert, M.; Rubin, A. B. *Plant Physiol.* **2003**, *131*, 1756.
- (180) van Gastel, M.; Lubitz, W. *Biolog. Magn. Res.*, in press.
- (181) Lubitz, W.; Brecht, M.; Foerster, S.; van Gastel, M.; Stein, M. In *Paramagnetic Resonance of Metallobiomolecules*; ACS Symposium Series 858; American Chemical Society, Washington, DC, 2003; p 128.
- (182) Abragam, A.; Bleaney, B. *Electron Paramagnetic Resonance of Transition Metal Ions*; Oxford University Press: Oxford, 1970.
- (183) Pilbrow, J. R. *Transition Ion Electron Paramagnetic Resonance*; Clarendon: Oxford, 1990.
- (184) Bencini, A.; Gatteschi, D. *EPR of Exchange Coupled Systems*; Springer-Verlag: Heidelberg, Germany, 1990.
- (185) Palmer, G. In *Physical Methods in Bioinorganic Chemistry*; Que, L., Jr., Ed.; University Science Books: Sausalito, 2000; Chapter 3, p 121.
- (186) Lancaster, C. R. D. *The Bioinorganic Chemistry of Nickel*; VCH Publishers: New York, 1988.
- (187) Gessner, C.; Trofanchuk, O.; Kawagoe, K.; Higuchi, Y.; Yasuoka, N.; Lubitz, W. *Chem. Phys. Lett.* **1996**, *256*, 518.
- (188) Trofanchuk, O.; Stein, M.; Gessner, C.; Lendzian, F.; Higuchi, Y.; Lubitz, W. *J. Biol. Inorg. Chem.* **2000**, *5*, 36.
- (189) Grinberg, O. Y.; Berliner, L. J. *Very high frequency (VHF) ESR/EPR*; Biological Magnetic Resonance, Vol. 22; Kluwer Academic-Plenum: New York, 2004.
- (190) Lubitz, W.; Möbius, K.; Dinse, K. P. *Magn. Reson. Chem.* **2005**, *43*, S2.
- (191) Möbius, K. *Appl. Magn. Res.* **2001**, *21*, 255.
- (192) Feher, G. *Phys. Rev.* **1956**, *103*, 834.
- (193) Schweiger, A.; Jeschke, G. *Principles of Pulse Electron Paramagnetic Resonance*; Oxford University Press: Oxford, 2001.
- (194) Dikanov, S. A.; Tsvetkov, Y. D. *Electron Spin Echo Envelope Modulation (ESEEM) Spectroscopy*; CRC Press: Boca Raton, FL, 1992.

- (195) Höfer, P.; Grupp, A.; Nebenführ, H.; Mehring, M. *Chem. Phys. Lett.* **1986**, *132*, 279.
- (196) Schosseler, P.; Wacker, T.; Schweiger, A. *Chem. Phys. Lett.* **1994**, *224*, 319.
- (197) Berliner, L. J.; Eaton, S. S.; Eaton, G. R. *Distance Measurements in Biological Systems by EPR: Biological Magnetic Resonance*; Kluwer Academic-Plenum Publishers: New York, 2000.
- (198) Milov, A. D.; Tsvetkov, Y. D.; Formaggio, F.; Crisma, M.; Toniolo, C.; Raap, J. *J. Am. Chem. Soc.* **2001**, *123*, 3784.
- (199) Milov, A. D.; Tsvetkov, Y. D.; Formaggio, F.; Crisma, M.; Toniolo, C.; Raap, J. *J. Am. Chem. Soc.* **2000**, *122*, 3843.
- (200) Milov, A. D.; Maryasov, A. G.; Tsvetkov, Y. D. *Appl. Magn. Res.* **1998**, *15*, 107.
- (201) Jeschke, G. *ChemPhysChem* **2002**, *3*, 927.
- (202) Koch, W.; Holthausen, M. C. A. *Chemist's Guide to Density Functional Theory*; Wiley-VCH: Weinheim, Germany, 2000.
- (203) Kaupp, M.; Bühl, M.; Malkin, V. G. *Calculation of NMR and EPR Parameters*; Wiley-VCH: Weinheim, 2004.
- (204) Neese, F. In *Electron paramagnetic resonance*; Gilbert, B. C., Davies, M. J., Murphy, D. M., Eds., Royal Society of Chemistry: Cambridge, 2006; Chapter 20, p in press.
- (205) Lalla-Maharajh, W. V.; Hall, D. O.; Cammack, R.; Rao, K. K.; LeGall, J. *Biochem. J.* **1983**, *209*, 445.
- (206) Hatchikian, C. E.; Traore, A. S.; Fernandez, V. M.; Cammack, R. *Eur. J. Biochem.* **1990**, *187*, 635.
- (207) Sorgenfrei, O.; Müller, S.; Pfeiffer, M.; Sniezko, I.; Klein, A. *Arch. Microbiol.* **1997**, *167*, 189.
- (208) Romao, C. V.; Pereira, I. A. C.; Xavier, A. V.; LeGall, J.; Teixeira, M. *Biochem. Biophys. Res. Commun.* **1997**, *240*, 75.
- (209) LeGall, J.; Dervarta, D. V.; Spilker, E.; Lee, J. P.; Peck, H. D. *Biochim. Biophys. Acta* **1971**, *234*, 525.
- (210) Nakos, G.; Mortenson, L. E. *Biochemistry* **1971**, *10*, 2442.
- (211) Nakos, G.; Mortenson, L. E. *Biochim. Biophys. Acta* **1971**, *227*, 576.
- (212) LeGall, J.; Ljungdahl, P. O.; Moura, I.; Peck, H. D.; Xavier, A. V.; Moura, J. J. G.; Teixeira, M.; Huynh, B. H.; DerVartanian, D. V. *Biochem. Biophys. Res. Commun.* **1982**, *106*, 610.
- (213) Graf, E. G.; Thauer, R. K. *FEBS Lett.* **1981**, *136*, 165.
- (214) Przybyla, A. E.; Robbins, J.; Menon, N.; Peck, H. D. *FEMS Microbiol. Rev.* **1992**, *88*, 109.
- (215) Albracht, S. P. J.; Graf, E.-G.; Thauer, R. K. *FEBS Lett.* **1982**, *140*, 311.
- (216) Krüger, H. J.; Huynh, B. H.; Ljungdahl, P. O.; Xavier, A. V.; DerVartanian, D. V.; Moura, I.; Peck, H. D.; Teixeira, M.; Moura, J. J. G.; LeGall, J. *J. Biol. Chem.* **1982**, *257*, 4620.
- (217) Moura, J. J. G.; Moura, I.; Huynh, B. H.; Krüger, H. J.; Teixeira, M.; DuVarney, R. C.; DerVartanian, D. V.; Xavier, A. V.; Peck, H. D., Jr.; LeGall, J. *Biochem. Biophys. Res. Commun.* **1982**, *108*, 1388.
- (218) Kojima, N.; Fox, J. A.; Hausinger, R. P.; Daniels, L.; Orme-Johnson, W. H.; Walsh, C. *Proc. Natl. Acad. Sci. U.S.A.* **1983**, *80*, 378.
- (219) Huyett, J. E.; Carepo, M.; Pamplona, A.; Franco, R.; Moura, I.; Moura, J. J. G.; Hoffman, B. M. *J. Am. Chem. Soc.* **1997**, *119*, 9291.
- (220) Schneider, K.; Patil, D. S.; Cammack, R. *Biochim. Biophys. Acta* **1983**, *748*, 353.
- (221) Erkens, A.; Schneider, K.; Müller, A. *J. Biol. Inorg. Chem.* **1996**, *1*, 99.
- (222) Burgdorf, T.; Lenz, O.; Buhrke, T.; Van der Linden, E.; Jones, A. K.; Albracht, S. P. J.; Friedrich, B. *J. Mol. Microbiol. Biotechnol.* **2005**, *10*, 181.
- (223) Müller, A.; Erkens, A.; Schneider, K.; Müller, A.; Nolting, H. F.; Sole, V. A.; Henkel, G. *Angew. Chem., Int. Ed. Engl.* **1997**, *36*, 1747.
- (224) Happe, R. P.; Roseboom, W.; Egert, G.; Friedrich, C. G.; Massanz, C.; Friedrich, B.; Albracht, S. P. J. *FEBS Lett.* **2000**, *466*, 259.
- (225) Van der Linden, E.; Burgdorf, T.; Bernhard, M.; Bleijlevens, B.; Friedrich, B.; Albracht, S. P. J. *J. Biol. Inorg. Chem.* **2004**, *9*, 616.
- (226) Löscher, S.; Burgdorf, T.; Zebger, I.; Hildebrandt, P.; Dau, H.; Friedrich, B.; Haumann, M. *Biochemistry* **2006**, *45*, 11658.
- (227) Foerster, S. EPR Spectroscopic Investigation of the Active Site of [NiFe]-Hydrogenase: A Contribution to the Elucidation of the Reaction Mechanism. Doctoral Thesis, Technische Universität Berlin, 2003.
- (228) Stein, M. Insight into the Mechanism of [NiFe] Hydrogenase by means of Magnetic Resonance Experiments and DFT Calculations. Doctoral Thesis, Technische Universität Berlin, 2001.
- (229) Albracht, S. P. J.; Ankelfuchs, D.; Bocher, R.; Ellermann, J.; Moll, J.; Vanderzwaan, J. W.; Thauer, R. K. *Biochim. Biophys. Acta* **1988**, *955*, 86.
- (230) Buhrke, T.; Brecht, M.; Lubitz, W.; Friedrich, B. *J. Biol. Inorg. Chem.* **2002**, *7*, 897.
- (231) Buhrke, T.; Lenz, O.; Krauss, N.; Friedrich, B. *J. Biol. Chem.* **2005**, *280*, 23791.
- (232) Flores, M.; Goenka-Agrawal, A.; van Gastel, M.; Gärtner, W.; Lubitz, W. submitted, 2007.
- (233) Albracht, S. P. J.; Kröger, A.; van der Zwaan, J. W.; Unden, G.; Böcher, R.; Mell, H.; Fontijn, R. D. *Biochim. Biophys. Acta* **1986**, *874*, 116.
- (234) He, S. H.; Teixeira, M.; LeGall, J.; Patil, D. S.; Moura, I.; Moura, J. J. G.; DerVartanian, D. V.; Huynh, B. H.; Peck, H. D. *J. Biol. Chem.* **1989**, *264*, 2678.
- (235) Sorgenfrei, O.; Duin, E. C.; Klein, A.; Albracht, S. P. J. *J. Biol. Chem.* **1996**, *271*, 23799.
- (236) Sorgenfrei, O.; Duin, E. C.; Klein, A.; Albracht, S. P. J. *Eur. J. Biochem.* **1997**, *247*, 681.
- (237) Stein, M.; Lubitz, W. *Phys. Chem. Chem. Phys.* **2001**, *3*, 5115.
- (238) Fan, C.; Teixeira, M.; Moura, J. J. G.; Moura, I.; Huynh, B. H.; LeGall, J.; Peck, H. D., Jr.; Hoffman, B. M. *J. Am. Chem. Soc.* **1991**, *113*, 20.
- (239) Gessner, C.; Stein, M.; Albracht, S. P. J.; Lubitz, W. *J. Biol. Inorg. Chem.* **1999**, *4*, 379.
- (240) van Gastel, M.; Stein, M.; Brecht, M.; Schröder, O.; Lenzian, F.; Bittl, R.; Ogata, H.; Higuchi, Y.; Lubitz, W. *J. Biol. Inorg. Chem.* **2006**, *11*, 41.
- (241) van Gastel, M.; Fichtner, C.; Neese, F.; Lubitz, W. *Biochem. Soc. Trans.* **2005**, *33*, 7.
- (242) Stadler, C.; De Lacey, A. L.; Hernandez, B.; Fernandez, V. M.; Conesa, J. C. *Inorg. Chem.* **2002**, *41*, 4417.
- (243) Stadler, C.; De Lacey, A. L.; Montet, Y.; Volbeda, A.; Fontecilla-Camps, J. C.; Conesa, J. C.; Fernandez, V. M. *Inorg. Chem.* **2002**, *41*, 4424.
- (244) Soderhjelm, P.; Ryde, U. *J. Mol. Struct. (THEOCHEM)* **2006**, *770*, 199.
- (245) Bleijlevens, B.; Faber, B. W.; Albracht, S. P. J. *J. Biol. Inorg. Chem.* **2001**, *6*, 763.
- (246) Chapman, A.; Cammack, R.; Hatchikian, E. C.; McCracken, J.; Peisach, J. *FEBS Lett.* **1988**, *242*, 134.
- (247) Goenka-Agrawal, A.; van Gastel, M.; Gärtner, W.; Lubitz, W. *J. Phys. Chem. B* **2006**, *110*, 8142.
- (248) Tan, S. L.; Fox, J. A.; Kojima, N.; Walsh, C. T.; Orme-Johnson, W. H. *J. Am. Chem. Soc.* **1984**, *106*, 3064.
- (249) Pershad, H. R.; Duff, J. L. C.; Heering, H. A.; Duin, E. C.; Albracht, S. P. J.; Armstrong, F. A. *Biochemistry* **1999**, *38*, 8992.
- (250) Cammack, R.; Patil, D. S.; Fernandez, V. M. *Biochem. Soc. Trans.* **1985**, *13*, 572.
- (251) Cammack, R.; Patil, D. S.; Aguirre, R.; Hatchikian, E. C. *FEBS Lett.* **1982**, *142*, 289.
- (252) Teixeira, M.; Moura, I.; Xavier, A. V.; DerVartanian, D. V.; LeGall, J.; Peck, H. D., Jr.; Huynh, B. H.; Moura, J. J. G. *Eur. J. Biochem.* **1983**, *130*, 481.
- (253) Fichtner, C. Spektroskopische und elektrochemische Untersuchung der [NiFe]-Hydrogenase aus *Desulfovibrio vulgaris* Miyazaki F. Doctoral Thesis, Universität Düsseldorf, 2005.
- (254) Adams, M. W. W.; Jin, S. L. C.; Chen, J. S.; Mortenson, L. E. *Biochim. Biophys. Acta* **1986**, *869*, 37.
- (255) Franco, R.; Moura, I.; LeGall, J.; Peck, H. D.; Huynh, B. H.; Moura, J. J. G. *Biochim. Biophys. Acta* **1993**, *1144*, 302.
- (256) Fernandez, V. M.; Rao, K. K.; Fernandez, M. A.; Cammack, R. *Biochimie* **1986**, *68*, 43.
- (257) Cammack, R.; Fernandez, V. M.; Schneider, K. *Biochimie* **1986**, *68*, 85.
- (258) Fernandez, V. M.; Hatchikian, E. C.; Patil, D. S.; Cammack, R. *Biochim. Biophys. Acta* **1986**, *883*, 145.
- (259) Roberts, L. M.; Lindahl, P. A. *J. Am. Chem. Soc.* **1995**, *117*, 2565.
- (260) Coremans, J. M. C. C.; van der Zwaan, J. W.; Albracht, S. P. J. *Biochim. Biophys. Acta* **1989**, *997*, 256.
- (261) Albracht, S. P. J.; Fontijn, R. D.; van der Zwaan, J. W. *Biochim. Biophys. Acta* **1985**, *832*, 89.
- (262) Barondeau, D. P.; Roberts, L. M.; Lindahl, P. A. *J. Am. Chem. Soc.* **1994**, *116*, 3442.
- (263) Roberts, L. M.; Lindahl, P. A. *Biochemistry* **1994**, *33*, 14339.
- (264) Vincent, K. A.; Parkin, A.; Lenz, O.; Albracht, S. P. J.; Fontecilla-Camps, J. C.; Cammack, R.; Friedrich, B.; Armstrong, F. A. *J. Am. Chem. Soc.* **2005**, *127*, 18179.
- (265) Albracht, S. P. J.; Kalkman, M. L.; Slater, E. C. *Biochim. Biophys. Acta* **1983**, *724*, 309.
- (266) Albracht, S. P. J.; van der Zwaan, J. W.; Fontijn, R. D. *Biochim. Biophys. Acta* **1984**, *766*, 245.
- (267) Brecht, M. Hochfeld- und Puls-EPR-Untersuchungen an den Kofaktoren von [NiFe]-Hydrogenasen: Beiträge zur Klärung des Mechanismus der biologischen Wasserspaltung. Doctoral Thesis, Technische Universität Berlin, 2001.
- (268) Fan, C. L.; Houseman, A. L. P.; Doan, P.; Hoffman, B. M. *J. Phys. Chem.* **1993**, *97*, 3017.
- (269) Elsässer, C.; Brecht, M.; Bittl, R. *J. Am. Chem. Soc.* **2002**, *124*, 12606.
- (270) Elsässer, C.; Brecht, M.; Bittl, R. *Biochem. Soc. Trans.* **2005**, *33*, 15.

- (271) Armstrong, F. A.; Albracht, S. P. J. *Phil. Trans. R. Soc. A* **2005**, 363, 937.
- (272) Krüger, H. J.; Holm, R. H. *Inorg. Chem.* **1989**, 28, 1148.
- (273) Krüger, H. J.; Holm, R. H. *J. Am. Chem. Soc.* **1990**, 112, 2955.
- (274) Krüger, H. J.; Peng, G.; Holm, R. H. *Inorg. Chem.* **1991**, 30, 734.
- (275) Choudhury, S. B.; Pressler, M. A.; Mirza, S. A.; Day, R. O.; Maroney, M. J. *Inorg. Chem.* **1994**, 33, 4831.
- (276) Teixeira, M.; Moura, I.; Xavier, A. V.; Huynh, B. H.; DerVartanian, D. V.; Peck, H. D., Jr.; LeGall, J.; Moura, J. J. G. *J. Biol. Chem.* **1985**, 260, 8942.
- (277) Guigliarelli, B.; More, C.; Fournel, A.; Asso, M.; Hatchikian, E. C.; Williams, R.; Cammack, R.; Bertrand, P. *Biochemistry* **1995**, 34, 4781.
- (278) Dole, F.; Medina, M.; More, C.; Cammack, R.; Bertrand, P.; Guigliarelli, B. *Biochemistry* **1996**, 35, 16399.
- (279) Bertrand, P.; Camensuli, P.; More, C.; Guigliarelli, B. *J. Am. Chem. Soc.* **1996**, 118, 1426.
- (280) Müller, A.; Tscherny, I.; Kappl, R.; Hatchikian, E. C.; Hüttermann, J.; Cammack, R. *J. Biol. Inorg. Chem.* **2002**, 7, 177.
- (281) Brugna-Guiral, M.; Tron, P.; Nitschke, W.; Stetter, K. O.; Burlat, B.; Guigliarelli, B.; Bruschi, M.; Giudici-Ortoni, M. T. *Extremophiles* **2003**, 7, 145.
- (282) Guiral, M.; Aubert, C.; Giudici-Ortoni, M. T. *Biochem. Soc. Trans.* **2005**, 33, 22.
- (283) Stein, M.; Lubitz, W. *J. Inorg. Biochem.* **2004**, 98, 862.
- (284) Fernandez, V. M.; Rua, M. L.; Reyes, P.; Cammack, R.; Hatchikian, E. C. *Eur. J. Biochem.* **1989**, 185, 449.
- (285) Kamachi, T.; Uno, S.; Hiraishi, T.; Okura, I. *J. Mol. Catal. A: Chem.* **1995**, 96, 329.
- (286) Zorin, N. A.; Dimon, B.; Gagnon, J.; Gaillard, J.; Carrier, P.; Vignais, P. M. *Eur. J. Biochem.* **1996**, 241, 675.
- (287) Fichtner, C.; van Gastel, M.; Lubitz, W. *Phys. Chem. Chem. Phys.* **2003**, 5, 5507.
- (288) Johnson, M. K.; Zambrano, I. C.; Czechowski, M. H.; Peck, H. D.; DerVartanian, D. V.; LeGall, J. *Biochem. Biophys. Res. Commun.* **1985**, 128, 220.
- (289) Medina, M.; Hatchikian, E. C.; Cammack, R. *Biochim. Biophys. Acta: Bioenerg.* **1996**, 1275, 227.
- (290) Fan, H. J.; Hall, M. B. *J. Am. Chem. Soc.* **2001**, 124, 394.
- (291) Arendsen, A. F.; Veenhuizen, P. T.; Hagen, W. R. *J. Bacteriol.* **1996**, 178, 163.
- (292) Silva, P. J.; de Castro, B.; Hagen, W. R. *J. Biol. Inorg. Chem.* **1999**, 4, 284.
- (293) Zorin, N. A.; Medina, M.; Pusheva, M. A.; Gogotov, I. N.; Cammack, R. *Fems Microbiol. Lett.* **1996**, 142, 71.
- (294) Rakhely, G.; Zhou, Z. H.; Adams, M. W. W.; Kovacs, K. L. *Eur. J. Biochem.* **1999**, 266, 1158.
- (295) Sapra, R.; Verhagen, M. F. J. M.; Adams, M. W. W. *J. Bacteriol.* **2000**, 182, 3423.
- (296) Filatov, M.; Cremer, D. *J. Chem. Phys.* **2005**, 123.
- (297) Niu, S. Q.; Thomson, L. M.; Hall, M. B. *J. Am. Chem. Soc.* **1999**, 121, 4000.
- (298) Stein, M.; van Lenthe, E.; Baerends, E. J.; Lubitz, W. *J. Am. Chem. Soc.* **2001**, 123, 5839.
- (299) Neese, F. *J. Chem. Phys.* **2001**, 115, 11080.
- (300) Stein, M.; Lubitz, W. *Phys. Chem. Chem. Phys.* **2001**, 3, 2668.
- (301) Ogata, H.; Flores, M.; van Gastel, M.; Lubitz, W. Unpublished work.
- (302) Amara, P.; Volbeda, A.; Fontecilla-Camps, J. C.; Field, M. J. *J. Am. Chem. Soc.* **1999**, 121, 4468.
- (303) Bruschi, M.; Zampella, G.; Fantucci, P.; De Gioia, L. *Coord. Chem. Rev.* **2005**, 249, 1620.
- (304) De Gioia, L.; Fantucci, P.; Guigliarelli, B.; Bertrand, P. *Inorg. Chem.* **1999**, 38, 2658.
- (305) De Lacey, A. L.; Pardo, A.; Fernandez, V. M.; Dementin, S.; Adryanczyk-Perrier, G.; Hatchikian, E. C.; Rousset, M. *J. Biol. Inorg. Chem.* **2004**, 9, 636.
- (306) Gross, R.; Pisa, R. S. M.; Lancaster, C. R. D.; Simon J. *J. Biol. Chem.* **2004**, 279, 274.
- (307) Pavlov, M.; Siegbahn, P. E. M.; Blomberg, M. R. A.; Crabtree, R. H. *J. Am. Chem. Soc.* **1998**, 120, 548.
- (308) Pavlov, M.; Blomberg, M. R. A.; Siegbahn, P. E. M. *Int. J. Quantum Chem.* **1999**, 73, 197.
- (309) De Gioia, L.; Fantucci, P.; Guigliarelli, B.; Bertrand, P. *Int. J. Quantum Chem.* **1999**, 73, 187.
- (310) Hagen, W. R.; van Berkel-Arts, A.; Krüse-Wolters, K. M.; Dunham, W. R.; Veeger, C. *FEBS Lett.* **1986**, 201, 158.
- (311) van Dijk, C.; van Berkel-Arts, A.; Veeger, C. *FEBS Lett.* **1983**, 156, 340.
- (312) Silakov, A. E. Investigation of the active site of the [FeFe] hydrogenase from *Desulfovibrio desulfuricans*. Doctoral Thesis, Heinrich-Heine-Universität Düsseldorf, 2007.
- (313) Silakov, A.; Reijerse, E. J.; Albracht, S. P. J.; Hatchikian, E. C.; Lubitz, W. *J. Am. Chem. Soc.* **2007**, 129, 11447.
- (314) Telsler, J.; Benecky, M. J.; Adams, M. W. W.; Mortenson, L. E.; Hoffman, B. M. *J. Biol. Chem.* **1986**, 261, 13536.
- (315) Krusic, P. J.; Filippo, J. S.; Hutchinson, B.; Hance, R. L.; Daniels, L. M. *J. Am. Chem. Soc.* **1981**, 103, 2129.
- (316) Krusic, P. J. *J. Am. Chem. Soc.* **1981**, 103, 2131.
- (317) Fiedler, A. T.; Brunold, T. C. *Inorg. Chem.* **2005**, 44, 9322.
- (318) Cao, Z. X.; Hall, M. B. *J. Am. Chem. Soc.* **2001**, 123, 3734.
- (319) Liu, Z. P.; Hu, P. *J. Am. Chem. Soc.* **2002**, 124, 5175.
- (320) George, S. J.; Cui, Z.; Razavet, M.; Pickett, C. J. *Chem. Eur. J.* **2002**, 8, 4037.
- (321) Darensbourg, M. Y.; Lyon, E. J.; Zhao, X.; Georgakaki, I. P. *Proc. Natl. Acad. Sci. U.S.A.* **2003**, 100, 3683.
- (322) Bruschi, M.; Fantucci, P.; De Gioia, L. *Inorg. Chem.* **2002**, 41, 1421.
- (323) Bruschi, M.; Fantucci, P.; De Gioia, L. *Inorg. Chem.* **2003**, 42, 4773.
- (324) Zhou, T. J.; Mo, Y. R.; Liu, A. M.; Zhou, Z. H.; Tsai, K. R. *Inorg. Chem.* **2004**, 43, 923.
- (325) Zhou, T. J.; Mo, Y. R.; Zhou, Z. H.; Tsai, K. R. *Inorg. Chem.* **2005**, 44, 4941.
- (326) Fan, H. J.; Hall, M. B. *J. Am. Chem. Soc.* **2001**, 123, 3828.
- (327) van Haaster, D. J.; Jongejan, J. A.; Hagedoorn, P. L.; Hagen, W. R. *Int. J. Hydrogen Energy* **2006**, 31, 1432.
- (328) Schenzle, A.; Wong, N. C.; Brewer, R. G. *Phys. Rev. A* **1980**, 22, 635.
- (329) Schenzle, A.; Wong, N. C.; Brewer, R. G. *Phys. Rev. A* **1980**, 21, 887.
- (330) Hahn, E. L. *Phys. Rev.* **1950**, 80, 580.
- (331) Rowan, L. G.; Hahn, E. L.; Mims, W. B. *Phys. Rev.* **1965**, 137, A61.
- (332) Mims, W. B. *Proc. R. Soc. London, Ser. A* **1965**, 283, 452.
- (333) Gemperle, C.; Sorensen, O. W.; Schweiger, A.; Ernst, R. R. *J. Magn. Reson.* **1990**, 87, 502.
- (334) Mehring, M.; Höfer, P.; Grupp, A. *Ber. Bunsen-Ges. Phys. Chem.* **1987**, 91, 1132.
- (335) Bowers, K. D.; Mims, W. B. *Phys. Rev.* **1959**, 115, 285.
- (336) Solomon, E. I.; Pavel, E. G.; Loeb, K. E.; Campochiaro, C. *Coord. Chem. Rev.* **1995**, 144, 369.
- (337) Bominaar, E. L.; Hu, Z. G.; Münck, E.; Girerd, J. J.; Borshch, S. A. *J. Am. Chem. Soc.* **1995**, 117, 6976.
- (338) Xia, J. Q.; Hu, Z. G.; Popescu, C. V.; Lindahl, P. A.; Münck, E. *J. Am. Chem. Soc.* **1997**, 119, 8301.
- (339) Belinsky, M. I. *J. Biol. Inorg. Chem.* **1996**, 1, 186.
- (340) Mouesca, J. M.; Noodleman, L.; Case, D. A.; Lamotte, B. *Inorg. Chem.* **1995**, 34, 4347.
- (341) Garcin, E., Ph.D. Thesis. Université Joseph Fourier-Grenoble 1, 1998.
- (342) Davies, E. R. *Phys. Lett.* **1974**, A47, 1.

CR050186Q